Thermodynamics of Aqueous Biopolymer Solutions and Fractionation of Dextran

Dissertation

Zur Erlangung des Grades
“Doktor der Naturwissenschaften”
im Fachbereich Chemie, Pharmazie und Geowissenschaften
Johannes Gutenberg-Universität Mainz

Rei Sugaya
geb. in Tokyo

Mainz 2005

Abstract

Flory-Huggins interaction parameters and thermal diffusion coefficients were measured for aqueous biopolymer solutions. Dextran (a water soluble polysaccharide) and bovine serum albumin (BSA, a water soluble protein) were used for this study. The former polymer is representative for chain macromolecules and the latter is for globular macromolecules.

The interaction parameters for the systems water/dextran and water/BSA were determined as a function of composition by means of vapor pressure measurements, using a combination of headspace sampling and gas chromatography (HS-GC). A new theoretical approach, accounting for chain connectivity and conformational variability, describes the observed dependencies quantitatively for the system water/dextran and qualitatively for the system water/BSA. The phase diagrams of the ternary systems water/methanol/dextran and water/dextran/BSA were determined via cloud point measurements and modeled by means of the direct minimization of the Gibbs energy using the information on the binary subsystems as input parameters.

The thermal diffusion of dextran was studied for aqueous solutions in the temperature range $15 < T < 55$ °C. The effects of the addition of urea were also studied. In the absence of urea, the Soret coefficient S_T changes its sign as T is varied; it is positive for $T > 45.0$ °C, but negative for $T < 45.0$ °C. The positive sign of S_T means that the dextran molecules migrate towards the cold side of the fluid; this behavior is typical for polymer solutions. While a negative sign indicates the macromolecules move toward the hot side; this behavior has so far not been observed with any other binary aqueous polymer solutions. The addition of urea to the aqueous solution of dextran increases S_T and reduces the inversion temperature. For 2 M urea, the change in the sign of S_T is observed at $T = 29.7$ °C. At higher temperature S_T is always positive in the studied temperature range. To rationalize these observations it is assumed that the addition of urea opens hydrogen bonds, similar to that induced by an increase in temperature.

For a future extension of the thermodynamic studies to the effects of poly-dispersity, dextran was fractionated by means of a recently developed technique called Continuous Spin Fractionation (CSF). The solvent/precipitant/polymer system used for the thermodynamic studies served as the basis for the fractionation of dextran The starting polymer had a weight average molar mass $M_w = 11.1$ kg/mol and a molecular non-uniformity $U = M_w / M_n - 1 = 1.0$. Seventy grams of dextran were fractionated using water as the solvent and methanol as the precipitant. Five fractionation steps yielded four samples with M_w values between 4.36 and 18.2 kg/mol and U values ranging from 0.28 to 0.48.

Contents

1 Introduction

The knowledge of the phase behavior in solvents plays an important role for the production and the use of technically important polymers. During the synthesis or the processing of polymers, it is necessary to know whether the polymer solution is stable, metastable or unstable.

The concentration dependence of the Gibbs energy of mixing leads to the thermodynamic description of the polymer containing mixtures. According to the Flory-Huggins theory, the residual term of the Gibbs energy of mixing is responsible for the stability or instability of the polymer solution. This term contains a parameter that describes the interaction between the segments of the polymer and the solvent molecules. The Flory-Huggins theory is very important for the basic understanding of the thermodynamics of polymer solutions, there are, however, significant deficiencies. In order to eliminate these shortcomings, a new approach based on "Chain Connectivity and Conformational Variability of Polymers"[1-3] was introduced. This approach has proven to be well applicable for linear synthetic polymers.[1-3] In this study, the applicability of the theory to solutions of biopolymers is investigated.

Dextran (a water soluble polysaccharide) and bovine serum albumin (BSA, a water soluble protein) were chosen for this purpose. Dextran was expected to follow the new approach because it is a linear or only slightly branched polymer. With BSA, a globular polymer, the situation was unpredictable. The main method used was the determination of vapor pressures via Headspace Gaschromatography (HS-GC), which leads to the Flory-Huggins interaction parameters. In the case of dextran the investigation was extended to the phenomenon of thermal diffusion (Soret effect), so far not studied with polysaccharides; in this context, the thermodynamic interactions quantified by the HS-GC measurements are important for the understanding of the Soret effect. The information concerning the *binary* systems named above is to be used for the theoretical modeling of the phase separation behavior of *ternary* systems by means of a "Direct Minimization of Gibbs Energy of Mixing".[4]

Two three-component mixtures were of particular interest: water/methanol/ dextran (I) and water/dextran/BSA (II). System (I), a polymer dissolved in a mixed solvent, was chosen because it constitutes the basis for the fractionation of dextran by means of a new large scale technique (Continuous Spin Fractionation). In view of later studies on the influences of polydispersity on thermodynamic properties the polymer was fractionated. For system (II), a solution of a chain polymer and a globular polymer in a common solvent was used, the goal was to investigate whether the phase diagram

measured by another member of the research group can be qualitatively modeled by use of the information obtained for the binary subsystems water/dextran and water/BSA.

2 Theory

2.1 Thermodynamics

In order to investigate the thermodynamics of polymer solutions, the thermodynamics of low-molecular materials is revised at first.[7] Secondly, the Flory-Huggins theory, the basics of the thermodynamics of polymer solutions,[7-10] and a new approach, "Chain Connectivity and Conformational Variability of Polymers",[1-3] which is introduced to eliminate the deficiencies of Flory-Huggins theory, are reviewed. In addition, for the experimental investigation, Headspace Gas Chromatography measurement is described. Then the way to model phase diagrams, called "Direct Minimization of the Gibbs Energy of Mixing"[4] is given.

2.1.1 Thermodynamics of Mixtures of Low-Molecular Materials

For mixtures of low molecular weight compounds, mole fractions, the quantities referring to one mole of mixture characterized by a stroke above the symbol, are used. Processes taking place at constant temperature and constant pressure are normally dealt with in terms of changes in the Gibbs energy ΔG, which are made up of an enthalpy contribution $\Delta\overline{H}$ and an entropy contribution $\Delta\overline{S}$ according to

$$\Delta\overline{G} = \Delta\overline{H} - T\Delta\overline{S} \tag{1}$$

where T is the absolute temperature.

Perfect mixing takes place athermally ($\Delta\overline{H}$ = 0) and the volume of the mixture does not differ from the sum of the volumes of its constituents (volume of mixing $\Delta\overline{V}$ = 0). In this case the driving force for the formation of a molecularly disperse mixture consists exclusively of the changes in entropy associated with the mixing process, i.e. in the higher number of arrangements of the molecules in the mixed state. The just described limiting situation is usually called perfect mixing (by approximation sometimes realized with mixtures of gases or mixed crystals) and the following relation holds true

$$\frac{-\Delta\overline{S}^{perf}}{R} = x_1 \ln x_1 + x_2 \ln x_2 \tag{2}$$

where R is the universal gas constant and x_i are mole fractions. For the Gibbs energy of mixing we thus obtain

$$\Delta\overline{G}^{perf} = -T\,\Delta\overline{S}^{perf} \tag{3}$$

Real mixture normally deviate considerably from the behavior described above. In order to maintain a well defined reference state one introduces so called excess quantities, measuring the deviation from perfect mixing, as formulated in the following equations.

$$\Delta\overline{G} = \Delta\overline{G}^{perf} + \Delta\overline{G}^{E} \tag{4}$$

where

$$\Delta\overline{G}^{E} = \Delta\overline{H} - T\,\Delta\overline{S}^{E} \tag{5}$$

2.1.2 Thermodynamics of polymer solutions

Although simple molecule solutions, which is described by the ideal solution law, seldom behave ideally over wide ranges in concentration, the correlation usually is adequate to justify adoption of the classically defined ideal solution as a standard for comparison. Solutions in which the solute is a polymer of high molecular weight exhibit very large deviations from ideality. According to Raoult's law (with $a = P / P_0$), the activity a of the solvent in the solution should equal to its mole fraction x_1 and the partial pressure P of the solvent in the solution should be very nearly equal to that of the pure solvent P_0 over the greater portion of the composition range. But experiments do not confirm this prediction. At higher concentrations the activity correlates better with the volume fraction, φ_1, than with the mole fraction. The underlying basis for the failure of the ideal solution law lies in its use of the mole fraction as the composition variable. Volume fraction is given as

$$\varphi_2 = \frac{n_2 V_2}{n_1 V_1 + n_2 V_2} \tag{6}$$

where V_i is molar volume of component i and n_i is moles of component i.

Ideal solution behavior over extended ranges in both composition and temperature requires that the following conditions be fulfilled:(i) the entropy of mixing must be given by Eq. 2; and (ii) the heat of mixing must equal zero($\Delta\overline{H} = 0$). Deviations from ideality may arise from failure of these conditions. In order to develop a concept of combinatorial mixing for polymer solutions, Flory and Huggins introduced a lattice model , where the number of segment N, the ratio of the molar volumes of the solute and solvent to the size of a segment, is used. One mole of segments is normally defined

by the volume of the solvent or set 100mL/segment. And the volume fractions are used instead of mole fractions and the quantities referring to volume fraction are characterized by double stroke. With this concept, entropy of mixing for polymer solutions are expressed as

$$\frac{-\Delta \overline{\overline{S}}^{comb}}{R} = \frac{1}{N_1}\varphi_1 \ln \varphi_1 + \frac{1}{N_2}\varphi_2 \ln \varphi_2 \tag{7}$$

The coexistence of different phases under equilibrium is bound to the condition that the chemical potential μ must be identical in all phases. Presently only liquid/liquid phase equilibria (i.e. the two phases have the same state of aggregation) is of interest; this means that it is only necessary to account for differences in the Gibbs energy of mixing and can be written

$$\Delta\mu_i^{'} = \Delta\mu_i^{''} \tag{8}$$

With the definition of the chemical potential of component 1

$$\Delta\mu_1 = \left(\frac{\partial \Delta G}{\partial n_1}\right)_{p,T,n_2} \tag{9}$$

and analogously of component 2 we obtain the following relations

$$\begin{aligned}\Delta\mu_1 = & \left(\frac{\partial\left[\left(n_1N_1 + n_2N_2\right)\Delta\overline{\overline{G}}\right]}{\partial\, n_1}\right)_{p,T,n_2} = \\ = & \; N_1\,\Delta\overline{\overline{G}} + \left(n_1N_1 + n_2N_2\right)\left(\frac{\partial\,\Delta\overline{\overline{G}}}{\partial\,\varphi_1}\right)\left(\frac{\partial\,\varphi_1}{\partial\, n_1}\right)\end{aligned} \tag{10}$$

where

$$\left(\frac{\partial\,\varphi_1}{\partial\, n_1}\right) = \frac{1}{n_1}\varphi_1\,\varphi_2 \tag{11}$$

After some rearrangement we obtain

$$\Delta\mu_1 = N_1\left(\Delta\overline{\overline{G}} + \left(1-\varphi_1\right)\frac{\partial\,\Delta\overline{\overline{G}}}{\partial\,\varphi_1}\right) \tag{12}$$

In terms of molar quantities this equation reads

$$\Delta\mu_1 = \Delta\overline{G} + (1 - x_1)\frac{\partial\,\Delta\overline{G}}{\partial\,x_1} \tag{13}$$

Phase Diagrams

Figure 1 shows the situation schematically for a system exhibiting a so called upper critical solution temperature (UCST, phase separation upon cooling). In this case the tie lines degenerate into a single point (at the critical temperature T_c and w_c, the critical weight fraction of the polymer) as T is raised. For the opposite case (phase separation upon heating) we speak of a system exhibiting a lower critical solution temperature (LCST).

According to Eq. 13, one can obtain the chemical potential of component 1 by means of the tangent to the curves describing the composition dependence of the Gibbs energy of mixing from the intercept with the ordinate (φ_1 =1), as demonstrated in the lower part of Figure 1. Analogously the chemical potential of component 2 results from the intercept at φ_2 =1. The chemical potentials of a given component must be identical in the coexisting phases as formulated in Eq. 8. In case the system exhibits limited mutual solubility it is therefore possible to determine the composition of the coexisting phases by means of a common tangent (cf. upper curves in the lower part of Figure 1). Repeating this construction for different temperatures and plotting T on the ordinate and the corresponding compositions on the abscissa yields the binodal curve shown in the upper part of Figure 1.

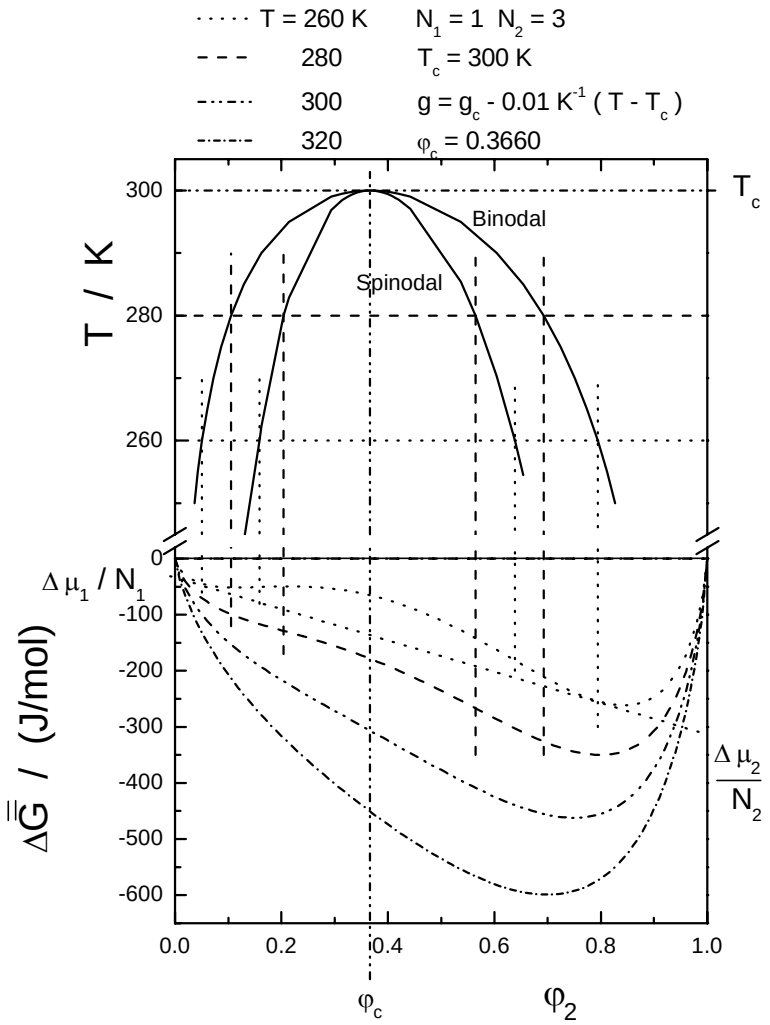

Figure 1. How to construct a phase diagram knowing the composition dependence of segment molar Gibbs energy of mixing. (textbook of Prof. B. A. Wolf, 2004)

The points of inflection of the curves of the lower part of Figure 1, representing the spinodal conditions in terms of Gibbs energy, are mathematically given by the condition

$$\frac{\partial^2 \overline{\overline{\Delta G}}}{\partial \varphi_2^2} = 0 \tag{14}$$

In the critical point of the system, where the binodal line and the spinodal line touch, the minima and the points of inflection coincide and the third derivative also becomes zero

$$\frac{\partial^3 \overline{\overline{\Delta G}}}{\partial \varphi_2^3} = 0 \tag{15}$$

In the vicinity of the critical composition of the system and close to the critical temperatures the curve $\overline{\overline{\Delta G}}(\varphi_2)$ is almost linear as demonstrated in Figure 1.

The description of three component systems requires three independent variables in the case of constant pressure: *T* and two composition variables. Because of the additional variable it is according to the Gibbs phase law possible that three phases coexist within a certain *range* of composition, in contrast to binary systems, for which only three phase *lines* are feasible. In order to avoid three-dimensional representations one normally depicts the isothermal situation and uses the so-called Gibbs phase triangle for that purpose as demonstrated in Figure 2.

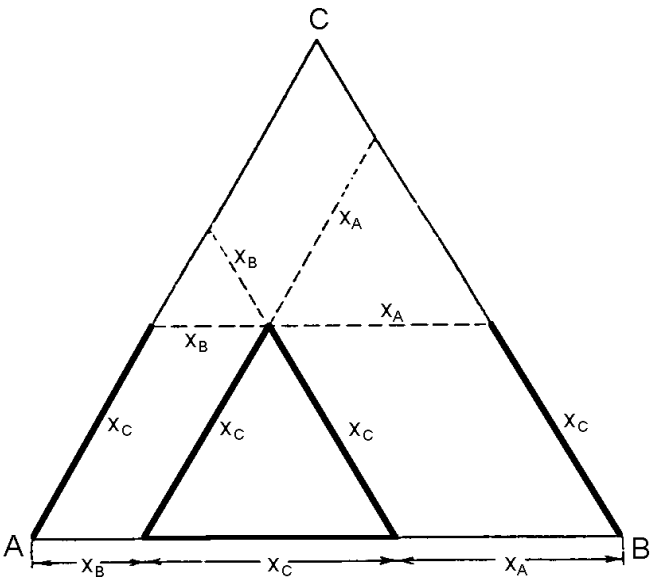

Figure 2. How to read the composition of a ternary mixture in a Gibbs phase triangle. (textbook of Prof. B. A. Wolf, 2004)

The corners of the triangle represent the pure components, the three edges (of unit length) the binary subsystems and the interior of the triangle stands for ternary mixtures. There are no restrictions concerning the particular nature of the composition variable, as long as the sum of all components yields unity. The most common method (out of several) to read the concentrations is demonstrated in Figure 2.

The extension of the integral Flory-Huggins equation to K components yields the following expression

$$\frac{\Delta\overline{\overline{G}}}{R\,T} = \sum_{i=1}^{K} \frac{1}{N_i}\,\varphi_i \ln \varphi_i + \sum_{i=1}^{K-1}\sum_{j=i+1}^{K} g_{ij}\,\varphi_i\,\varphi_j \tag{16}$$

For its derivation it was tacitly assumed that interactions between two types of segments (ij) suffice to describe the mixture and that no ternary interaction parameters g_{ijk} are required. For K = 3 we obtain the relation for mixtures of three components.

Flory-Huggins theory

By analogy to mixtures of low molecular weight components we quantify the deviation from this limiting behavior. To this end we introduce residual contribution according to

$$\Delta\overline{\overline{G}} = \Delta\overline{\overline{G}}^{comb} + \Delta\overline{\overline{G}}^{R} \tag{17}$$

Initially $\Delta\overline{\overline{G}}^{R}$ was considered to be exclusively of enthalpic nature and a composition independent interaction parameter, here called *g*', was introduced by means of the following relation

$$\frac{\Delta\overline{\overline{H}}}{R\,T} = g'\,\varphi_1\,\varphi_2 \tag{18}$$

g' was meant to measure ½ of the change in enthalpy associated with the destruction of a contact between two segments of component 1 and two segments of component 2 to yield two contacts between a segment of 1 and a segment of 2. Despite the fact that experiments have very early demonstrated convincingly that *g* is neither independent of composition nor necessarily of enthalpic nature, this formalism is still widespread and helpful for the understanding of some central features of polymer containing mixtures. For the integral Gibbs energy of mixing per mole of segments the Flory-Huggins equation reads

$$\frac{\Delta\overline{\overline{G}}}{R\,T} = \frac{1}{N_1}\,\varphi_1 \ln \varphi_1 + \frac{1}{N_2}\,\varphi_2 \ln \varphi_2 + g\,\varphi_1\,\varphi_2 \tag{19}$$

where integral interaction parameter *g* is redefined as

$$g = \frac{\Delta \overline{\overline{G}}^{R}}{R\,T\,\varphi_1\,\varphi_2} \tag{20}$$

and contains enthalpic as well as entropic contributions.

The integral Flory-Huggins interaction parameter g is experimentally inaccessible. The only information that is available stems from the measurement of chemical potentials, normally that of the solvent (e.g. via vapor pressure measurements or via osmosis). For crystalline polymers the chemical potential of the polymer in the mixture becomes accessible form liquid/solid equilibria. In view of this situation and because of the already mentioned concentration dependence of g we must differentiate the integral equation Eq. 19 and end up with the following expressions

$$\frac{\partial \dfrac{\Delta \overline{\overline{G}}}{R\,T}}{\partial \varphi_2} = -\frac{1}{N_1} + \frac{1}{N_2} - \frac{1}{N_1}\ln \varphi_1 + \frac{1}{N_2}\ln \varphi_2 + g\,(\varphi_1 - \varphi_2) + \frac{\partial g}{\partial \varphi_2}\varphi_1\varphi_2 \tag{21}$$

$$\frac{\partial^2 \dfrac{\Delta \overline{\overline{G}}}{R\,T}}{\partial \varphi_2^2} = \frac{1}{N_1\,\varphi_1} + \frac{1}{N_2\,\varphi_2} - 2\,g + 2\,\frac{\partial g}{\partial \varphi_2}(\varphi_1 - \varphi_2) + \frac{\partial^2 g}{\partial \varphi_2^2}\varphi_1\varphi_2 \tag{22}$$

$$\frac{\partial^3 \dfrac{\Delta \overline{\overline{G}}}{R\,T}}{\partial \varphi_2^3} = \frac{1}{N_1\,\varphi_1^2} - \frac{1}{N_2\,\varphi_2^2} - 6\,\frac{\partial g}{\partial \varphi_2} + 3\frac{\partial^2 g}{\partial \varphi_2^2}(\varphi_1 - \varphi_2) + \frac{\partial^3 g}{\partial \varphi_2^3}\varphi_1\varphi_2 \tag{23}$$

By means of the above relations one obtains the following expression for the chemical potential of component 1

$$\frac{\Delta \mu_1}{R\,T\,N_1} = \frac{1}{N_1}\ln \varphi_1 + \left(\frac{1}{N_1} - \frac{1}{N_2}\right)\varphi_2 + \chi\,\varphi_2^2 \tag{24}$$

where χ is given by

$$\chi = g + \varphi_1 \frac{\partial\, g}{\partial\, \varphi_1} = \frac{\Delta \mu_1^R}{RT\,N_1\,\varphi_2^2} \tag{25}$$

and for the chemical potential of component 2

$$\frac{\Delta\mu_2}{R\,T\,N_2} = \frac{1}{N_2}\ln\varphi_2 + \left(\frac{1}{N_2} - \frac{1}{N_1}\right)\varphi_1 + \xi\,\varphi_1^2 \tag{26}$$

where ξ is given by

$$\xi = g + \varphi_2\frac{\partial\, g}{\partial\,\varphi_2} = \frac{\Delta\mu_2^R}{RT\,N_2\,\varphi_1^2} \tag{27}$$

For the integral interaction parameter the following equations hold true

$$g = \frac{1}{\varphi_1}\int_0^{\varphi_1}\chi\; d\varphi_1 = \frac{1}{\varphi_2}\int_0^{\varphi_2}\xi\; d\varphi_2 \tag{28}$$

$$g = \varphi_2\;\chi + \varphi_1\;\xi \tag{29}$$

Demixing into two liquid phases is bound to the existence of a “hump” in the function $\Delta\overline{\overline{G}}(\varphi_2)$ as discussed earlier. The contribution $\Delta\overline{\overline{G}}^{comb}(\varphi_2)$ inevitably runs above its tangents and does consequently exclude demixing; it is only the residual contribution $\Delta\overline{\overline{G}}^{R}(\varphi_2)$, which may induce phase separation. Only if the interaction parameter *g* exceeds a certain critical value, depending on the chain lengths of the components, the deviation from combinatorial behavior becomes large enough to produce the required hump. Under the (unreasonable) assumption that *g* does not depend on composition, all interaction parameter become identical and one can calculate the critical interaction parameter g_c and the critical volume fractions φ_c from the condition that the binodal curve and the spinodal curve touch each other as the conditions become critical. By means of the Eqs. 14 and 22 one can calculate the spinodal if *g* is known and with the Eqs. 15 and 23 the critical point becomes accessible. From Eqs. 15 and 23 one obtains

$$\frac{1}{N_1\,\varphi_{1c}^2} = \frac{1}{N_2\,\varphi_{2c}^2} \tag{30}$$

$$\sqrt{N_1}\,\varphi_{1c} = \sqrt{N_2}\,(1-\varphi_{1c}) \tag{31}$$

$$\sqrt{N_1}\,\varphi_{1c} + \sqrt{N_2}\,\varphi_{1c} = \sqrt{N_2} \tag{32}$$

$$\varphi_{1c} = \frac{\sqrt{N_2}}{\sqrt{N_1}+\sqrt{N_2}} \tag{33}$$

and from the Eqs. 14 and 22

$$g_c = \frac{1}{2}\left(\frac{1}{N_1\,\varphi_{1c}} + \frac{1}{N_2\,\varphi_{2c}}\right) \tag{34}$$

Insertion of Eq. 33 yields

$$g_c = \frac{1}{2}\left(\frac{\sqrt{N_1}+\sqrt{N_2}}{N_1\sqrt{N_2}} + \frac{\sqrt{N_1}+\sqrt{N_2}}{N_2\sqrt{N_1}}\right) = \frac{1}{2}\left(\frac{\left(\sqrt{N_1}+\sqrt{N_2}\right)^2}{N_1\,N_2}\right) \tag{35}$$

Despite the deficiencies of the Flory-Huggins theory, namely its collapse in the region of low polymer concentrations and for its disability to account for the experimentally observed dependence of the Flory-Huggins interaction parameter, χ on chain length at high polymer concentrations, this approach is very helpful in understanding some basic features. For example the fact that the mutual miscibility associated with a certain unfavorable interaction between the components (positive g values) decreases rapidly as the number of segments N_i becomes larger. Similarly it explains that critical volume fractions around 0.5 can only be expected if the chain length of the components is not too different. Otherwise the critical composition is shifted to the side of the component containing fewer segments.

2.1.3 Chain Connectivity and Conformational Variability

In order to eliminate the deficiencies of Flory-Huggins theory, an approach, "Chain Connectivity and Conformational Variability",[1-3] has been designed that accounts for two important features of polymer containing systems, namely chain connectivity (impeding the uniform distribution of segments over the entire volume of a

system) and conformational response (accounting for the fact that coil dimensions may vary with composition).

According to the new approach, the equation for the integral interaction parameter reads

$$g = \frac{\alpha}{(1-\nu)(1-\nu\varphi)} - \zeta\left(1+(1-\lambda)\varphi\right) \tag{36}$$

The parameters of the above relation were introduced in the course of modeling the chemical potential of the solvent[1-3] as a function of composition, where the dilution was conceptually subdivided into two clearly separable steps, corresponding to the summands of Eq. 36. The first step consists in the addition of solvent without changing the conformation of the polymer chains and possible preferential orientations of solvent molecules. Equilibrium is reached in the second step, consisting of a conformational rearrangement such that the minimum in its Gibbs energy is achieved. The just outlined approach turned out to be very efficient for a quantitative modeling of the thermodynamic behavior of homogeneous and demixed polymer solutions[1-3,11-16] Moreover it could help to rationalize uncommon experimental observations concerning multiple critical points for binary systems.[17]

The different parameters of Eq. 36 have the following meaning.

α quantifies the effect of opening an intermolecular contact between polymer segments at infinite dilution by inserting a solvent molecule changing neither the conformation of the polymer chain nor possible orientations of the solvent.

ν was introduced to account for the interactions beyond the concentration regime of pair interaction and comprises two effects, (i) those resulting from differences in the surfaces of a polymer segment and of a solvent molecule and (ii) those stemming from changes in the entropy of dilution from the combinatorial value with the composition of the mixture.

ζ constitutes the conformational response; it results from the rearrangement of the components, in particular of the polymer chain, after the formation of new contacts. Positive ζ values decrease the Gibbs energies and enhance the mixing tendency. The theta condition for polymer solutions corresponds to $\zeta = 0$.

λ stands for chain connectivity, i.e. for the fact that the segments of a polymer molecule cannot spread out over the entire volume of a system. With polymer

solutions λ approaches 0.5 as the molar mass of the solute goes to infinity. For shorter chains the spatial constraints are larger and so is λ.

α and ζ are determined by following equation,[1]

$$\zeta = \frac{\sigma \rho_2^2 \overline{V_1}}{\kappa} \tag{37}$$

$$\alpha = \frac{1+\zeta}{2} + A_2^{\infty} \rho_2^2 \overline{V}_1 \tag{38}$$

where σ stands for the slope of A_2 vers. $N^{-(1-a)}$, ρ for the density and κ is determined as

$$\kappa = K_N \rho_2 \tag{39}$$

$$K_N = K\left(\frac{\rho_2}{\rho_1} M_1\right)^a \tag{40}$$

where a is the exponent of the Kuhn-Mark-Houwink equation, K the factor of the Kuhn-Mark-Houwink relation, and M the molar mass. A_2^{∞} stands for the second osmotic virial coefficient of infinitely long chains obtained as

$$A_2 = A_2^{\infty} + \sigma N^{-(1-a)} \tag{41}$$

And λ is determined as follows,

$$\lambda = \frac{1}{2} + \kappa N^{-(1-a)} \tag{42}$$

As for ν, some discrepancies are noted, though, ν lie in the order of magnitude[2] expected for γ, the differences in the surfaces of the polymer segments s_2 and the solvent molecules s_1, introduced as[18]

$$\gamma = 1 - \frac{s_2}{s_1} \tag{43}$$

Here it is refrained from using the same nomenclature because some of the observations can hardly be reconciled with the molecular picture underlying γ, despite the fact that others match reasonably. The disagreement applies above all the temperature

dependence of ν. Even if one interprets the changes in the free volume resulting from an augmentation of temperature as an increase in the surface of the solvent molecules, one cannot rationalize the pronounced reduction of ν. On the other hand, for some of the systems the ν values determined for room temperature lie on the order of magnitude expected for γ.

For the modeling of phase diagrams Eq. 36 suffices because the direct minimization of the Gibbs energy[19,20] for that purpose is used. However, for the evaluation of experimental information on the chemical potential of the solvent (e.g. via vapor pressures) as a function of composition, the corresponding differential expression is more adequate. According to the present approach it reads

$$\chi = \frac{\alpha}{\left(1-\nu\,\varphi\right)^2} - \zeta\lambda\left(1+2\left(\frac{1}{\lambda}-1\right)\varphi\right) \tag{44}$$

$$\xi = \frac{\alpha}{\left(1-\nu\right)\left(1-\nu\varphi\right)^2} - \zeta\left(1+2\left(1-\lambda\right)\varphi\right) \tag{45}$$

2.1.4 Determination of Interaction Parameters from Vapor Pressures

The vapor pressure of the solvent above a polymer solution (P), as compared with the vapor pressure of the pure solvent (P_0), yields access to the activity a of this component in the mixture, i.e. on the corresponding (differential) interaction parameter χ according to

$$\ln\frac{P}{P_0} = \ln a = \ln\left(1-\varphi\right) + \left(1-\frac{1}{N}\right)\varphi + \chi\,\varphi^2 \tag{46}$$

2.1.5 Direct Minimization of Gibbs Energy of Mixing

The calculation of phase diagrams on the basis of the Gibbs energy of mixing ΔG is a common procedure in the field of thermodynamics.[21] Normally the calculation of tie lines at constant temperature and pressure is carried out by numerically solving the equations describing the equality of the chemical potentials μ. μ is connected to the Gibbs energy and the derivatives of the Gibbs energy with respect to the composition variables. However the calculations become difficult when the number of components is increased. Therefore a method, called "Direct Minimization of Gibbs energy of mixing",[4,22] was developed where only ΔG is required, but not the derivatives. This method can be applied to any equation for the Gibbs energy and any number of components.

Calculation of spinodal lines

The calculation procedure of the spinodal line in binary systems is demonstrated in the scheme of Figure 3 where ΔG is plotted as a function of the volume fraction. For the calculation the composition axis, in the actual case the volume fraction, is divided into n points. For each of these points it is checked whether the system is unstable or not. The distance from one point to the next, the accuracy with which the spinodal line can be determined, is therefore 1/n. If the overall value of ΔG for the demixed system, $\Delta G^{o.a.}$ is less than ΔG of the homogeneous system the overall composition lies within the unstable area. This is demonstrated in Figure 3 for the second point of the calculation procedure ($\varphi^{o.a.}$=0.4). If $\Delta G^{o.a.}$ is larger than ΔG the homogeneous mixture is stable, or at least an energy barrier exists for the demixing process, i.e. $\varphi^{o.a.}$ lies in the metastable range (Figure 3, fourth point, $\varphi^{o.a.}$ =0.8). Checking all points yields the entire unstable area, and thus the spinodal line as its boundary.

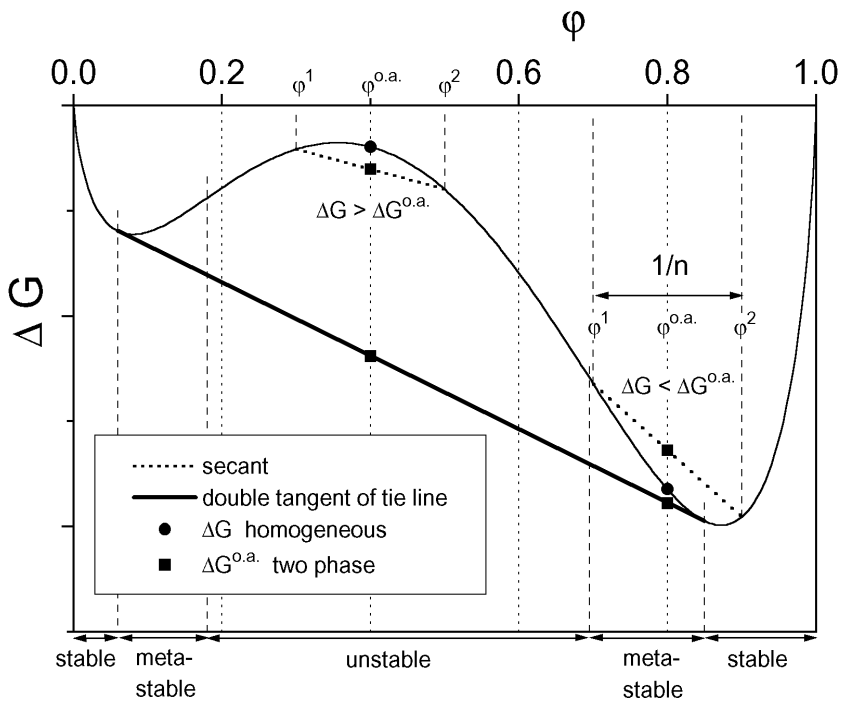

Figure 3. The Gibbs energy of mixing as a function of the volume fraction. The secants demonstrate how the overall value for a demixed system $\Delta G^{o.a.}$ can be read from the graph (Ref.[4]).

Calculation of tie lines and binodal lines

A system is at equilibrium for a given pressure and temperature when its ΔG becomes minimum. So a system demixes when the overall energy $\Delta G^{o.a.}$ of the demixed system is less than ΔG of the homogeneous mixture. This is demonstrated for a binary system in the scheme of Figure 3. The secant determining the tie line is the secant for which $\Delta G^{o.a.}$ for a given $\varphi^{o.a.}$ is minimum. This secant is also a double tangent to $\Delta G(\varphi)$.

2.2 Fractionation

For many pharmaceutical and technical applications, non-uniformity of polymer is often disturbing or harmful.[23,24] Also for the basic research, the availability of narrow-distributed polymers is necessary in order to make the correct interpretation from results of measurement, if it concerns to the influence of the molecular weight on the measurement (for example, viscosity[25-27] and interfacial tension[28-30]).

Almost all the polymers cannot be manufactured or got with a low polydispersity. If a polymer with a narrow molecular weight distribution is needed, there is therefore usually no other alternative to proceed but fractionate these broad-distributed sample. Exceptions here are polymers, which can be synthesized by living anion[31-34] or radical[35,36] polymerization. Most of these polymers possess a narrow polydispersity due to the absence of abort and transmission reactions.

Useful fractionation procedures for low-molecular materials are often not applicable for polymer. On the one hand polymers are not volatile. A distillate separation is not possible therefore. On the other hand the separation by different melting points, often cannot be used since the few polymer crystallize. The only way is via polymer solutions. There are different methods for analytic purposes, which are based on different separation principles. Examples are the HPLC(high performance liquid chromatography, separation due to different reciprocal effect of the polymer with a column filler),[37,38] the GPC(Gel Permeation Chromatography, separation due to different hydrodynamic radii)[39,40] and the FFF(field flow fractionation, separation due to

different migration speed in a field, like for example an electrical field, a shear rate or a transverse flux).[41,42]

For preparative fractionation liquid-liquid extraction is available. The conventional extraction for low-molecular materials cannot be used, however. With this method, a material is extracted from a solution by means of a second solvent which is not mixable with first solution. For polymers this procedure is not suited, since the solution differences for different molecular weights are not sufficient. The entire polymer would be found only in one solvent. The solvent quality of the two phases may differ only slightly, in order to use efficiently smallest difference of the solubility. This is reached with one liquid-liquid separation.

Continuous Spin Fractionation

The Continuous Spin Fractionation (CSF)[43,44] is a large scale fractionation technique to produce narrowly distributed polymers using a starting material with a broad molecular weight distribution. This method is in principle applicable to all soluble polymers. Further requirements are the existence of a non-solvent enabling the realization of liquid/liquid phase separation upon heating or cooling. Two fractions that have a lower nonuniformity than the starting material are achieved with each fractionation step. As a rule of the thumb the non-uniformity $U = (M_w/M_n) - 1$ of the fractions is approximately half of that of the starting material. Narrowly distributed samples can be obtained by applying the CSF repeatedly to the same polymer, using the acquired fraction as starting material for the next step.

CSF is based on the liquid-liquid phase separation. It overcomes some of the disadvantages of its precursor method, namely the Continuous Polymer Fractionation.[45-47] The most outstanding advantage lies in the considerably larger polymer concentrations that can be realized and the elimination of damming back, which sometimes constitutes a problem with extraction columns. Both methods rest on the fractionation that takes place if a homogenous polymer solution demixes into a polymer rich phase (called gel) and a polymer lean phase (called sol) due to a change in the solvent power. Such a phase separation can be achieved either through a change in temperature or in composition (see Figure 4). This process leads to an enriched of the

long chain material of an initially broadly distributed polymer in the gel phase because of enthalpic reasons, while the low molecular weight material accumulates in the sol phase due to entropic reasons. As a result of this fractionation the compositions of the gel and of the sol phase do not lie on the cloud point curve of the starting material.

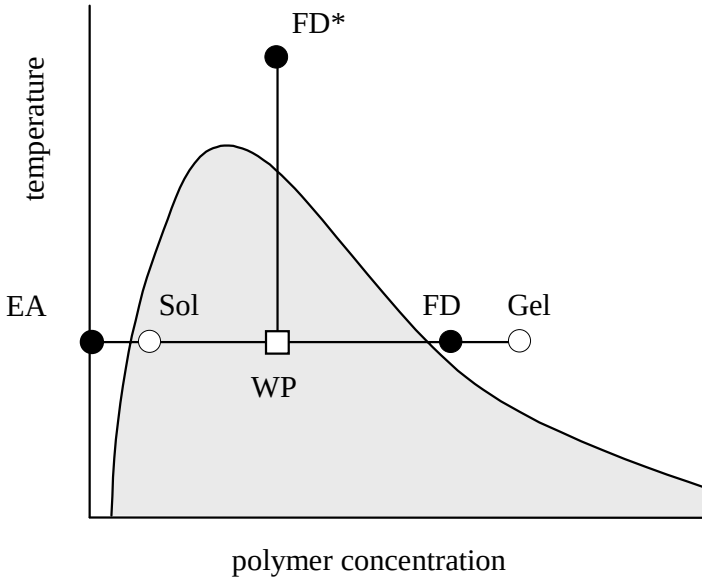

Figure 4. Schematic phase diagram for a polymer/solvent system that can be used for fractionation. The temperature/composition area within which demixing takes place is shaded. The cloud point curve (full line) states the temperatures at which homogeneous solutions segregate the first droplet of a second phase upon cooling. FD stands for feed, EA for extracting agent and WP for working point (over-all composition of a given experiment). The state of WP can either be achieved by mixing FD and EA by constant temperature or by keeping the composition of FD* constant and reducing the temperature. Due to polymer fractionation the points representing the coexisting polymer lean phase (sol) and polymer rich phase (gel) do not fall on the cloud point curve (Ref.[44]).

Even though phase separation can already be realized with a binary system, by either changing the temperature at constant composition or by mixing a polymer solution (called feed, FD) with the solvent (extracting agent, EA) in an appropriate ratio at a constant temperature, ternary systems are much more practical. In this case the single solvent is replaced by a mixed solvent system consisting of a solvent and a non-solvent component. This additional degree of freedom provides considerably more opportunities to find convenient working conditions. In all cases FD and EA are mixed in such a way that the obtained overall composition (working point, WP) lies inside the miscibility gap and that the system therefore demixes into gel and sol (as shown in Figure 5)

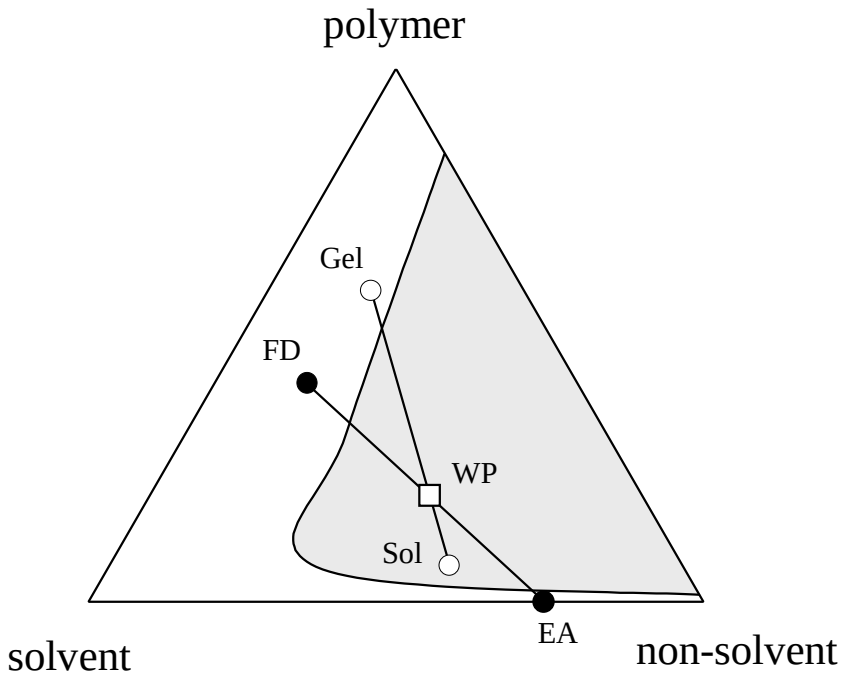

Figure 5. Schematic isothermal phase diagram of a ternary system used for CSF. The two phase area is shaded and the abbreviations are the same as in Figure 1. The solvent is completely miscible with the polymer and with the nonsolvent, whereas a miscibility gap exists between polymer and non-solvent (Ref.[44]).

With the precursor method of the CPF the mixing is achieved by pumping feed and extracting agent into a thermostated glass column. The desired overall composition is reached inside the column and due to differences in their densities, gel and sol separate. One of the drawbacks of this method lies in the limitation to low polymer concentrations of the feed. For high concentrations the viscosity of the feed reduces the mobility of the polymer chains contained in the small droplets of the source phase to such an extent that no equilibrium is reached when the droplets reached the bottom of the column. This implies that short chain material is retained in the gel phase and the fractionation efficiency becomes poor. In principle this problem can be solved by means of filling the column with carrier material (e.g. glass beads) to increase the residence time. However, this procedure increases the probability of damming back dramatically.

CSF overcomes these drawbacks by using ordinary spinning nozzles, like they are used in the fiber industry. The feed is pressed through it to produce a large number (one spinning nozzle has about 1000 holes) of very thin threads with diameters in the range of 60-100 micrometers. Because of the Rayleigh instability[48-50] these threads break immediately up into tinny droplets of typically 50 μm in diameter with a high surface to

volume ratio. Due to the short transport distances the easier soluble component can leave the droplets much faster and equilibrium conditions are reached. For that reason the CSF apparatus is constructed somewhat differently as compared with CPF. It mainly consists of a mixing vessel into which the extracting agent is pumped freely and the feed through a spinning nozzle. From this container the mixture is continuously transported into a device that allows macroscopic phase separation. In the simplest case this is again a column in which the phases separate due to their difference in density. In case of too similar densities of the coexisting phases one can successfully use continuously working centrifuges. CSF setup is shown in Figure 6.

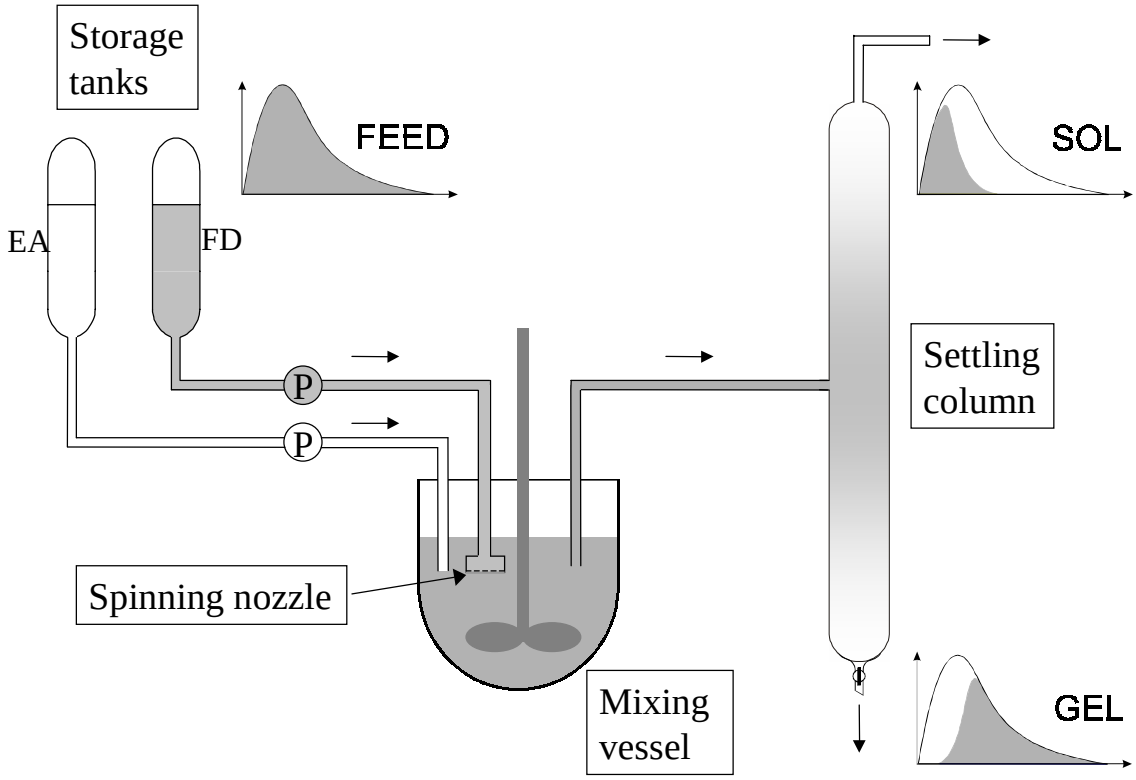

Figure 6. Scheme of a typical apparatus suitable for CSF. Feed and extracting agent are transported by means of two precision pumps at the rate required to realize the desired working point (cf. Figures 4 and 5) and the feed is spun through a spinning nozzle into a vigorously stirred vessel. The two phase mixture produced in this manner flows freely into a column where one phase (normally the polymer rich gel phase) sediments and leaves at the lower end, whereas the other phase (normally the polymer lean sol phase) exits at the upper end. The differential molecular weight distributions of the initial polymer and the two obtained fractions are depicted in the inserts. (Ref.[44])

Even with a laboratory scale device of rather low capacity it is possible to reach polymer throughputs in the order of 10-100g/hour. It is obvious that modifications, like the use of more spinning nozzles and a centrifugal separator to detach sol and gel, make very large fractions accessible.

2.3 Thermal Diffusion

The Ludwig-Soret effect, also called thermal diffusion, concerns the mass flows of fluid mixtures, which are induced by a temperature gradient.[51-53] The Soret coefficient characterizes the magnitude of the effect. For steady state conditions and binary mixtures the Soret coefficient, S_T, is defined as

$$S_T = -\frac{1}{w_0\left(1-w_0\right)}\frac{\nabla w}{\nabla T} \tag{47}$$

where w is the mass fraction of component 1, w_0 means its equilibrium value, and ∇ indicates the gradient.[54,55] The Soret coefficient of component 1 in Eq. 47 has a positive sign when component 1 migrates to the cold side.[54] The Soret coefficient can also be expressed as

$$S_T = \left(D_T / D\right) \tag{48}$$

where D_T is the thermal diffusion coefficient and D is the ordinary translational diffusion coefficient.[56]

The interpretation of TDFRS signals for the ternary system of polymer in the mixed solvent has already been reported in detail.[55] Briefly, the normalized heterodyne signal intensity ζ_{het} of the read out laser for binary mixtures is expressed as

$$\zeta_{het} = 1-e^{-t/\tau_{th}} - \frac{\left(\partial n/\partial w_1\right)_{P,T}}{\left(\partial n/\partial T\right)_{P,w_1}} w_{10}\left(1-w_{10}\right)\times S_T\left(1-e^{-q^2Dt}\right) \tag{49}$$

where τ_{th} is the time constant of the temperature grating, n is the index of refraction, P is the pressure, w_1 is the mass fraction of component 1, w_{10} its equilibrium value, q is the wave vector, $q = (4\pi\nu/\lambda_0)\sin(\theta/2)$. For ternary mixtures,

$$\zeta_{het} = 1 - e^{-t/\tau_{th}} - \frac{\left(\partial n / \partial w_1\right)_{P,T,w_2}}{\left(\partial n / \partial T\right)_{P,w_1,w_2}} w_{10}\left(1 - w_{10}\right) \times S_{1T}\left(1 - e^{-q^2 D_{11} t}\right) - \frac{\left(\partial n / \partial w_2\right)_{P,T,w_1}}{\left(\partial n / \partial T\right)_{P,w_1,w_2}} w_{20}\left(1 - w_{20}\right) \times S_{2T}\left(1 - e^{-q^2 D_{22} t}\right) \tag{50}$$

where w_k and w_{k0} are the mass fraction of component k and its equilibrium value, respectively, and D_{11} and D_{22} are diagonal elements of the matrix of diffusion coefficients.

Eqs. 49 and 50 imply that a single diffusive process is expressed with the time constant $\tau = 1/(q^2 D)$ for binary mixtures, while two diffusive processes are expected with time constants $\tau_1 = 1/(q^2 D_{11})$ and $\tau_2 = 1/(q^2 D_{22})$ for the ternary system of a polymer in mixed solvent. The experiments for dextran in urea/water showed a two-mode decay behavior (see Sec. Appendix) with time constants on the order of 10^{-3} s as the faster process associating with solvent diffusion and 10^{-1} s as the slower process corresponding to the polymer diffusion. These typical time constants of the diffusive processes were well separated on the time scale of the experiment. In analogy to binary mixtures, cf. Eq. 47, the Soret coefficients, S_{kT}, for each process are defined as[55]

$$S_{kT} \equiv -\frac{1}{w_{k0}\left(1 - w_{k0}\right)} \frac{\nabla w_k}{\nabla T} \tag{51}$$

3 Experiment

3.1 Material

3.1.1 Dextran

Dextran is a water soluble polysaccharide, used extensively in medical science,[57] flocculation,[58] pharmaceutical[59] and agricultural[60] industries. It is mainly composed of α–*D*–(1$\rightarrow$6) linked glucose units and some short α–*D*–(1$\rightarrow$3) -linked glucose branch units.(Figure 7) All known dextrans are branched at different branching points and to different extents. Differences in the three-dimensional structures of different dextrans are due to the percentage and manner in which the branches are arranged.

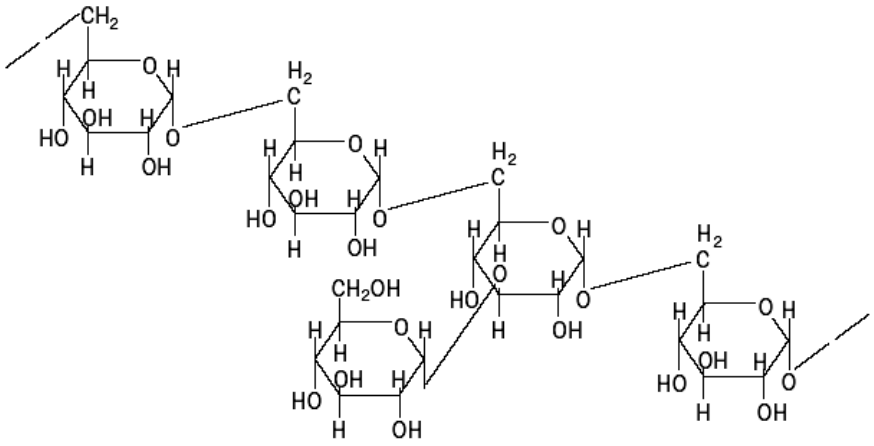

Figure 7. Structure of dextran molecule.

Dextran aqueous concentrated solution is known to segregate crystals (precipitation).[61] This crystallization is considered to be due to hydrogen bonds and they are easily broken by DMSO or boiling for 1 or 2 hours.

In this study three different dextrans, Dx10k, Dx70k, Dx10000k were donated from Polymer Standard Service GmbH (Mainz, Germany). For the determination of the phase diagram of the ternary system water/dextran/BSA measured by Yurij Antonov, Dx2000k was used. Dx2000k was purchased from Amersham Pharmacia Biotech AB (Uppsala, Sweden) and the weight and number average molecular weight, reported by the manufacturer, is 2100kg/mol and 300kg/mol respectively.

3.1.2 BSA

Bovine serum albumin (BSA) is a water soluble protein and it is a globular molecule. The molecular weight is 66kg /mol[62] based on amino acid sequence information. BSA is a single polypeptide chain consisting of about 583 amino acid residues and no carbohydrates. At pH5-7, it contains 17 intrachaindisulfide bridges and 1 sulfhydryl group.[62,63] It is used extensively in food[64] and pharmceutical[65] industries. Physical properties from literature are listed in Table I.

Table I. Physical Properties of BSA

pH of 1% Solution[63]		5.2-7
Stokes Radius[66]	(r_s)	3.48nm
Diffusion constant[63]	$D_{20,w} \times 10^7$	5.9
Partial specific constant[63]	V_{20}	0.733
Intrinsic viscosity[63]	η	0.0413
Refractive index increment[63]	(578nm) x 10^{-3}	1.90
Estimated -α-helix[63]	%	54
Estimated -β-form[63]	%	18

The BSA Fraction V , pH 5 (Lot A018080301) was obtained from the Across Organics (New Jersey, USA). Protein content ≅ 98-99%, Trace analysis: Na <5000 ppm, CI <3000 ppm, no fat acids were detected. The isoelectric point of the protein is about 4.8-5.0,[67] radius of gyration at pH 5.3 is equal to 30.6 A.[67]

3.1.3 Other chemicals

Deionized water was used for all the experiments. Methanol (MeOH), acetone (AC), iso-propanol (iPOH), ethanol (EtOH), tetra-hydrofuran (THF), acetic acid (AA), and dimethyl-acetamid (DMAC), puriss. quality from Fluka, served as precipitant for dextran without further purification.

3.2 Methods

3.2.1 Gel Permeation Chromatography (GPC)

These experiments were carried out in aqueous solutions (containing 8.5 g $NaNO_3$ and 4.2 g $NaHCO_3$ per liter) using the columns HEMA BIO 40, HEMA BIO 1000, SUPREMA 300, supplied by PSS (Polymer Standard Service, Germany) for GPC-measurements at room temperature. The differential refractometer Gynkotek RI-71 was employed as detector and dextran standards (PSS) served for calibration. The molar masses resulting for dextran from GPC were obtained by means of universal calibration using the following Kuhn-Mark-Houwink parameters for pure water: $K_{Dextran}$ = 0.0978 mL/g, $a_{Dextran}$ = 0.5.[68] Because of the fact that the eluent contains salt, the obtained molar masses are only apparent values, as indicated by asterisks.

3.2.2 Light Scattering (LS)

Static light scattering (SLS) measurements were performed in water at 25 °C with a modified (SLS, G. Baur, Freiburg, Germany) static light scattering apparatus Fica 50 (Sofica, Paris) using a laser (wavelength λ = 632 nm) and measuring at angles 20° < θ < 145°. Dynamic light scattering (DLS) was carried out in the angular range 25° < θ < 150°. Kr-ion laser was used as the light source (wavelength λ = 647.1 nm). ALV-5000E correlator was used to measure the correlation function of scattered light.

Polymer solutions in the range of 0.2 to 1 g/mL for SLS and 1, 3 and 6 g/mL for DLS were prepared and filtered through a 0.45 μm membrane filter (Millipore) directly into the thoroughly cleaned optical cells (Hellma, Müllheim, Germany) and thermo-stated in the light scattering apparatus for 15 min. The refractive index increments (dn/dc) at 25 °C was measured as 0.1358 mL/g.

The absolute Rayleigh ratio R, the excess intensity of scattered light corrected with the instrument constant, is expressed as

$$\frac{Kc}{R(q)} = \frac{1}{M_w P(q)} + 2A_2 c \tag{52}$$

where K is the optical constant ($K = 4\pi^2 n^2 (\partial n/\partial C)^2/(N_A \lambda_0^4)$ = 13.3 x 10^{-6} cm^2 g^{-2} mol). c, A_2, and $P(q)$ are the concentration of polymer in g cm^{-3}, second virial coefficient, and particle scattering factor, respectively. q is the wave vector, $q = (4\pi n/\lambda_0)\sin(\theta/2)$. $P(q)$ depends on the dimension of polymer and is related to the radius of gyration R_g as

$$\frac{1}{P(q)} = 1 - \frac{1}{3} q^2 \left\langle R_g^2 \right\rangle + \cdots. \tag{53}$$

The autocorrelation function of the scattered light intensity $g^{(2)}(q, t)$ is related to the normalized field correlation function $g^{(1)}(q, t)$ by

$$g^{(2)}(q,t) = B\,(1 + \beta \left| g^{(1)}(q,t) \right|^2) \tag{54}$$

where B and β are the base line and a constant relating to the coherence of detection, respectively. The measured correlation functions were analyzed by the cumulant method to obtain the average decay rates Γ,

$$\ln \left| g^{(1)}(t) \right| = -\Gamma t + \frac{\mu_2}{2!} t^2 - \frac{\mu_3}{3!} t^3 + \cdots, \tag{55}$$

where μ_i is the ith cumulant and μ_2 / Γ^2 gives the normalized dispersion of distribution of Γ. If the fluctuation of the scattering light intensity is due to the translational diffusion of the polymer chains, the decay rate has the form

$$\Gamma / q^2 = D_0 \left(1 + k_d c + \cdots\right). \tag{56}$$

Here D_0 is the translational diffusion coefficient at infinite dilution and k_d is a constant for the effect of polymer concentration. The hydrodynamic radius R_h is related to D_0 by the Stokes-Einstein equation, $R_h = k_B T/(6\pi\eta D_0)$, where k_B is Boltzmann's constant and η denotes the solvent viscosity.

3.2.3 Differential Scanning Calorimetry (DSC)

The crystallinity and thermal behavior of original and crystallized dextran were obtained by differential scanning calorimetry (DSC). Crystallized samples were prepared in the same way as the samples for vapor pressure measurements(cf. 3.4.1). The thus prepared samples were kept for 6 months at room temperature.

DSC measurements were carried out under nitrogen with a heating rate 5 ^{o}C/min on a Mettler DS TA 3000 instrument. DSC runs were carried out from –65 up to 200 ^{o}C in order to cover the whole range of the glass-to-melt transition. The glass transition temperature (T_g) were taken as the onset temperature of the glass transition. The crystallization temperature (T_{cr}) and melting temperature (T_m) were determined as the peak values of the corresponding exo- and endo-thermic phenomena.

3.2.4 Thermogravimetric Analysis (TGA)

Thermal stabilities of the original dextran were investigated by thermogravimetric analysis (TGA) with a Mettler TG-50. The samples were heated with a rate of 10K min^{-1} from room temperature to 800 ^{o}C under an inert atmosphere.

3.2.5 Turbidimetry and Phase Analysis

The way to determine phase diagram is described in detail elsewhere.[69] Cloud points were detected turbidimetrically by titrating homogeneous polymer solutions in an automated manner with the non-solvent, using equipment described earlier.[70] The critical polymer concentration was determined by means of phase volume ratios.[71] In order to obtain tie lines we have pressed homogenous polymer solution through a spinning nozzle into the extracting agent in such a manner, that the resulting over all composition lies within the miscibility gap and demixing into two liquid-liquid phases takes place. After macroscopic separation the coexisting phases were detached and analyzed with respect to their composition. To this end we collected the volatile components in a cooling trap and determined the composition of this mixture by means of refractometry. The remaining polymer was weighted.

3.2.6 Headspace Sampling –Gaschromatography (HS-GC)

Vapor pressure measurements were performed at 25^{o}C for the systems water/Dx70k, water/10000k and water/BSA. As Dx10k does not make a film, the measurements were not performed for the system water/Dx10k.

Sample Preparation

The measuring cell consists of a glass tube of 10 cm length with an inner diameter of 1 cm and a wall thickness of 0.5 cm (Schott, Mainz, Germany). The tube is held by metal fittings and sealed by Teflon backings. The glass tubes can withstands pressures up to 10 bar. Valves and connecting metal capillaries were purchased from SITEC (Sieber Engineering AG, Switzerland); the fine valve enables a reproducible adjustment of the opening.

In order to achieve phase equilibria within reasonable time, the bulk polymer was not filled into the measuring cell, but thin films were prepared (typically 0.005 to 0.02 mm thick) on glass beads of 4 mm diameter, instead. To this end the cell was charged

with the bare beads and sealed on both ends by means of metal grids to keep them in place. Using sufficiently viscous solutions (20 wt.% of the polymer in water) the voids between the spheres can be filled without seeping. In this manner the solution was evenly distributed to cover all beads and the cell was loaded with the required amount of polymer. After that the major part of solvent was removed at room temperature by applying vacuum. The amount of deposited polymer (typically some 200 mg) was calculated from the weight gain of the cell.

After drying completely, water was absorbed to the polymer film by adsorbing water vapor to be the polymer concentration from 97 wt% to 80 wt% and by dropping liquid water from 70 wt% to 40 wt%. These polymer solutions were kept at 25 ^{o}C to reach the equilibrium. In order to know whether the polymer solutions were in equilibrium or not, the measurements were performed 1 day, 1 week and 3 weeks after the sample preparation (see. Figure 8).

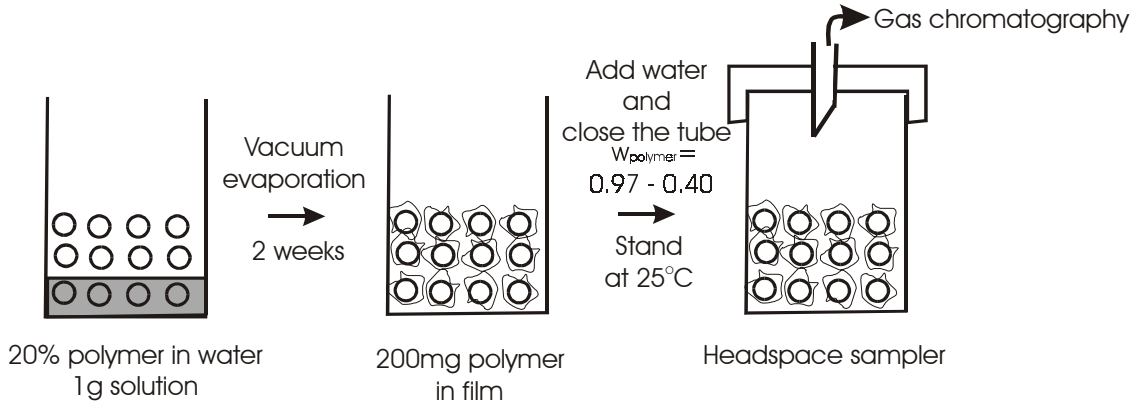

Figure 8. Procedure of the sample preparation for HS-GC.

Headspace Sampling-Gaschromatography (HS-GC)

The combination of headspace sampling and gas chromatography for the determination of vapor pressures is already described in detail.[72,73] The measurements were performed at 25 °C using a pneumatically driven thermostatted head-space sampler (Dani HSS 3950, Milano, Italy) which takes 50 μL of the equilibrium gas phase and injects this mixture of solvent and air into a gas chromatograph (Shimadzu GC 14B, Kyoto, Japan). The amount of solvent contained in the sample volume – being proportional to the vapor pressure – is detected by a thermal conductivity detector and registered by means of an integrator (Shimadzu, Chromatopac C-R6A). The capillary column AT-WAX (Alltech Associates Inc., Deerfield, USA) had a length of 15 m, a diameter of 0.53 mm and a film thickness of 2.5 μm. In order to obtain reliable equilibrium data we have applied the method of Multiple Head-Space Extraction (MHSE).[74-76]

4 Results and Discussion

4.1 Gel Permeation Chromatography of Dextran

Gel Permeation Chromatography (GPC) was applied for dextran samples. The results are shown in Figure 9 and Table II .

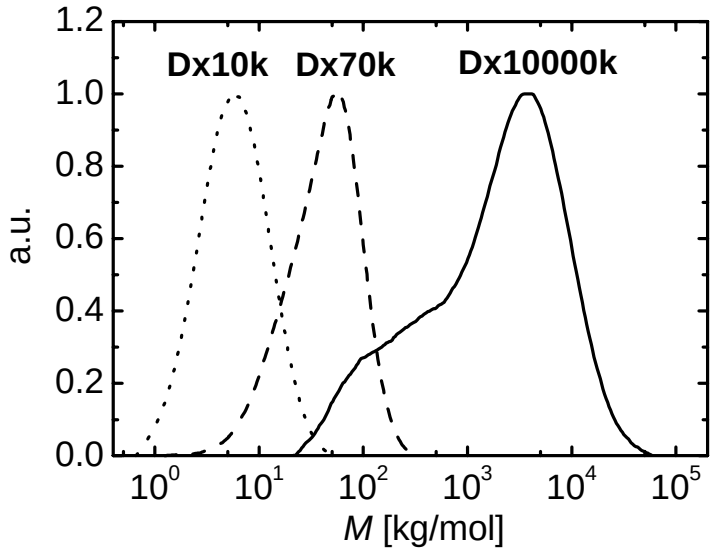

Figure 9. Molecular weight distributions of the original dextran samples normalized to the same height.

Table II. Molecular weights and non-uniformities of the original dextran samples.

	Mw kg/mol	*Mn* kg/mol	Non-Uniformity U=*Mw*/*Mn* -1
Dx10k	11.1	5.5	1.0
Dx70k	59.5	27.8	1.1
Dx10000k	3420	395	7.7

4.2 Densities of the Polymers

Dextran

Densities (ρ) of Dx70k and Dx10000k were determined at 25 ^{o}C by a picnometer. As Dx10k does not form into films, it was not possible to determine the density using this method. The results of these measurements are shown in Figure 10. The results from literature[77] are also shown. The trendline is determined as ρ [g/mL] = 0.890 * EXP (-10^2/*Mn*/1.416) +1.306. The molecular weight scales proportionally to the density. The experimental results agree with reported values; however, the errors are large. For this reason the literature values are used for further experimentation: 1.306g/mL for Dx10k, 1.376g/mL for Dx70k, 2.009g/mL for Dx2000k and 2.050g/mL for Dx10000k.

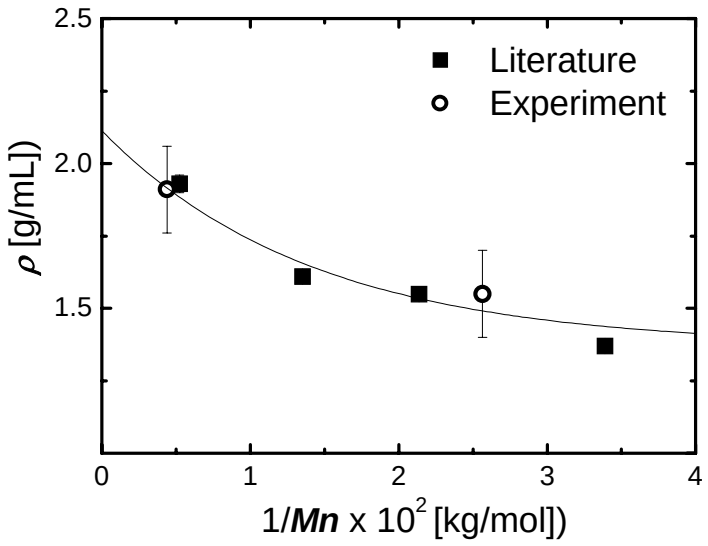

Figure 10. Densities of the dextran samples plotted as a function of 1/*Mn*. The closed squares are given in literature[77] and the open circles are from own picnometer measurements conducted at 25 ^{o}C. A exponental fit of the literature data is also presented.

BSA

The density of BSA was determined by the method previously described which was applied to dextran. The density was found to be 1.31 +/- 0.07 g/mL.

4.3 Light Scattering of the Polymer Solutions

Dx70k

Static Light Scattering (SLS) and Dynamic Light Scattering (DLS) experiments were performed for Dx70k at 25 ^{o}C using water as the solvent; dn/dc was determined as 0.1358 mL/g. Figure 11 shows the Zimm Plot obtained for the system Dx70k/H_2O, the concentrations range from 2g/L to 12g/L. The following results were obtained from the Zimm plot: M_W = 161 kg/mol, A_2 = 2.590 x 10^{-4} (cm^3 mol/g^2) and Rg = 72 nm.

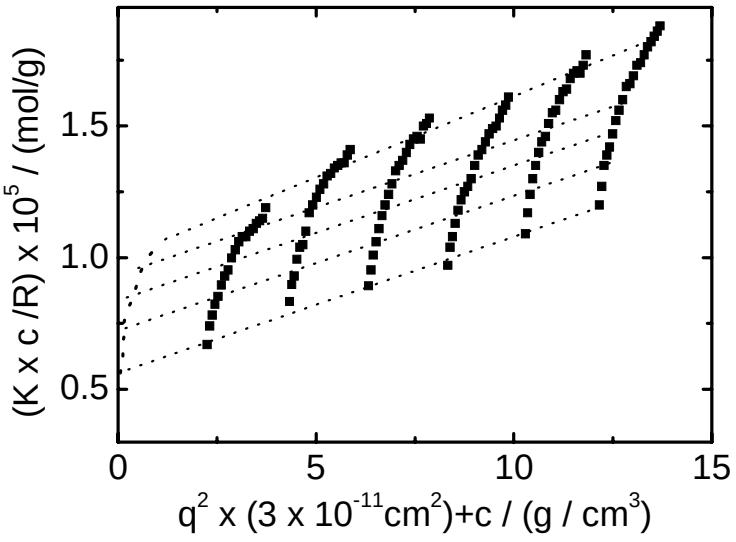

Figure 11. Zimm plot for aqueous solutions of Dx70k at 25 **^{o}C**.

Figure 12 shows the result from DLS of Dx70k/ H_2O at 1 g/L, 3 g/L and 6 g/L. For all concentrations one observes a peak at R_h = 6.6 nm. But peaks at larger R_h appear with increasing concentration. This means dextran molecules aggregate at higher concentrations (c>3 g/L). That is the reason why M_W and Rg obtained from SLS (measurement were done at 2.0 g/L < c < 12 g/L) are so large. A_2 values reported in literature, where SLS was done at sufficiently high dilution 0.5 g/L < c < 2.0 g/L[78] and 0.5 g/L < c < 5.0 g/L [79,80], are used for the following data analysis (Table III).

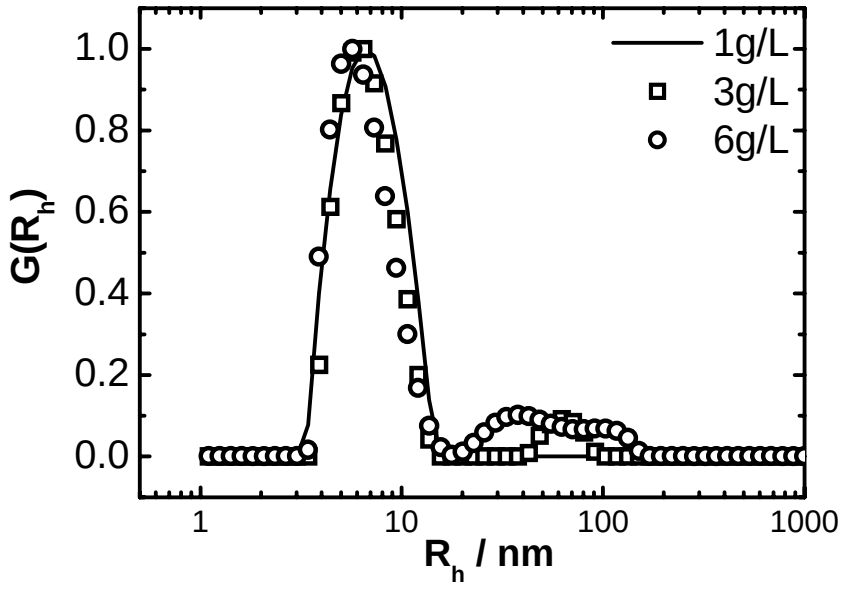

Figure 12. $G(R_h)$ vs R_h obtained by DLS.

Table III. Light scattering data from literature. (a [78] b [79])

Mw Kg/mol	dn/dc mL/g	Non Uniformity U=*Mn*/*Mw* -1	R_g nm	R_h nm	A_2 10^{-4} (cm^3 mol/g^2)
9.0[b]	0.151			3.0	7.5
37[b]	0.151			5.0	4.2
59[b]	0.151		-1	10.0	4.56
80[a]	0.148	0.3-0.6	8.6	6.4	7.14
132[b]	0.151		12.0	11.0	3.28
334[b]	0.151		19.0	15.0	2.02
400[a]	0.148	0.3-0.6	16.4	12.9	1.88
506[b]	0.151		21.0	17.0	1.76
2000[a]	0.148	0.3-0.6	33.6	27.5	0.74
2660[b]	0.151		47.0	11.0	0.54
7400 [a]	0.148	0.3-0.6	56.5	48.3	0.29

BSA

SLS data for BSA were taken from the literature.[81,82] The plot of K^*c/R_θ as a function of concentration is curved. At high dilution A_2 is found to be -1.47×10^3 cm^3 mol/g^2 (Figure 13).

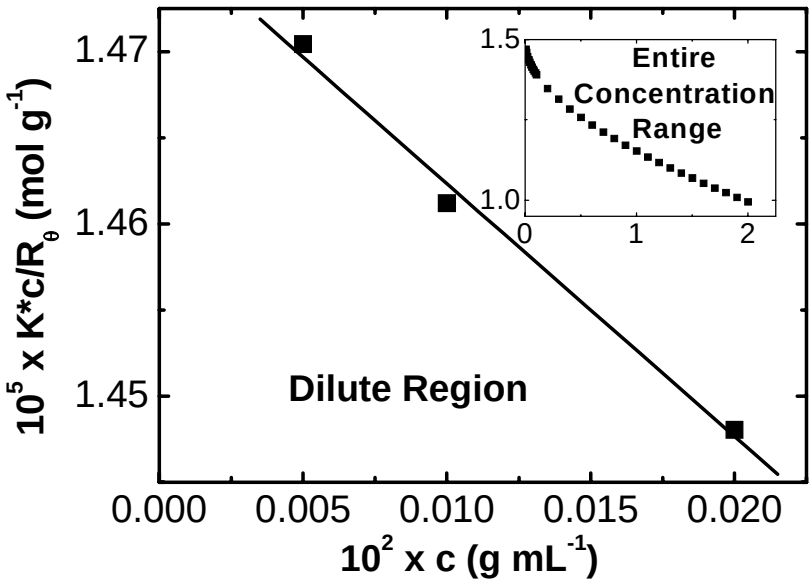

Figure 13. Light scattering data for solutions of BSA at its isoelectric point in deionized water in dilute region. The inset gives the data in the entire concentration range.[81,82]

4.4 Crystallization of Dextran

In highly concentrated solution (ca. 20 – 80 wt%) dextran precipitates into crystals, which are insoluble in water.[61] The influence of molecular weight on crystallization was observed visually for aqueous solutions of Dx10k, Dx70k and Dx10000k at $w_{dextran} = 0.3$. Dx10k, Dx70k and Dx10000k started to crystallize from the solutions 1 day, 4 days and 1 week after the solution preparation, respectively. The smaller the molecular weight is, the faster the crystallization begins.

In order to investigate the influence of polymer concentration on crystallization, water was absorbed into dextran films (Dx70k and Dx10000k) deposited on glass beads until constant water content from $w_{dextran}$=0.4 to $w_{dextran}$=1.0 as controlled by weighing (The procedure of the film preparation is described in 3.4.1 in detail). Ten concentrations of the solutions for each polymer were prepared and kept for six months.

After this period, Dx70k crystallized for concentrations between w_{Dx70k}=0.4 to w_{Dx70k}=0.85; the corresponding data for Dx10000k are $w_{Dx10000k}$=0.4 to $w_{Dx10000k}$=0.8. This indicates that crystallization occurs up to higher dextran concentration for shorter chains. Generally, it can be stated that lower molecular weight dextran crystallizes easier than higher molecular weight dextran. Literature reports[61] that the crystals are dissolved again in water by boiling for one to two hours, were confirmed experimentally.

Differential Scanning Calorimetry (DSC) was used to investigate the influence of polymer concentration on the crystallization of dextran (Dx70k) from solution in more detail. Four concentrations out of the ten concentrations of Dx70k solutions mentioned above were chosen for this purpose. For easier understanding, the experimental procedure is visualized in Figure 14. The glass tubes containing the polymer solutions, in Figure 14 these mixtures correspond to the picture (I)-(IV) in third line, stood for 6 months at room temperature to complete crystallization and they were kept in an open container until the weight of the polymer film was constant (about 3 weeks). The dextran samples obtained were taken from the glass beads and measured by DSC.

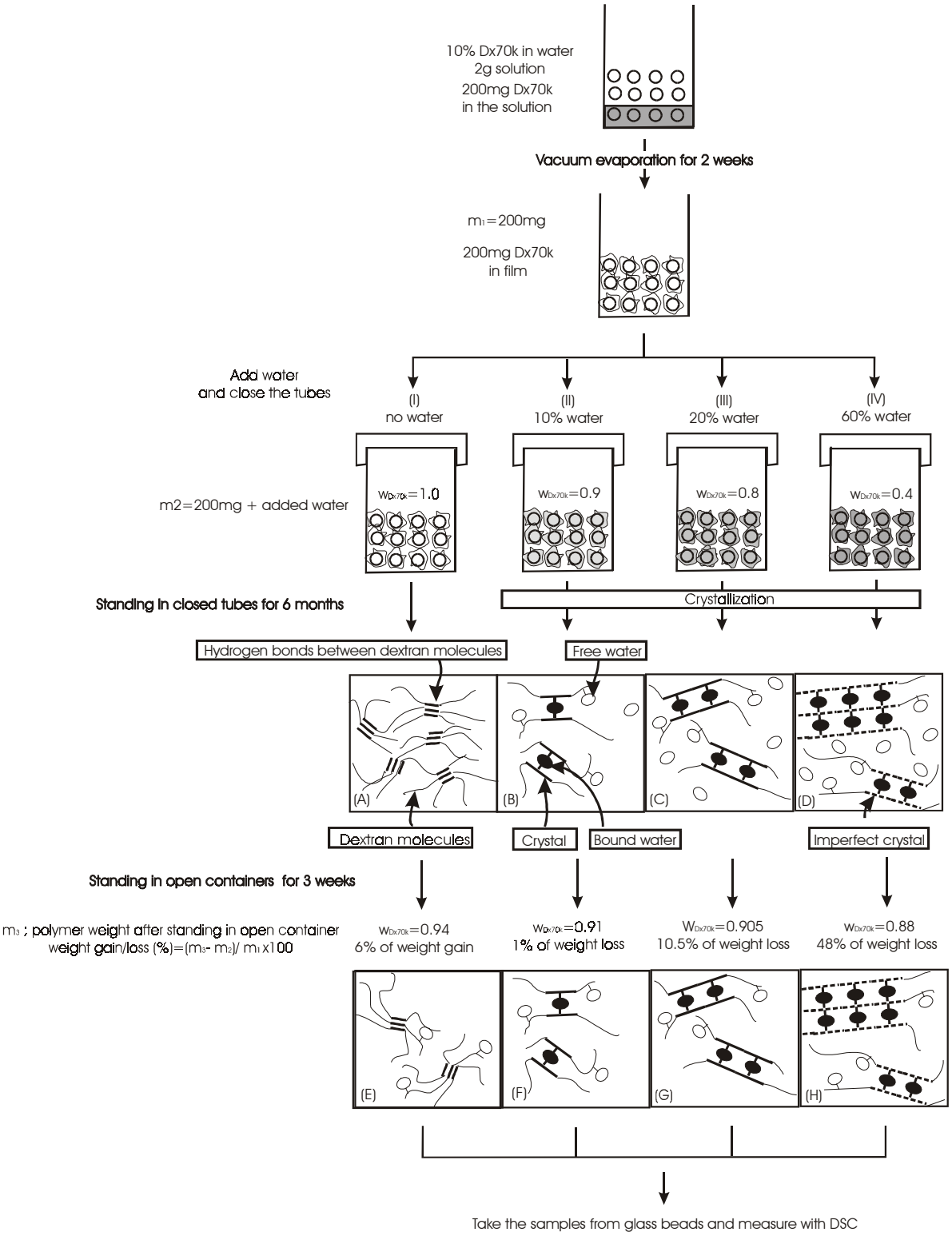

Figure 14. Procedure of sample preparation for DSC and weight changes by the uptake or release of water.

One may tentatively interpret the thermal behavior observed in the DSC measurements in terms of the water content of the solution from which dextran crystals (sketched in third line in Figure 14) are segregated and in terms of water content of the DSC samples of dextran (sketched in the fifth line in Figure 14). As mentioned in the literature,[83,84] the main chain motions of polysaccharides in the dry state are restricted by a large number of hydrogen bonds, which are altered by the addition of water because water acts as "plasticizer". When further water is added into the dextran solution, dextran starts to crystallize. In this case water is considered to be incorporated into the crystals and to exist as "bound (or unfreezing) water".[83]

Based on this interpretation, the state of our samples is considered as follows. After the film preparation via vacuum drying, the samples do not contain water. Many hydrogen bonds exist in dextran molecules as sketched in Figure 14 (A). The weight of polymer is indicated as m_1. As sample (I) is opened and kept in contact with air, it absorbs ca. 6 wt% of water from the atmosphere. Part of the hydrogen bonds between dextran molecules are broken and substituted by hydrogen bonds between dextran and water molecules(Figure 14 (E)). We call this absorbed water "free water" because it can be totally removed by vacuum drying again. The amount of "free water" must depend on the relative humidity of the atmosphere. The sample containing 10 wt% of water and standing for 6 months (w_{Dx70k}=0.9(II)) loses water in open containers just up to w_{Dx70k}=0.91, indicating that ca. 1 wt% of water is removed by evaporation in open containers. Upon a vacuum drying afterwards, only ca. 8.6 wt% of water can be removed. This means ca. 0.4wt% of water interacts with the polymer so strongly that it can not be removed by vacuum drying. Therefore, we call it "bound water". This situation is depicted in Figure 14 (B) and (F). Analogously, samples standing for 6 months at w_{Dx70k}=0.8 (III) and at w_{Dx70k}=0.4 (IV) lose ca. 10.5 wt% and 48 wt% of water in open containers, respectively. The weights of polymer solution during the standing time in closed tubes and after standing in open containers are indicated as m_2 and m_3. If the samples after standing in open containers are subjected to vacuum drying, the weight of sample (I) is m_1, indicating that the sample released ca. 6 wt% of "free water", where the weights of samples (II), (III) and (IV) are ca. 0.4 wt%, 1 wt% and 1.7 wt% more than m_1.(Table IV) This means that the amount of "bound water" increases with water content during the standing time.

Table IV. Estimated state of water contained in DSC samples.

	w_{Dx70k} during the standing time	w_{Dx70k} DSC samples	Total water content ca. (wt%)	Free water content ca. (wt%)	Bound water content ca. (wt%)
(I)	1.0	0.94	6	6	0
(II)	0.9	0.91	9	8.6	0.4
(III)	0.8	0.905	9.5	9.5	1
(IV)	0.4	0.88	12	10.3	1.7

DSC findings are shown in Figure 15 and the glass transition temperature (T_g), the crystallization temperature (T_{cr}), the heat of crystallization (ΔH_{cr}), the melting temperature (T_m) and the heat of melting (ΔH_m) are collected in Table V and Figure 16.

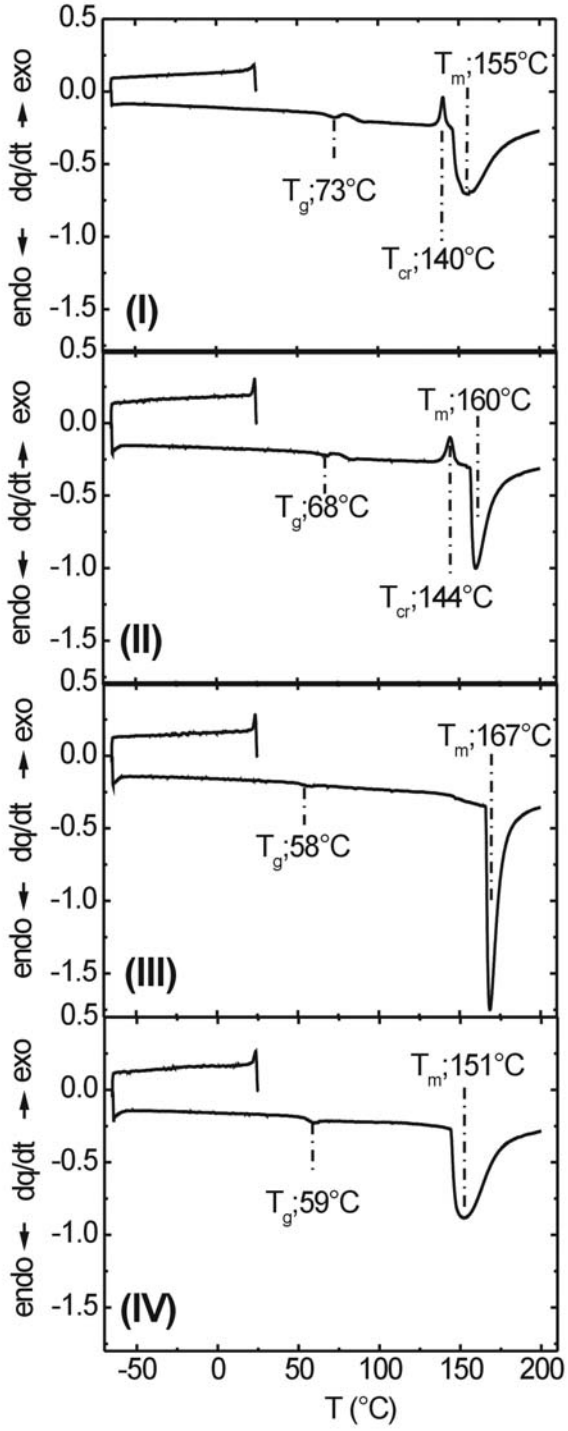

Figure 15. Results of DSC experiments at a heating rate of 5 ^{o}C/min for original and crystallized dextran samples. T_g, T_{cr} and T_m are shown.

Table V. Results from DSC measurements

	w_{Dx70k} during the standing time	w_{Dx70k} DSC samples	T_g (^oC)	T_{cr} (^oC)	ΔH_{cr} (J/g*)	T_m (^oC)	ΔH_m (J/g*)
(I)	1.0	0.94	73	140	-8.4	155	111
(II)	0.9	0.91	68	144	-12.5	160	91
(III)	0.8	0.905	58			167	125
(IV)	0.4	0.88	59			151	148

*per weight of DSC samples

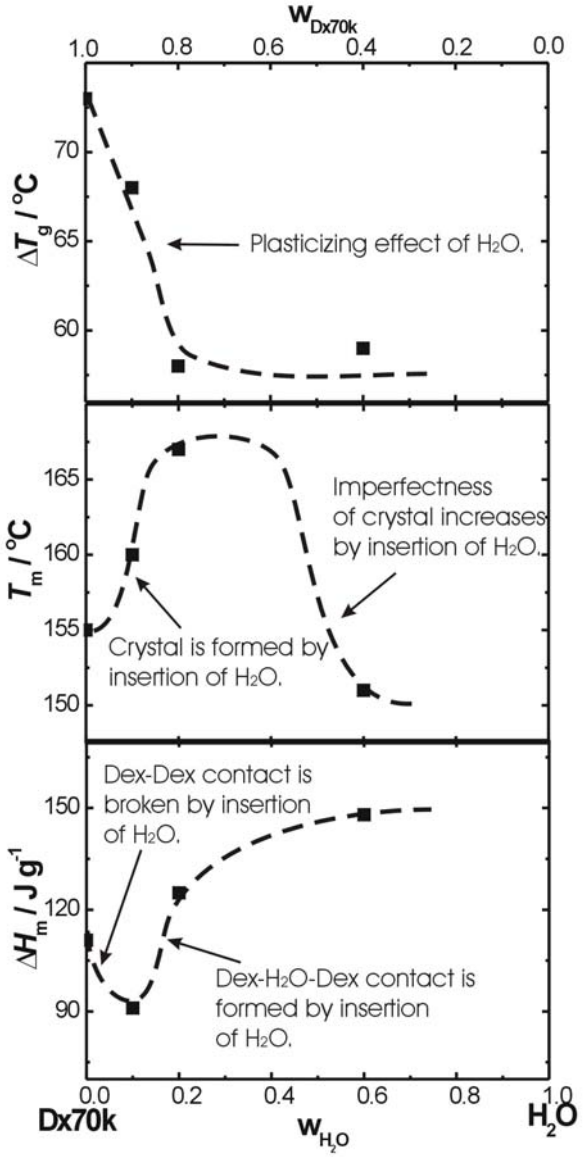

Figure 16. T_g, T_m and ΔH_m as a function of weight fraction of the components during the standing time.

Within the range $0.8<w_{Dx70k}<1.0$, T_g decreases with increasing water content of the solution from which the crystals are segregated during the standing time and within this range, T_m increases, whereas ΔH_m passes a minimum. For the sample standing at $w_{Dx70k}=0.4$, i. e. at much higher dilution, T_g remains the same as at $w_{Dx70k}=0.8$, T_m becomes lower than for $w_{Dx70k}=0.8$ and ΔH_m assumes to be maximum value within this condition.

The behaviors of T_g reflect the amounts of "free water" and "bound water". It is tentatively assumed that the "free water" leads to the reduction of T_g due to its plasticizing effect. As for T_m, within the range $0.8< w_{Dx70k}<1.0$, the higher water content during the standing time leads to a higher mobility of dextran molecules as sketched in Figure 14 (C). The higher mobility of molecules enables the formation of more perfect crystals, which require a higher melting energy, leading to an increase of T_m. A reduction of ΔH_m with increasing water content during the standing time within the range $0.9<w_{Dx70k}<1.0$ is assumed to be due to the fact that rigid hydrogen bonds between dextran molecules are destroyed by water molecules. The observation that T_m becomes much smaller and ΔH_m much larger as dextran concentrations of the solutions from which crystals are segregated falls can be interpreted in following manner. The higher mobility of polymer chains leads to the crystallization of a larger fraction of dextran but to the formation of less perfect crystals.

4.5 Thermal Gravimetric Analysis

Thermal Gravimetric Analysis (TGA) was applied to Dx70k and Dx10000k. Figure 17 shows the results. The thermal decomposition temperatures are determined as 278^{o}C for Dx70k and 264 ^{o}C for Dx10000k. Dx70k contains 15 wt% ash, while Dx10000k contains 23 wt% ash. The reason why Dx10000k decomposes at lower temperature and contains more ash than Dx70k is considered because the impurity of Dx10000k is higher than Dx70k.

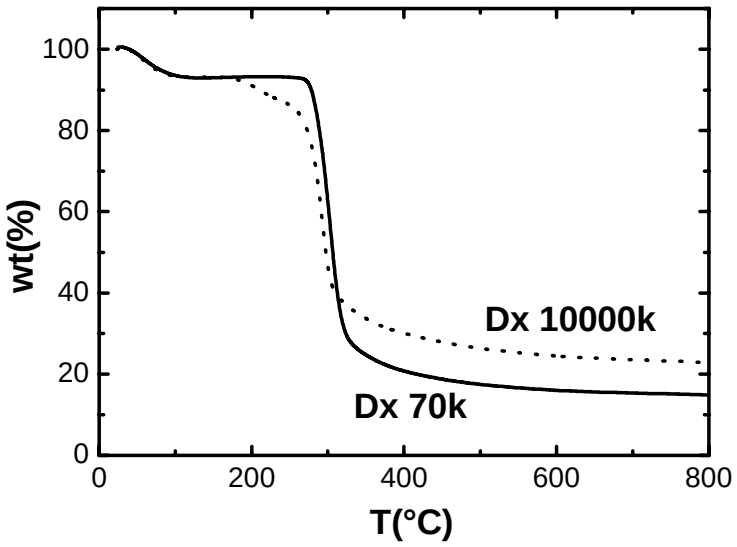

Figure 17. Thermal Gravimetric Analysis results for Dx70k and Dx10000k.

4.6 Measured Phase Diagrams

4.6.1 Solvent / Non Solvent / Dextran

For the fractionation of dextran it is necessary to select suitable solvents and non solvents. The selection of suitable solvents not only depends on the convenience to purify but also on the economics. It is natural to choose water as solvent for both reasons. Figure 18 shows the phase diagram for the ternary system water/different non solvents/Dx70k at 25 ^{o}C. It can be seen that the precipitation strength of the non solvents investigated here is in the order AC > iPOH > EtOH > MeOH > THF > AA > DMAC. So to choose aceton as a non solvent should be the best choice economically as well as environmentally. But as is mentioned in a literature[120], the fractionation efficiency is inversely proportional to the precipitation strength. That is, with too strong non solvents, most of the polymer precipitates in the gel phase and the fractionation efficiency is low. According to orienting fractionation experiments, MeOH is the best non solvent for dextran. Therefore we used it, even if it is poisonous. Figure 19 shows the phase diagrams of water/methanol/Dx70k and water/aceton/Dx70k at 25 ^{o}C for comparison. This diagram contains cloud points, swelling points and critical compositions. For the system water/aceton/Dx70k, some tie lines are also shown.

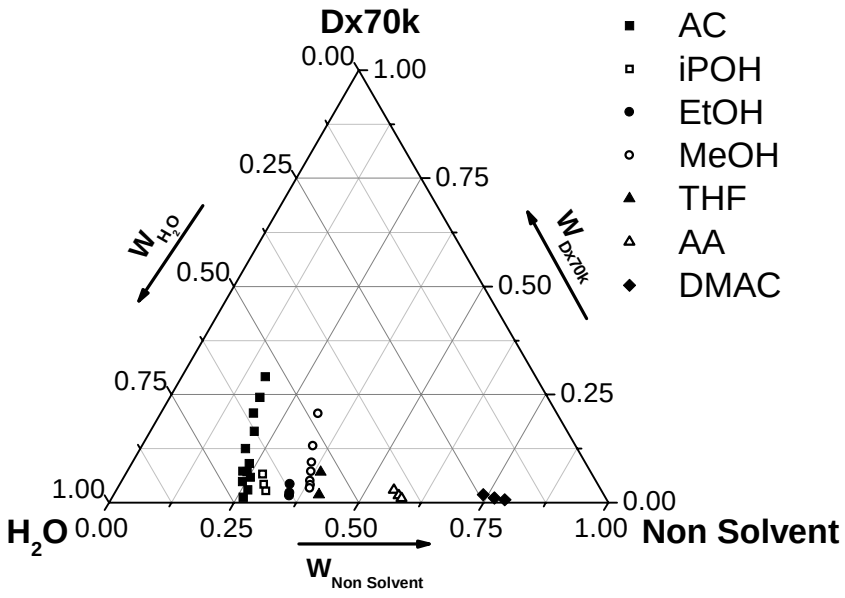

Figure 18. Cloud points of different ternary system water /non solvent/Dx70k at 25 ^{o}C.

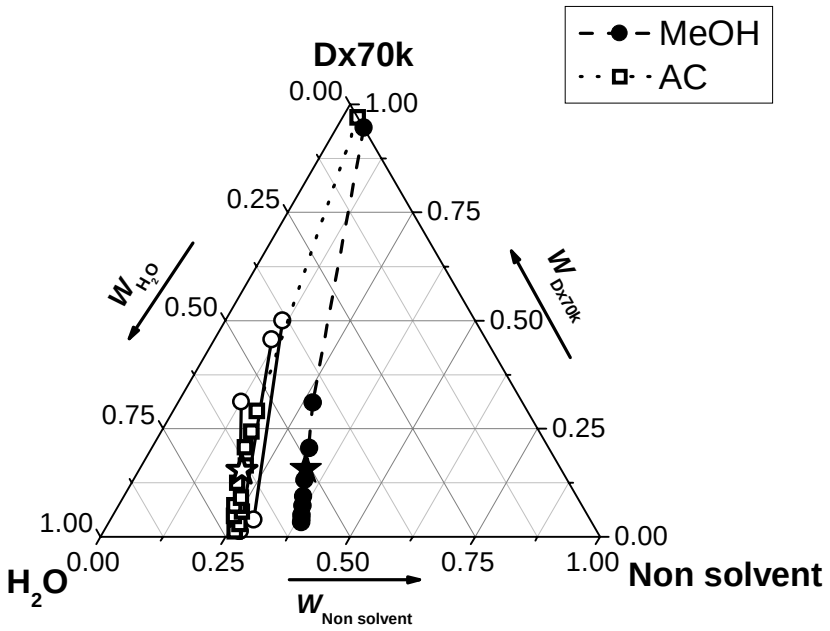

Figure 19. Comparison of the phase diagrams of the systems water/methanol/ Dx70k and water/aceton/Dx70k at 25 °C. Full circles and open squares represent cloud points and swelling points for the system of methanol and aceton, respectively. The full star and the open star are critical points for the non solvent of methanol and aceton. Open circles give the ends of tie lines for the system of aceton.

Figure 20 shows the phase diagram of the water/methanol/Dx10k, Dx70k and Dx10000k at 25 °C. This graph contains the cloud points and the swelling points for Dx70k and Dx10000k. For Dx10k it was impossible to determine the swelling point because Dx10k does not form a film. For Dx70k it also shows the critical composition. For the other two dextran samples critical compositions were not determined due to the facts that the gel phase of Dx10k crystallizes during the measurement of the critical point and the solutions of Dx10000k are extremely viscous and yellow at even less than 5 wt%.

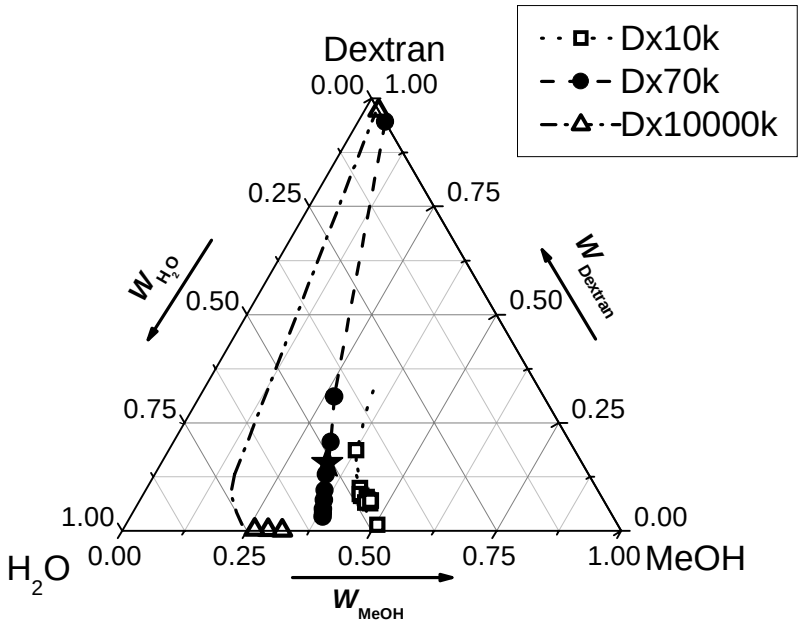

Figure 20. Phase diagrams of the systems water/methanol/dextran for the three indicated dextran samples at 25 °C. Open squares, full cirlcles, and open triangles represent cloud points and swelling points for Dx10k, Dx70k, and Dx10000k, respectively. The dashed lines give the expected cloud point curves. The star is the critical point for Dx70k.

4.6.2 Water / Dextran / BSA

Figure 21 shows the phase diagram of water/Dx2000k/BSA at 25°C measured by Yurij A. Antonov (unpublished results).

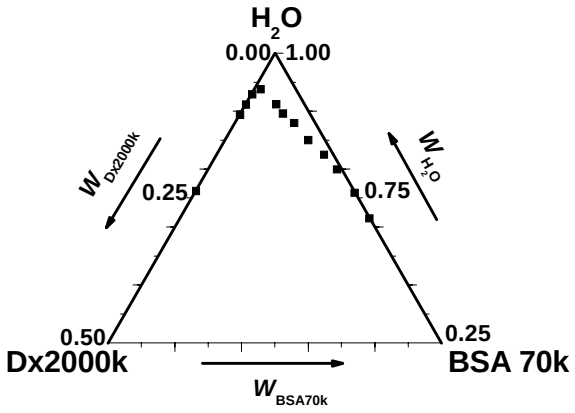

Figure 21. Upper part of the phase diagram of the system water/Dx2000k/ BSA at 25 °C measured by Yurij A. Antonov (unpublished results).

4.7 Modeled Phase Diagrams

The modeling of ternary system is performed by using the binary interaction parameters of the components. There are three options to determine composition dependencies of the interaction parameters for binary systems. If the system consists of two solvents, the composition dependencies of χ and ξ are obtained from the vapor pressures of each component. If the system consists of a solvent and a polymer, the composition dependencies of χ results from the vapor pressures of the solvent. A further option for a solvent/polymer system is the evaluation of data for dilute solution obtained for polymers of different molecular weight. This evaluation yields the parameters α, ζ, λ and ν by means of which χ can be described.

The vapor pressures for the system water/Dx70k were measured for the modeling of the ternary system water/methanol/Dx70k and those for the system water/BSA were measured for the modeling of the ternary system water/Dx2000k/BSA.

In many cases there are several possibilities to express composition dependencies of interaction parameters analytically with comparable precision. For the parameter sets of binary and ternary systems, the following abbreviations are used: water/methanol=L, water/dextran=D, water/BSA=B, methanol/dextran=M, water/methanol/dextran=X, water/dextran/BSA=Y, dextran/BSA=Z. The abbreviations and the number of Figures showing the interaction parameter as a function of compositions are summarized in Table VI for the binary systems and in Table VII for the ternary systems. In Table VII, the combinations of the binary systems which are used for the modeling of the ternary system are also shown.

Table VI. Abbreviations and Figure numbers of the parameter sets used in the descriptions of binary systems.

	H_2O/ MeOH	H_2O/ Dx70k			H_2O/ BSA			MeOH/ Dx70k			Dx70k/ BSA
Abbreviation	L	D1	D2	D3	B1	B2	B3	M1	M2	M3	Z1
Figure No.	26	27	29	35	37	38	39	31	33	36	41

Table VII. Abbreviations, combinations of binary systems and Figure numbers of parameter sets used in the descriptions of ternary systems.

	H_2O/MeOH/Dx70k			H_2O/Dx70k/BSA
Abbreviation	X1	X2	X3	Y1
combination	L+D1+M1	L+D2+M2	L+D3+M3	D3+B3+Z1

	H_2O/MeOH/Dx70k			H_2O/Dx70k/BSA
Figure No.	30	32	34	40

4.7.1 Vapor Pressures

Vapor pressures were measured by means of Headspace Sampling-Gaschromatography (HS-GC) for the systems water/Dx70k and water/BSA at 25 °C. In order to determine if the sample solutions were in equilibrium or not, the measurements were performed after various periods of rest. The vapor pressures for the system water/Dx10000k are shown in Appendix (6.2).

Water/Dextran

Figure 22 shows the results of the vapor pressure measurement for the system water/Dx70k for different resting periods. The samples at $0.4 < \varphi_{Dx70k} < 0.6$ kept for 1 week or for 3 weeks were white and contained crystals.

There is deviation between data for the different resting periods but no tendency toward equilibrium is recognized. Because of crystallization, the data of the samples kept for 1day is used for further modeling, though it is unclear whether the sample is in equilibrium or not.

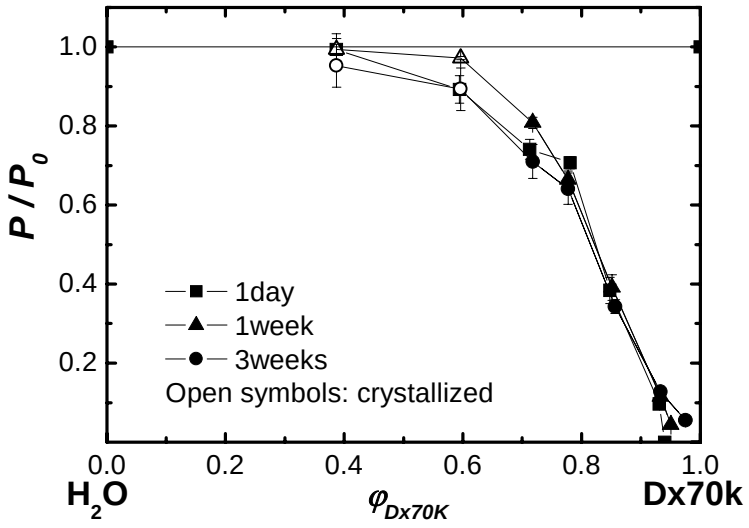

Figure 22. Vapor pressures for the system water/Dx70k at 25°C. Squares, triangles and circles represent P/P_0 of the samples 1 day, 1 week and 3 weeks after the preparation of solutions, respectively. The open symbols mark samples, which were white, indicating crystallization.

Water/BSA

Figure 23 shows the results of the vapor pressure measurement for the system water/BSA for different resting periods. Similar to the behavior for the system water/Dx70k, no tendency toward equilibrium is recognized. The data for resting periods of 3 weeks is used for the further modeling, because the system is considered to be in equilibrium.

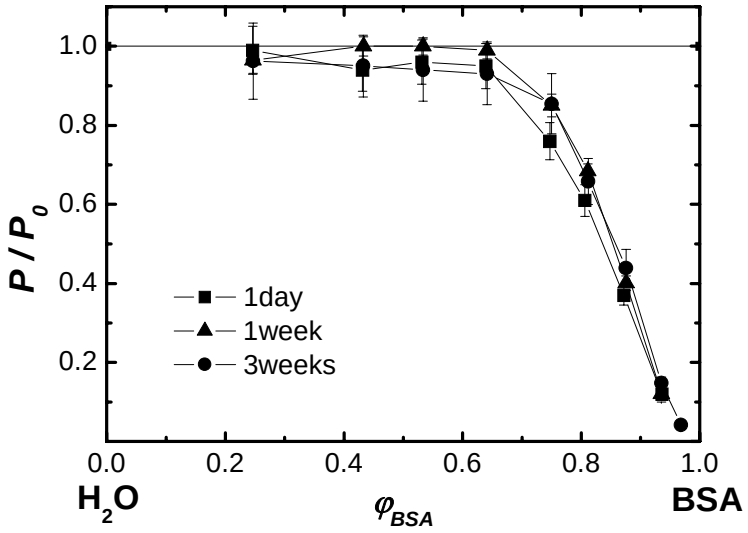

Figure 23. Vapor pressures for the system water/BSA at 25 °C. Symbols are the same as Figure 22.

4.7.2 Water/Methanol/Dextran

For the ternary system water/methanol/Dx70k, the following indices are used: water=1, methanol=2 and dextran=3. The volume of water was defined as the unit volume, i.e. it constitutes of one segment, N_1=1, N_2=2.256 and N_3=2245.

Water/Methanol

Figure 24 shows literature data of vapor pressures of the system water/ methanol.[85,86]

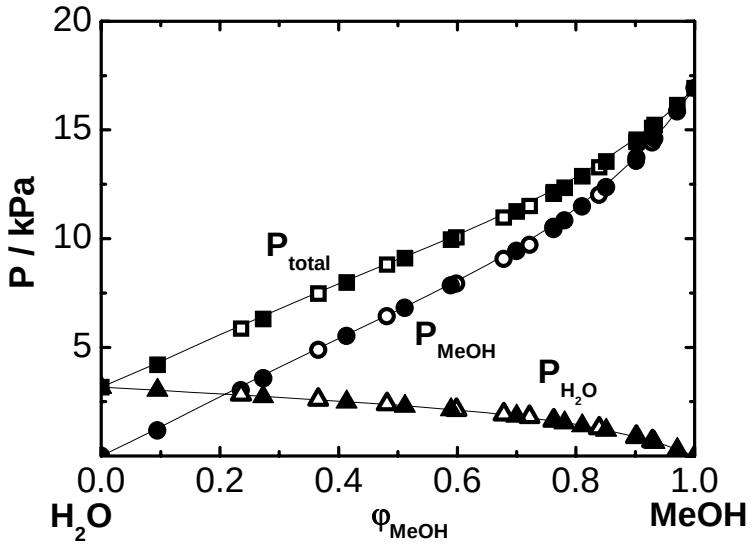

Figure 24. Vapor pressures of the system water/methanol at 25 °C. Open symbols are the data from Ref.[85]. Full symbols are from Ref.[86].

The Flory-Huggins interaction parameters in the differential form for water (χ) and methanol (ξ) are obtained according to the following equations (cf. Eqs. 24, 26 and 46) and shown in Figure 25.

$$\chi = \frac{\Delta G_1^R}{RT\varphi_2^2} = \frac{\ln a_1 - \ln(1-\varphi_2) - \left(1 - \frac{1}{N_2}\right)\varphi_2}{\varphi_2^2} \tag{57}$$

$$\xi = \frac{\Delta G_2^R}{RT\varphi_1^2} = \frac{\ln a_2 - \ln \varphi_2 - (1-N_2)(1-\varphi_2)}{N_2(1-\varphi_2)^2} \tag{58}$$

The activities of water and methanol are determined as follows using the data from Ref.[87].

$$a_1 = \frac{P_1}{P_{x_1=1}} = \frac{P_1}{3.17} \tag{59}$$

$$a_2 = \frac{P_2}{P_{x_2=1}} = \frac{P_2}{16.91} \tag{60}$$

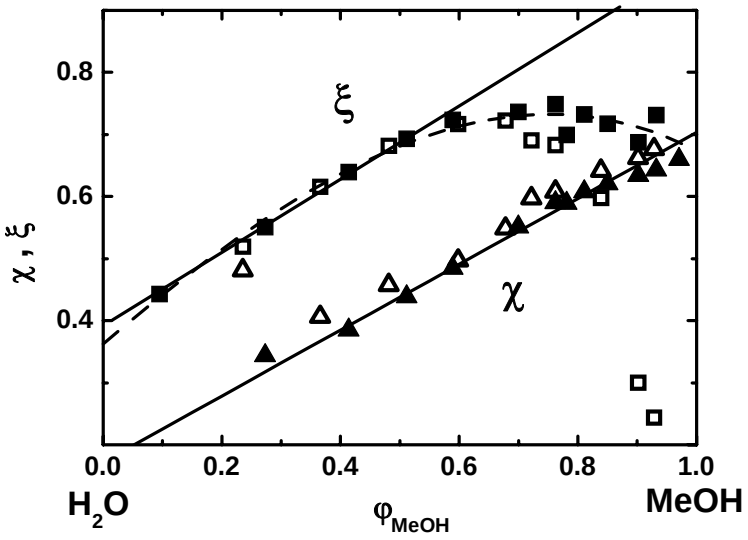

Figure 25. χ and ξ for the system water/methanol at 25 ^{o}C. Triangles and squares represent $\chi(\varphi_{MeOH})$ and $\xi(\varphi_{MeOH})$, respectively. Open symbols are the data from Ref.[85] and full symbols are from Ref.[86]. The solid lines represent a linear fit of $\chi(\varphi_{MeOH})$ and $\xi(\varphi_{MeOH})$ and the dashed line represents a polynomial fit of $\xi(\varphi_{MeOH})$.

The dependence of $\xi(\varphi_{MeOH})$ shown in Figure 25 indicates that at high concentration of methanol, the error of the activity for methanol is very large. Also, for simplicity $\xi(\varphi_{MeOH})$ and g were assumed to depend linearly on composition. This

assumption does not make a big difference for the calculation of g or for modeling of the ternary system.

The calculation of the concentration dependencies of interaction was performed by means of the dependence of $\chi(\varphi_{MeOH})$ due to its small error. The integral interaction parameter, g, depends linearly on φ_{MeOH}, so it can be described as

$$g = a + b\varphi_2 \tag{61}$$

The differential interaction parameter of water, χ, can be represented as

$$\chi = g + \varphi_1 \frac{\partial g}{\partial \varphi_1} = a + b\varphi_2 - (1-\varphi_2)b = (a-b) + 2b\varphi_2 \tag{62}$$

From the dependence of $\chi(\varphi_{MeOH})$ shown in Figure 25, we obtain a =0.43789 and b =0.26522. Therefore the following relations hold true:

$$\chi = 0.1727 + 0.5304\varphi_2 \tag{63}$$

$$g = 0.43789 + 0.26522\varphi_2 \tag{64}$$

$$\xi = g + x\frac{\partial g}{\partial x} = a + 2bx = 0.4349 + 0.53044\varphi_2 \tag{65}$$

According to Eqs. 19 and 64 , the Gibbs energy of mixing per one mole of segments is given by the following equation:

$$\frac{\Delta\overline{\overline{G}}_{12}}{RT} = \frac{1}{N_1}\varphi_1 \ln\varphi_1 + \frac{1}{N_2}\varphi_2 \ln\varphi_2 + \left(0.43789 + 0.26522\varphi_2\right)\left(1-\varphi_2\right)\ln\varphi_2 \tag{66}$$

Figure 26 shows the calculated interaction parameters and the segment molar Gibbs energy of mixing for the system water/methanol. Thus the interaction parameters obtained for the system water/methanol shown in Figure 26 is called L.

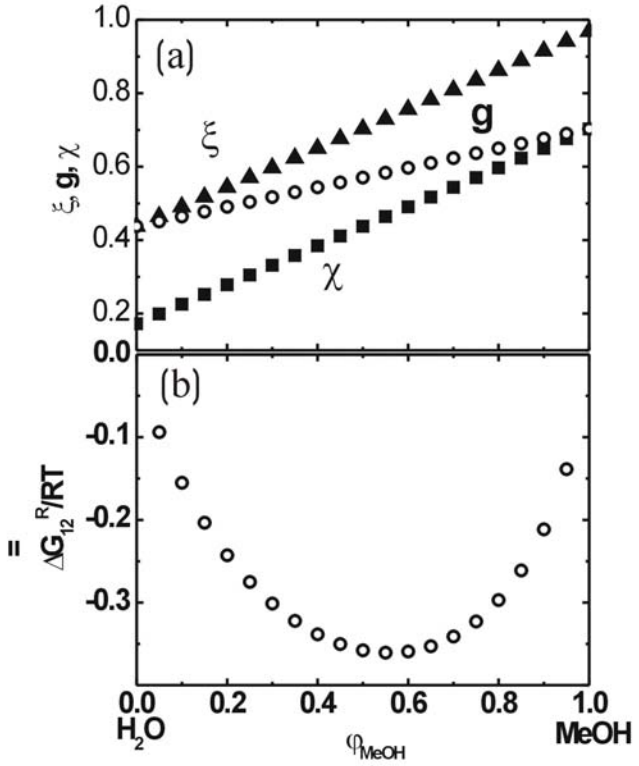

Figure 26. Water/methanol at 25 °C. Interaction parameters (L). (a) Interaction parameters. (b) Segment molar Gibbs energy of mixing.

Water/Dextran

For the system water/Dx70k, it is possible to obtain the vapor pressures and the dilute solution information of different molecular weight.

Figure 27 shows the fitting of the measured vapor pressures with the values α_{13}=–0.0178, ζ_{13}=–0.6294, λ_{13}=0.5313 and ν_{13}=0.9761. This set of parameters is called D1. The measured vapor pressures as a function of composition can be well fit by means of the parameters α, ζ, λ and ν as shown in Figure 27 (a). However, as indicated in the inset of Figure 27 (b), χ_{13} of φ_{Dx70k}=0 ($\chi_{0,13}$) is 0.32, whereas $\chi_{0,13}$ = 0.48 is obtained from light scattering (A_2 = 4.560 * 10^{-4} cm^3 mol g^{-2}) according to the following phenomenological relation equation.[121]

$$\chi_0 = \frac{1}{2} - A_2 \ \overline{V}_1 \ \rho_2^2 \tag{67}$$

Therefore, D1 seems to be unrealistic, at least for dilutes solution. Nevertheless the parameter set D1 will also be used to model the ternary system.

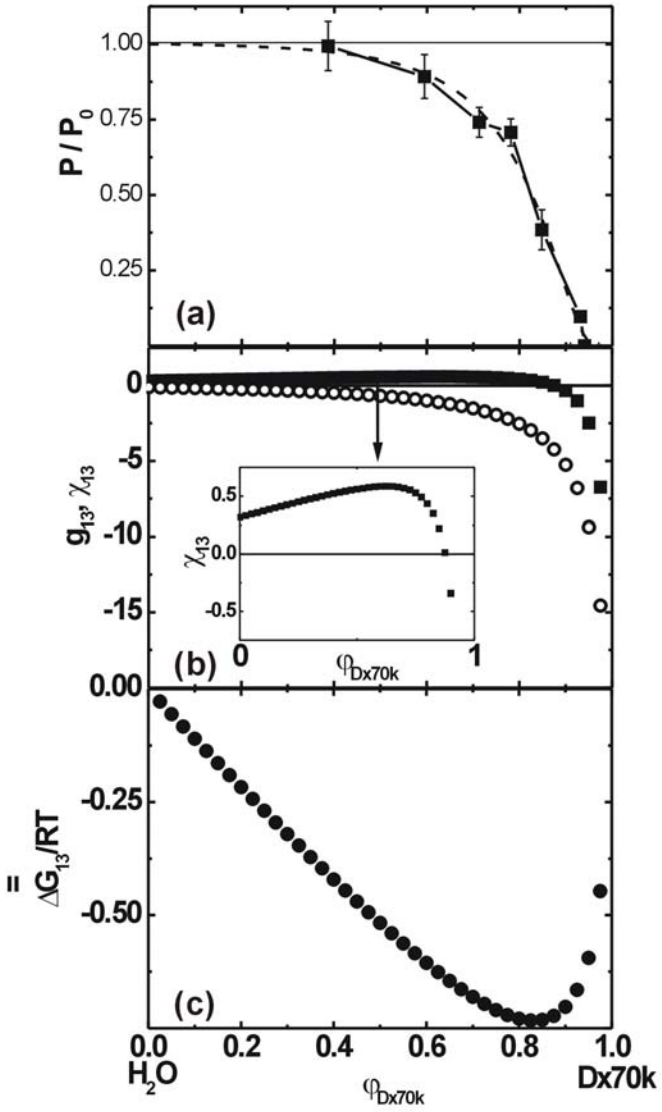

Figure 27. Water/Dx70k at 25 °C. Parameter set D1 was used: α_{13} = -0.0178, ζ_{13} = -0.6294, λ_{13} = 0.5313 and ν_{13} = 0.9761. (a) The dashed line gives the vapor pressures from the fitting and the full symbols are from experiment. (b) Full symbols represent χ, and open symbols represent g. The inset shows an enlarged picture for χ. (c) Segment molar Gibbs energy of mixing.

The parameter set D1 describes the vapor pressures for the system water/Dx70k well but all four parameters, α_{13}, ζ_{13}, λ_{13} and ν_{13} are adjusted to vapor pressures. For this reason α_{13}, ζ_{13} and λ_{13} will be determined from the dilute solution information and ν_{13} will be estimated from surface areas.

ζ_{13} is obtained according to Eq. 37 by using σ, a dependence of A_2 on the molecular weight of dextran. Figure 28 shows A_2 of dextran aqueous solution[78,80] as a function of N. From the odependence of A_2 ($N^{-(1-a)}$) in Figure 28, σ is determined as $3.386*10^{-4}$ (cm^3 mol / g^2). Thus ζ_{13}=0.0203 is obtained.

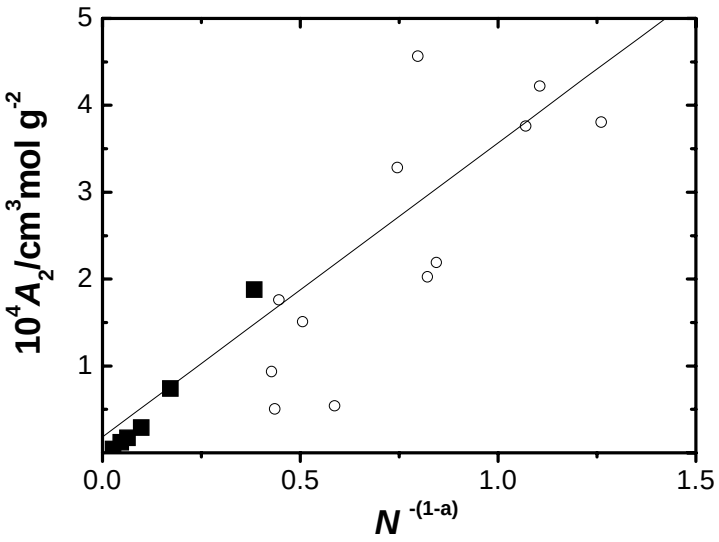

Figure 28. A_2 as a function of N. Open symbols are data from Ref.[79] and full symbols are from Ref.[78]. The line represents a linear fit of A_2 ($N^{-(1-a)}$).

α_{13} and λ_{13} are determined from Eqs. 38 and 42. In Table VIII all the parameters required for the determination of α and λ are collected from the literature.[88,89] The following values are obtained: α_{13}=0.5152 and λ_{13}=0.5134.

Table VIII. Collection of the parameters required for the determination of the α and λ.[88,89]

Method	LS
Mw / kg mol^{-1}	20-100
10^2 K / mL mol^{-1}	9.78
a	0.5
K_N	0.5049
κ / mL g^{-1}	0.7425
$10^4\,\sigma$ / cm^{-3} mol^{-1} g^{-2}	3.386
$10^4\ A_2^{\infty}$ / cm^{-3} mol^{-1} g^{-2}	3.439

ν_{13} may be estimated from γ for the present system, γ is calculated according to Eq. 43. Table IX shows the surface areas of the different functional groups and the molecular surface areas of water and the repeating unit of dextran, glucose.[90]

Table IX. Estimation of ν_{13} with surface areas.[90]

	Functional group	Surface area per group 10^9cm^2/mol	number	Surface area per same functional group	Surface area per molecule
H2O	-OH	1.46	1	1.46	**1.50**
Glucose	-CH3	2.12	1	2.12	**11.2**
	-CH	0.57	5	2.85	
	-OH	1.46	3	4.38	
	-O-	0.60	3	1.80	

From the data of Table IX one obtains

$$\gamma_{13} = 1 - \frac{11.2}{1.5} = -6.5 \tag{68}$$

This value represents the relative surface area per molecule. However, the relative surface area per volume is needed. The molar volume of glucose and water are

$$V_{glucose} = \frac{M_{glucose}}{\rho_{Dx70K}} = \frac{162}{1.4706} = 110.2\left(cm^3 / mol\right) \tag{69}$$

$$V_{H_2O} = \frac{M_{glucose}}{\rho_{Dx70K}} = \frac{18}{0.9970} = 18.1\left(cm^3 / mol\right) \tag{70}$$

Molar volume of glucose is 110.2/18.1=6.1 times of that of water. So the effective γ value, called $\gamma*$ is given as

$$\gamma_{13}^* = 1 - \frac{11.2}{6.1*1.5} = -0.22 \tag{71}$$

this γ_{13}^* is considered to be identical with ν_{13}.

With the parameters, α_{13}=0.5152, ζ_{13}=0.0203 and λ_{13}=0.5134, obtained by means of dilute solution information and ν_{13}= -0.22, by means of surface area, the vapor pressures of the system water/Dx70k were predicted according to Eq. 46. This set of parameters is called D2. Figure 29 shows the vapor pressures obtained from the experiments and the predictions. The modeled vapor pressure (P/P_0) coincides reasonably with the measurements within experimental error.

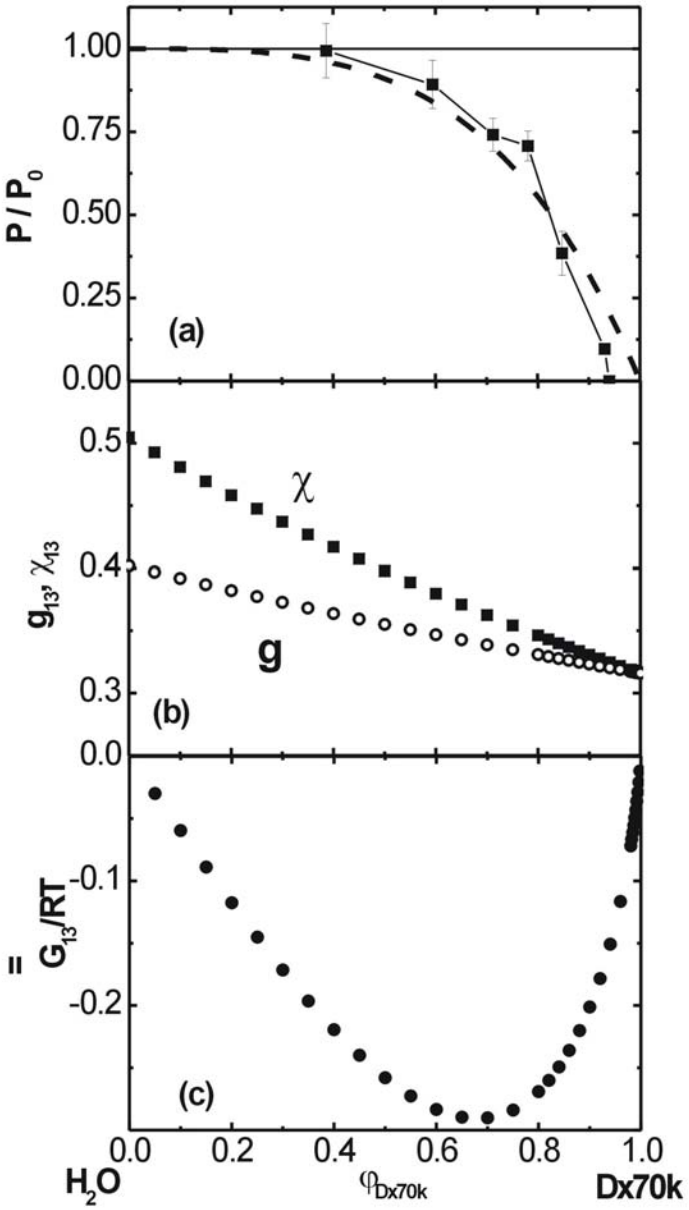

Figure 29. Water/Dx70k at 25 °C. Parameter set D2 was used: $\alpha_{13} = 0.5152$, $\zeta_{13} = 0.0203$, $\lambda_{13} = 0.5134$ and $\nu_{13} = -0.22$. (a) The dashed line gives the vapor pressures calculated from the information on dilute solution and the full symbols are from experiment. (b) Full symbols represent χ, and open symbols represent g. (c) Segment molar Gibbs energy of mixing.

Methanol/Dextran

For the system methanol/Dx70k, only the information about surface areas for the estimation of ν_{23} and the swelling point can be obtained. At the volume fraction of the swelling point, the segment molar Gibbs energy of mixing should have a tangent to the origin of the coordinates (φ_{Dx70k}=0). The dilute solution information for the determination of α_{23}, ζ_{23} and λ_{23} and the vapor pressures cannot be measured because of the large miscibility gap between methanol and dextran.

Therefore, ν_{23} is estimated and the modeling of this binary system will be attempted after the modeling of the ternary system water/methanol/Dx70k.

In the same way as ν_{13}, ν_{23} is estimated using the surface areas of methanol (Table X) and dextran (Table IX).

Table X. Estimation of ν_{23} with surface areas.[90]

	Functional group	Surface area per group 10^9cm^2/mol	Number	Surface area per functional group	Surface area per molecule
Methanol	-CH_3	2.12	1	2.12	**3.58**
	-OH	1.46	1	1.46	

Thus we obtain γ_{23} as

$$\gamma_{23} = 1 - \frac{11.2}{3.58} = -2.1 \tag{72}$$

where the molar volume of methanol is

$$V_{MeOH} = \frac{M_{MeOH}}{\rho_{MeOH}} = \frac{32}{0.7910} = 40.5 cm^3 / mol \tag{73}$$

The molar volume of glucose is 110.2/40.5=2.72 times of that of methanol. Thus γ^* is given as

$$\gamma_{23}^* = 1 - \frac{11.2}{2.7 * 3.58} = -0.16 \tag{74}$$

Water/Methanol/Dextran

The parameter sets D1 and D2 obtained for the system water/Dx70k are used to model the phase diagram for the system water/methanol/Dx70k by varying the parameters for the system methanol/Dx70k.

With the parameter set D1, it was not possible to obtain a reasonable ternary phase diagram. Figure 30 shows an example of the modeled phase diagram indicating the large miscibility gap. Trials were performed with $\nu_{23} \neq -0.16$, i.e. the ν_{23} value obtained not from the surface area, but they also did not yield a reasonable phase diagram. The parameter set used to model the ternary system shown in Figure 30 is called X1 (cf. Table XI). The parameter set for the system methanol/Dx70k obtained to model the phase diagram for the ternary system shown in Figure 30 is called M2. The interaction parameters and the segment molar Gibbs energy of mixing for the system methanol/dextran with the parameter set M1 are shown in Figure 31.

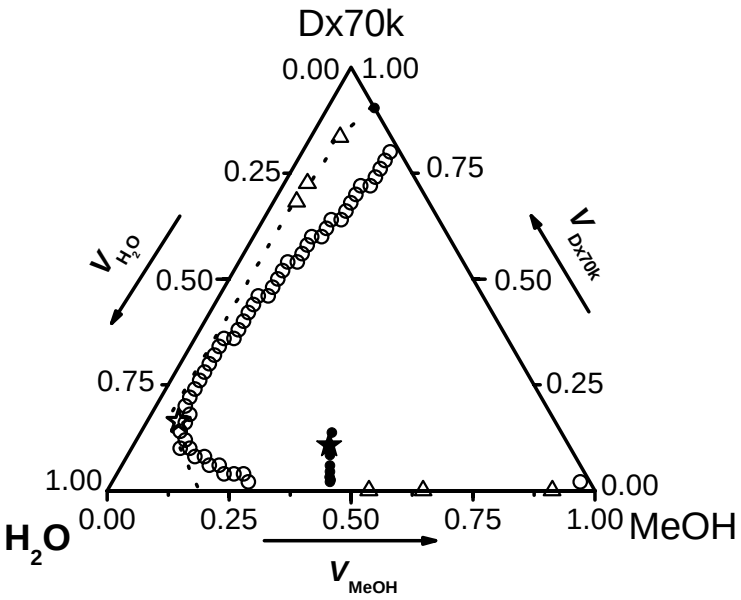

Figure 30. Water/methanol/Dx70k at 25°C was modeled using the parameter set X1(cf. Table XI). Full circles represent the experimental cloud points and the swelling point. The full star gives the experimental critical point. Open circles are the modeled spinodal curve. Open triangles represent the ends of tie lines from the modeling and dashed line is the expected binodal line.

Table XI. Interaction parameters used for modeling with parameter set X1.

system	interaction parameter
water / methanol	$g = 0.4379 + 0.2652\varphi_2$
water / Dx70k (D1)	$g = \frac{-0.0178}{(1-0.9761)(1-0.9761\varphi_3)} + 0.6294\left(1+(1-0.5313)\varphi_3\right)$
methanol / Dx70k (M1)	$g = \frac{0.1}{(1+0.16)(1+0.16\varphi_3)} + 0.5\left(1+(1-0.5)\varphi_3\right)$

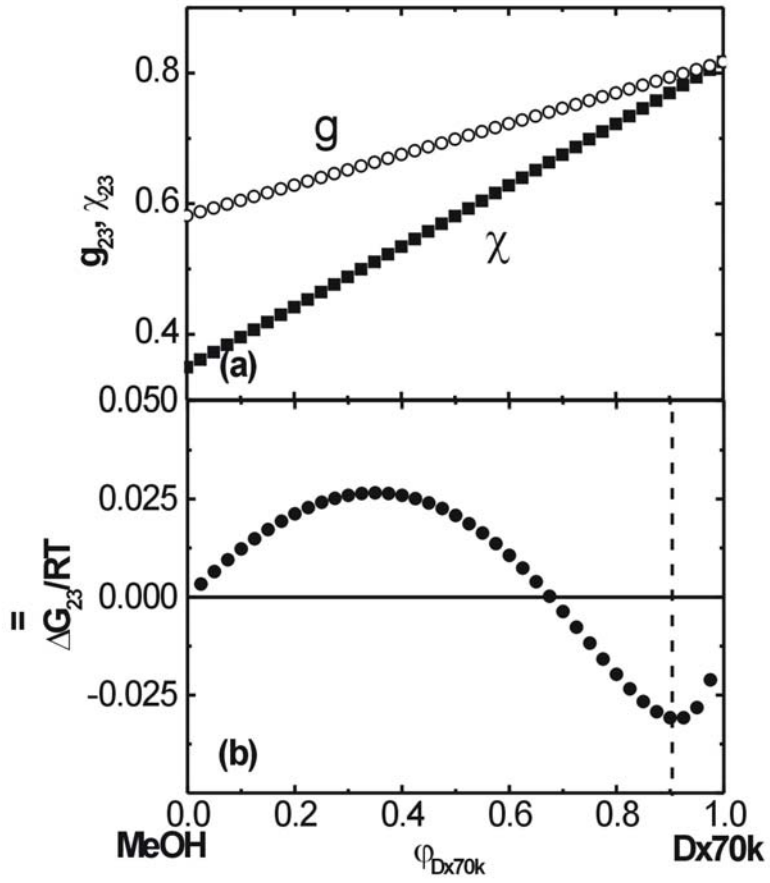

Figure 31. Methanol /Dx70k at 25°C. Parameter set M1 was used: α_{23} = 0.1, ζ_{23} = -0.5, λ_{23} = 0.5 and ν_{23} = -0.16. (a) Full symbols represent χ, and open symbols represent g from the modeling. (b) Modeled segment molar Gibbs energy. The dashed line represents the swelling point, φ_{Dx70k}=0.9030.

Because of the unrealistic results obtained with the parameter set D1, the next modeling was performed with the parameter set D2. Figure 32 shows the modeled phase diagram. The spinodal curve, binodal curve, swelling point and critical point for the system water/methanol/Dx70k are represented in a realistic manner.

The parameter set used to model the ternary system shown in Figure 32 is called X2 (cf. Table XII). The parameter set for the system methanol/Dx70k obtained to model the phase diagram for the ternary system shown in Figure 32 is called M2. The interaction parameters and the segment molar Gibbs energy of mixing for the system methanol/Dx70k with the parameter set M2 are shown in Figure 33.

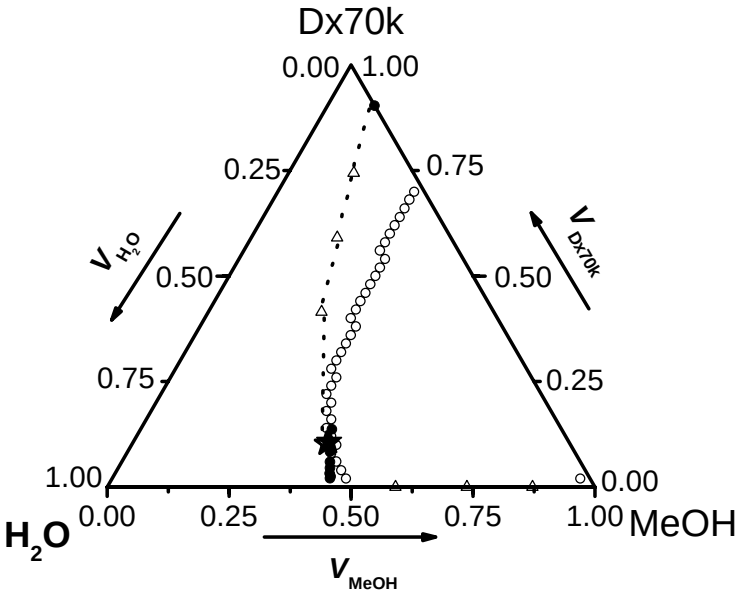

Figure 32. Water/methanol/Dx70k at 25°C was modeled using the parameter set X2 (cf. Table XII). Symbols are the same as Figure 30. The modeled critical point coincides within experimental error with the experimental critical point.

Table XII. Interaction parameters used for modeling with parameter set X2.

Components	calculated parameters
water / methanol	$g = 0.4379 + 0.2652\varphi_2$
water / Dx70k (D2)	$g = \frac{0.5152}{(1+0.22)(1+0.22\varphi_3)} - 0.0203\left(1+(1-0.5134)\varphi_3\right)$
methanol / Dx70k (M2)	$g = \frac{0.155}{(1+0.16)(1+0.16\varphi_3)} + 0.45\left(1+(1-0.5)\varphi_3\right)$

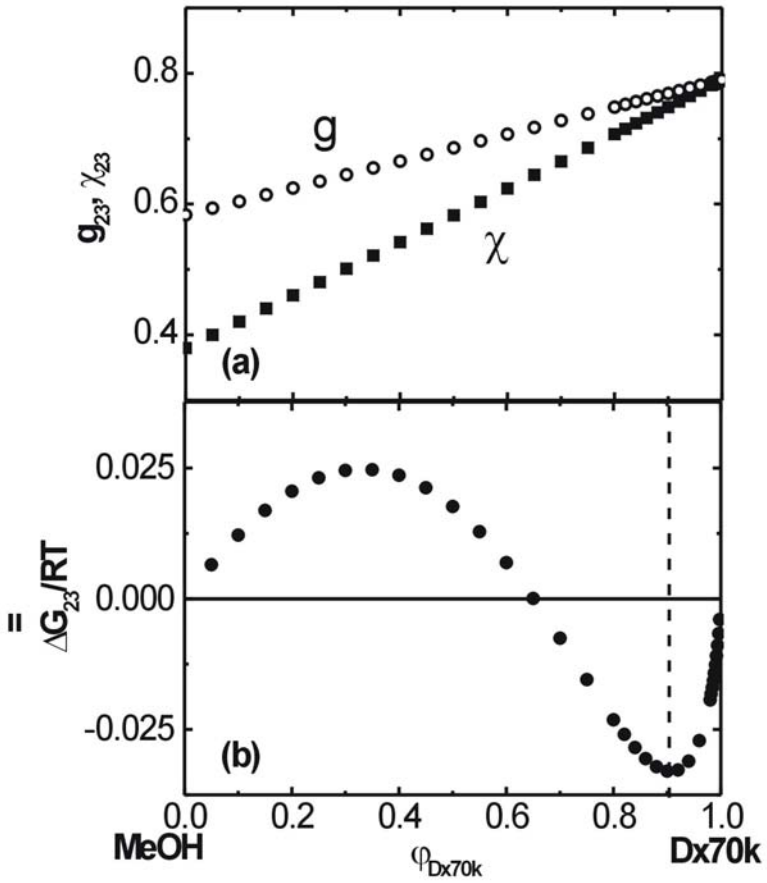

Figure 33. Methanol /Dx70k at 25 °C. Parameter set M2 was used: α_{23} = 0.155, ζ_{23} = 0.0203, λ_{23} = 0.5134 and ν_{23} = -0.22. Symbols are the same as Figure 31.

The parameter set X2 gives reasonable results but there is one puzzling issue regarding the interaction parameter between methanol and dextran. Figure 33 indicates that χ_{23} at φ_2=0 is relatively low ($\chi_{0,\,23}$ =0.38), though the segment molar Gibbs energy of mixing leads to a miscibility gap. The χ_0 value between polymer and non solvent is presently unknown, but it is expected to be higher than 0.5 for the immiscible system. For this reason, further modeling with $\chi_{0,\,23} > 0.5$ is attempted as described in the next section.

If we change the parameters for the system methanol/Dx70k to be $\chi_{0,\,23} > 0.5$, in order to model the phase diagram for the system water/methanol/Dx70k at the same time, other parameters for the other binary systems, water/methanol and water/Dx70k need to also be changed. The parameters, except for ν, are considered to be un-suspected, while negative ν values for the system water/Dx70k and methanol/Dx70k are rather unrealistic. Therefore, modeling of the phase diagram is attempted to be $\chi_{0,\,23} > 0.5$, $\nu_{13} > 0$ and $\nu_{23} > 0$ by setting $\chi_{0,\,23}$=0.55. This means that the following relation must hold true because of Eq. 44.

$$\chi_{0,23} = 0.55 = \alpha_{23} - \zeta_{23}\lambda_{23} \tag{75}$$

where λ_{23} is approximated to 0.5; only α_{23} and ζ_{23} were varied. Under these conditions, the modeling of the ternary system water/methanol/Dx70k was performed (Figure 34). For this modeling, the parameters ν_{13}=0.22, α_{23}=0.72, ζ_{23}=0.34, λ_{23}=0.5 and ν_{23}=0.22 are used. The spinodal curve, binodal curve, swelling point and critical point for the system water/methanol/Dx70k are represented in a realistic manner.

The parameter set used to model the ternary system shown in Figure 34 is called X3 (cf. Table XIII). The vapor pressures, the interaction parameters and the segment molar Gibbs energy of mixing are shown for the system methanol/Dx70k in Figure 35 and for the system methanol/Dx70k (M3) in Figure 36.

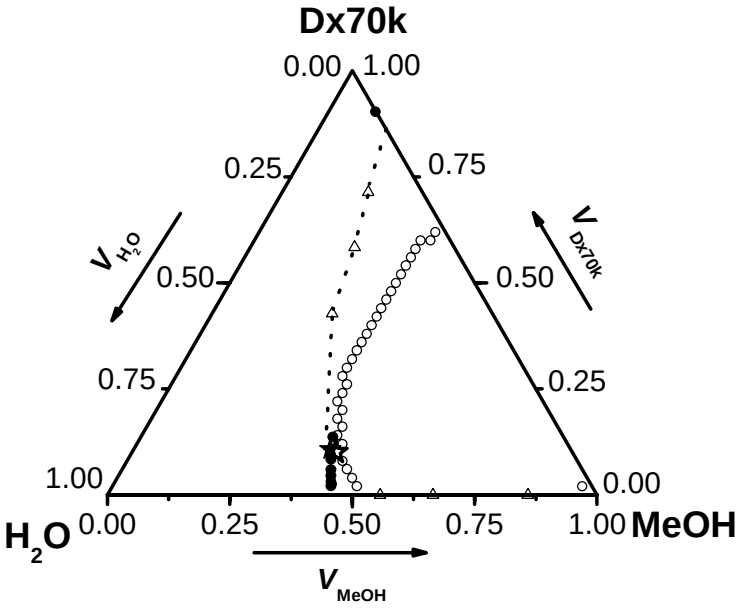

Figure 34. Water/methanol/Dx70k at 25 °C was modeled using the parameter set X3 (cf. Table XIII). Symbols are the same as Figure 30.

Table XIII. Interaction parameters used for modeling with parameter set X3.

system	Interaction parameters
water/methanol	$g = 0.43789 + 0.26522\varphi_2$
water/Dx70k (Model D3)	$g = \frac{0.5152}{(1-0.22)(1-0.22\varphi_3)} - 0.0203\left(1+(1-0.5134)\varphi_3\right)$
methanol/Dx70k (Model M3)	$g = \frac{0.72}{(1-0.22)(1-0.22\varphi_3)} - 0.34\left(1+(1-0.5)\varphi_3\right)$

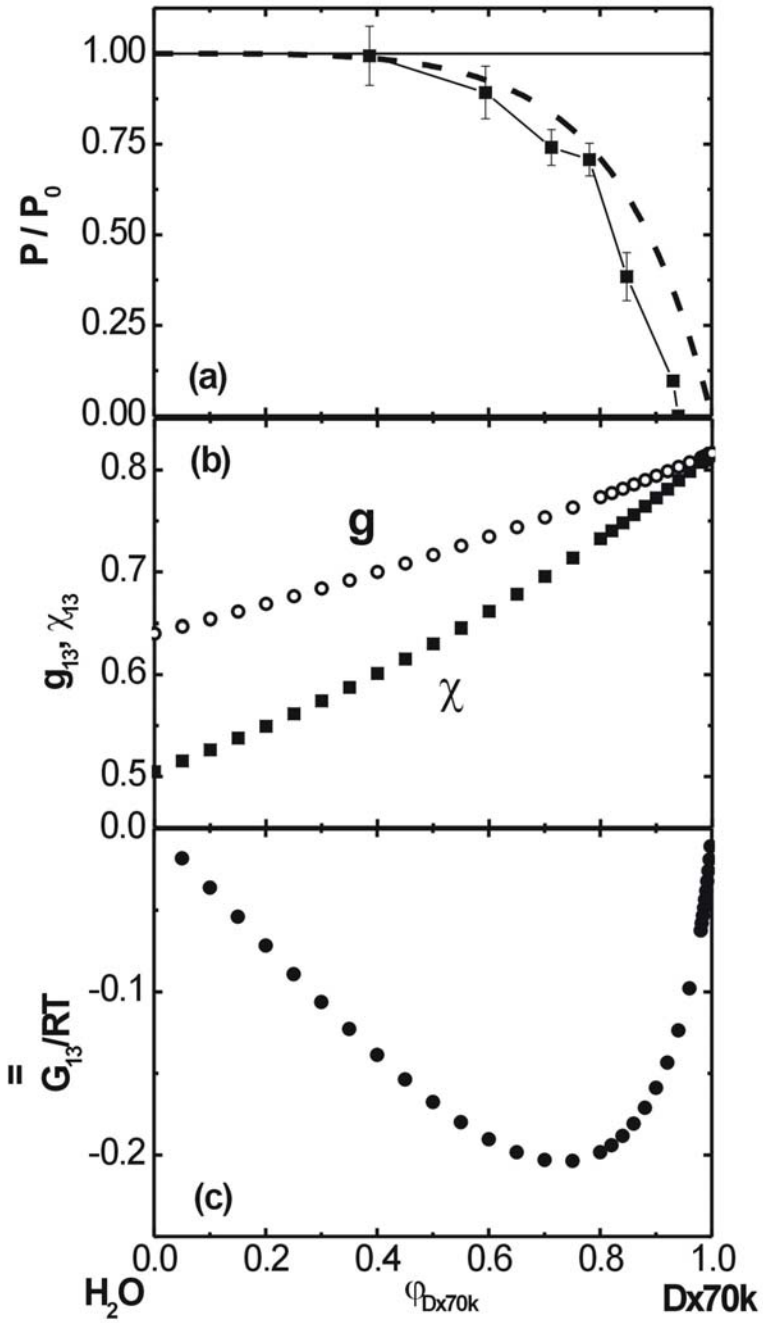

Figure 35. Water/Dx70k at 25°C. Parameter set D3 was used: $\alpha_{13} = 0.5152$, $\zeta_{13} = 0.0203$, $\lambda_{13} = 0.5134$ and $\nu_{13} = 0.22$. The symbols are the same as Figure 31.

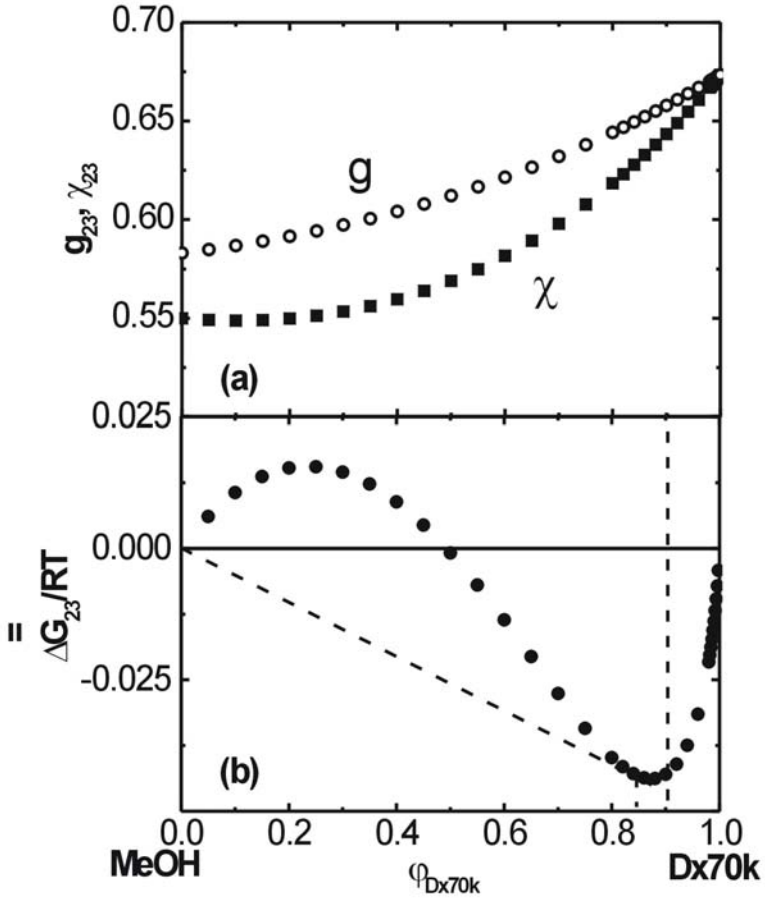

Figure 36. Methanol/Dx70k at 25 °C. Parameter set M3 was used; $\alpha_{23} = 0.72$, $\zeta_{13} = 0.34$, $\lambda_{13} = 0.5$ and $\nu_{23} = 0.22$. Symbols are the same as Figure 31.

Figure 34 indicates that the parameter set X3 is similarly realistic as X2 (Figure 32). On the other hand, the parameter set M3 does not represent the swelling point with sufficient accuracy as seen from Figure 36. Nevertheless, X3 is considered to be the best modeling for the system water/methanol/Dx70k, because $\chi_{0,23}$ is higher than 0.5.

The vapor pressures for the system water/Dx70k with the parameter set D3 (Figure 35 (a)) represents the experimental results with lower accuracy than D1 and D2. This could be because the dextran solutions for HS-GC measurements were not in equilibrium for the sample 1 day after the solution preparation. However, if the solutions are kept longer than 1 day, crystals aggregate.

To sum up the results, the modeling for the system water/methanol/ Dx70k can be stated that the parameter sets D3 for the system water/Dx70k and M3 for the system

methanol/Dx70k represent the phase diagram for the ternary system water/methanol/ Dx70k in a realistic manner. The concentration independent parameters, α_{13}, ζ_{13} and λ_{13} for the system water/Dx70k were determined from dilute solutions. It was not possible to calculate ν from the surface areas for the systems water/Dx70k and methanol/Dx70k. The concentration independent parameters do not represent the experimental vapor pressures reasonably. The reason could be the dextran solutions were not in equilibrium 1 day after the sample preparation.

4.7.3 Water/Dextran/BSA

For the system water/Dx2000k/BSA, the following indices are used: water=1, dextran=2 and BSA=3. The volume of water was defined as the unit volume, i.e. it constitutes of one segment, N_1=1, N_2=55300 and N_3=2815. In the same way as with the previous system water/methanol/Dx70k, the modeling of the phase diagram for the ternary system is performed by means of the binary interaction parameters.

Though the molecular weights of dextrans used for the modeling of the binary system water/Dx70k (M_w=63.6 kg/mol) and for the determination of the phase diagram of the ternary system water/Dx2000k(M_w=2100 kg/mol)/BSA are different, the modeling was performed on the assumption that the molecular weight of the polymers does not influence the interaction parameter considerably.

For the binary system water/dextran, the parameter set D3 turned out to be most realistic in the previous section. However, to be on the safe side, D2 was used for the modeling of the system water/dextran/BSA as well. For the binary polymer blend dextran/BSA, it is impossible to measure the interaction parameters, so it is necessary to guess reasonable values. For the interaction parameters of the binary system water/BSA, partial information is obtained by means of the light scattering and vapor pressures measurements as described in the next section.

Water/BSA

For the binary system water/dextran, α, ζ, and λ were determined by means of σ, i.e. the dependence of A_2 on the molecular weight of dextran. But BSA is mono-disperse and it is consequently impossible to obtain σ. We can only obtain A_2 and measure vapor pressures. From A_2, we get $\chi_{0,13}$ according to Eq. 67. Furthermore, we know how χ_0 is related to α, ζ, and λ (see Eq. 76).

From literature data on light scattering (A_2=1.66*10^{-4} cm^3 mol g^{-2}),[81,91] the following relation holds true according to Eqs. 44 and 67:

$$\chi_{0,13} = 0.51 = \alpha_{13} - \varsigma_{13}\lambda_{13} \tag{76}$$

In this case λ_{13} cannot be approximated to 0.5 because this approximation may not hold true for globular macromolecules like BSA. In addition to the relationship between $\chi_{0,13}$, α_{13}, ζ_{13} and λ_{13} (Eq. 76), qualitative information on the composition dependence of the segment molar Gibbs energy of mixing can be found. Because water and BSA are readily miscible, the second derivative of the segment molar Gibbs energy of mixing as a function of concentration should be positive at all concentrations. There is no information regarding ν_{13}, and so it is necessary to guess this value. Under these restraints, the vapor pressures for the system water/BSA is modeled by varying α_{13}, λ_{13} and ν_{13}. First, λ_{13} is systematically changed, and all the other parameters are adjusted to fit the vapor pressures. We choose all the parameters within physically reasonable ranges; -2 <α_{13} <2, ,-2 <ζ_{13}<2, 0<λ_{13} <1 and 0<ν_{13}<1.

From these attempts to fit the experimental findings, three parameter sets were chosen. The results are shown in Figure 37 (B1: α_{13} = -0.1, ζ_{13} = -0.813, λ_{13} = 0.75 and ν_{13} = 0.6973), Figure 38 (B2: α_{13} = 2, ζ_{13} = 1.863, λ_{13} = 0.8 and ν_{13} = 0.1354) and Figure 39 (B3: α_{13} = 0.5, ζ_{13} = -0.1, λ_{13} = 0.1 and ν_{13} = 0.1). These graphs show vapor pressures, interaction parameters and the segment molar Gibbs energy of mixing, plus its first and second derivatives. Parameter set B1 has negative α_{13} and ζ_{13} values, indicating favorable contact and unfavorable relaxation between BSA and water. On the other hand, B2 has positive α_{13} and ζ_{13} values, i.e. unfavorable contact and favorable relaxation and B3 has positive α_{13} and negative ζ_{13} values, i.e. unfavorable contact and unfavorable relaxation. In regards to the globular nature of BSA, B1 seems to be reasonable. Whereas the parameter set B3 represents the measured vapor pressures most reasonably.

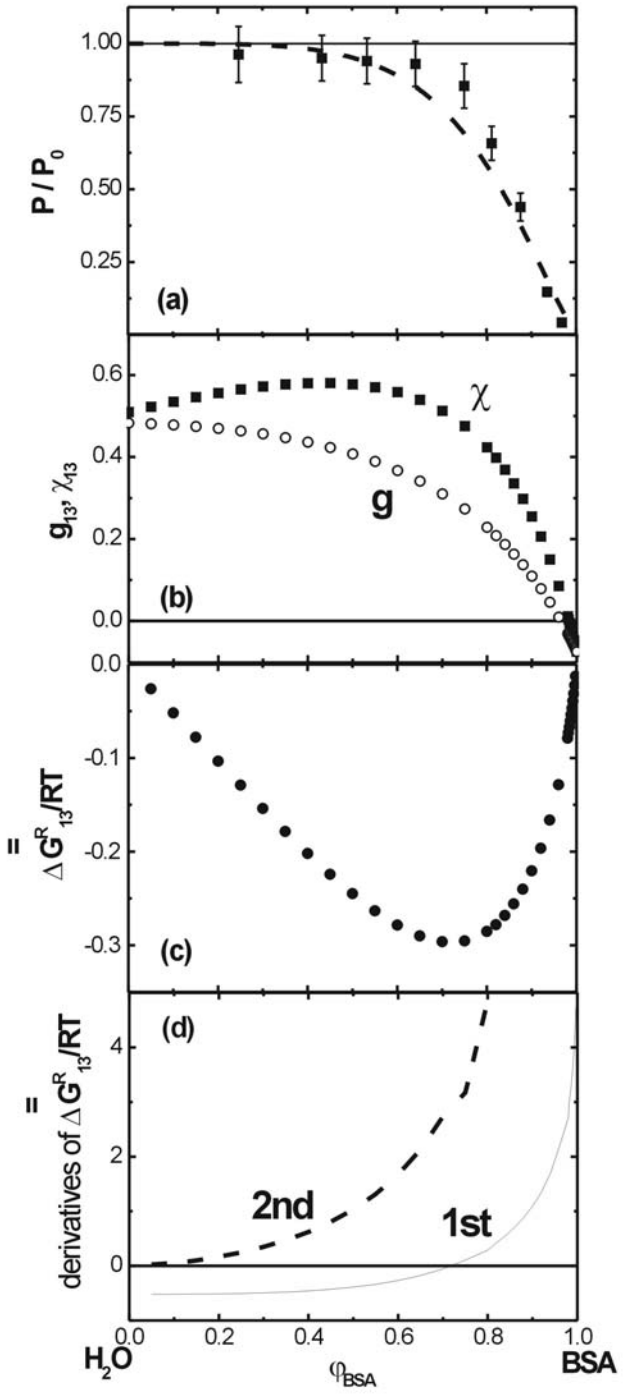

Figure 37. Water/BSA at 25 °C. Parameter set B1 was used: α_{13} = -0.1, ζ_{13} = -0.813, λ_{13} = 0.75 and ν_{13} = 0.6973. (a) Dashed line gives the vapor pressures from the modeling and full symbols are from experiments. (b) Full symbols represent χ, and the open symbols represent g from the modeling. (c) The modeled segment molar Gibbs energy of mixing. (d) Solid line gives the first derivative and dashed line gives the second derivative of the segment molar Gibbs energy of mixing.

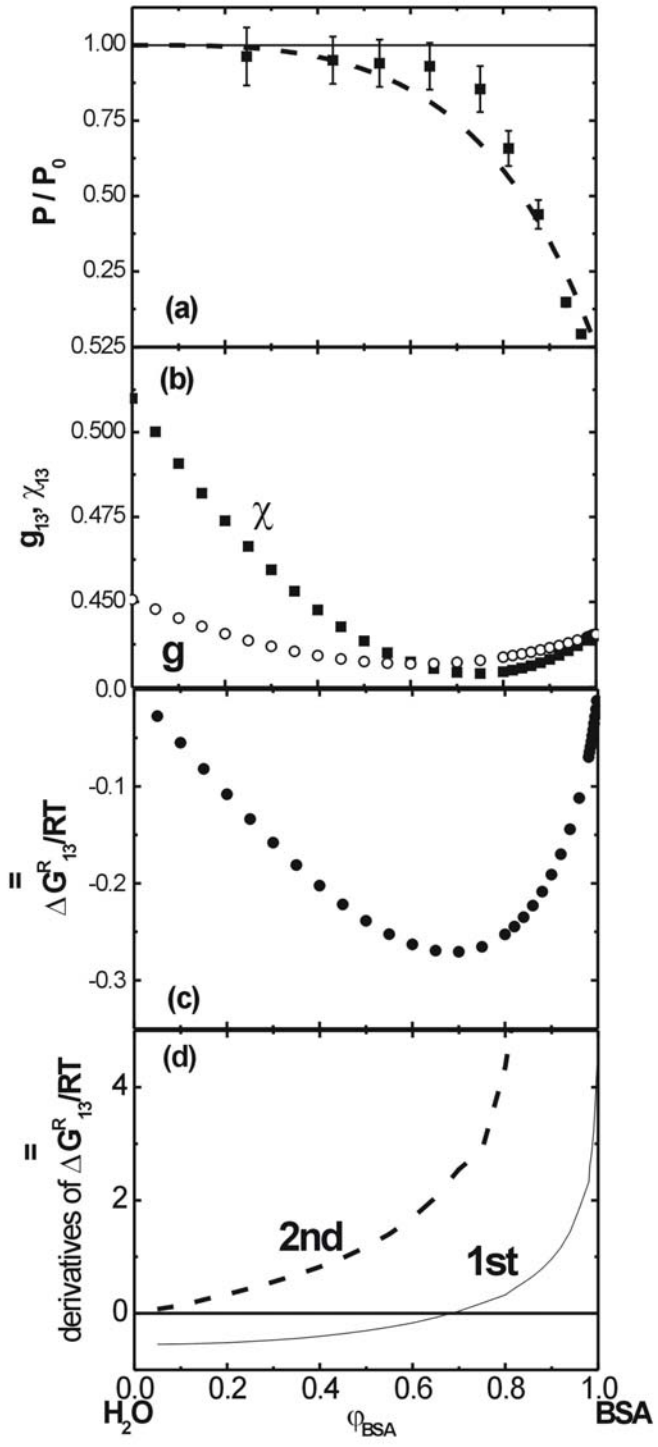

Figure 38. Water/BSA at 25 °C. Parameter set B2 was used: $\alpha_{13} = 2$, $\zeta_{13} = 1.863$, $\lambda_{13} = 0.8$ and $\nu_{13} = 0.1354$. Symbols are the same as Figure 37.

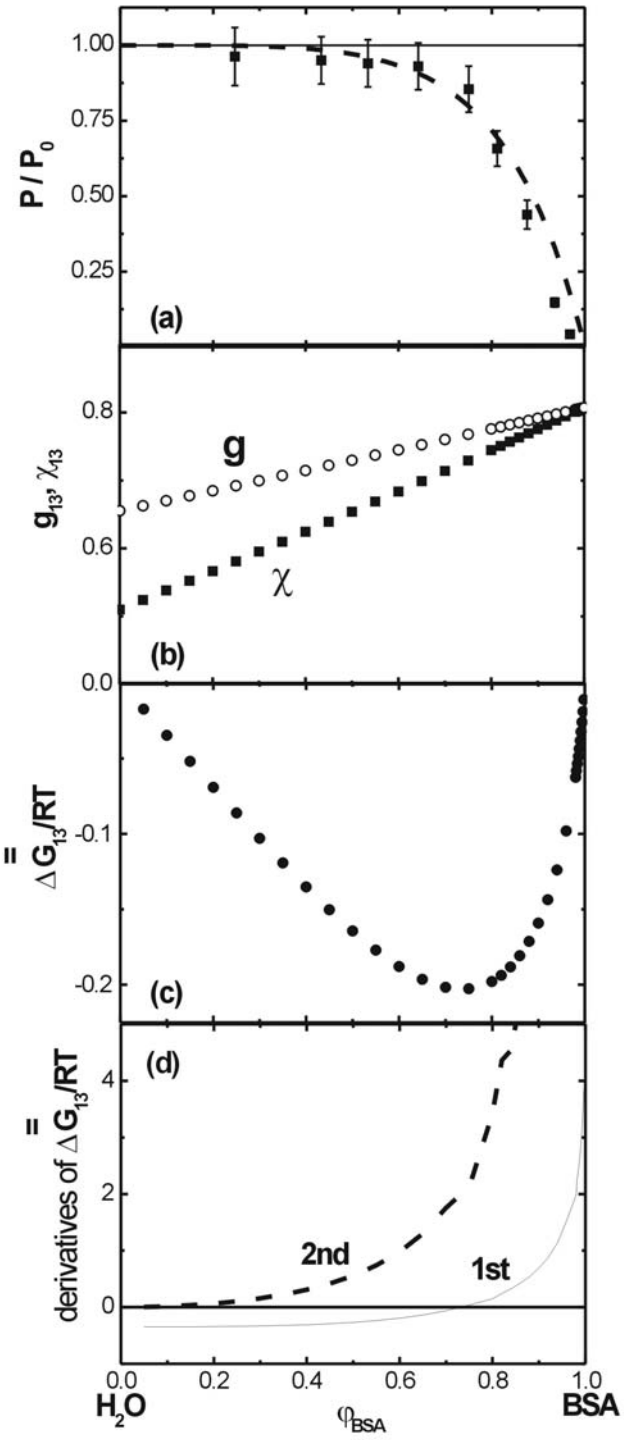

Figure 39. Water/BSA at 25 ^{o}C. Parameter set B3 was used: α_{13} = 0.5, ζ_{13} = -0.1, λ_{13} = 0.1 and ν_{13} = 0.1. Symbols are the same as Figure 37.

Water/Dextran/BSA

With the parameter sets obtained for the binary systems, water/dextran (D2 and D3) and water/BSA (B1, B2 and B3), the phase diagram of the ternary system water/Dx2000k/BSA was modeled by adjusting the parameters for the binary system Dx2000k/BSA. There are different possibilities to model the different binary subsystem and there is a tremendous number of combinations of parameters. Furthermore, for globular macromolecules the theory of "Chain Connectivity and Conformational Variability"[1-3] may not hold true. Nevertheless, the model calculation was performed to obtain additional information on the suitability of the different options. In the following the results that are closest to the experimental observation are presented.

Figure 40 shows the corresponding phase diagram and the parameter set used for this modeling is called Y1. For the parameter set Y1, the parameter sets for the binary systems, D3, B3 and Z1 ($\alpha_{23} = 1$, $\zeta_{23} = 0.8$, $\lambda_{23} = 0.5$ and $\nu_{23} = 0.17$**,** shown in Figure 41) are used (cf. Table XIV). Though a part of the modeled spinodal curve lies outside of the measured cloud point curve, the tie lines are considered to be realistic in their position. The two tie lines and the critical point shown in this graph indicate that there must be an intersection of tie lines and at least two critical points. The existence of the intersection of tie lines agree with the experimental observation of a three phase separation.[92] The spinodal line should continue as indicated by the dashed line, but in the calculation it was not possible to model this feature. The segment molar Gibbs energy mixing with parameter set Z1 shown in Figure 41(b) indicates that dextran and BSA are highly immiscible as expected for these very different kinds of macromolecules. So far, except for the modeling with parameter set Y1, reasonable modeling has not been achieved.

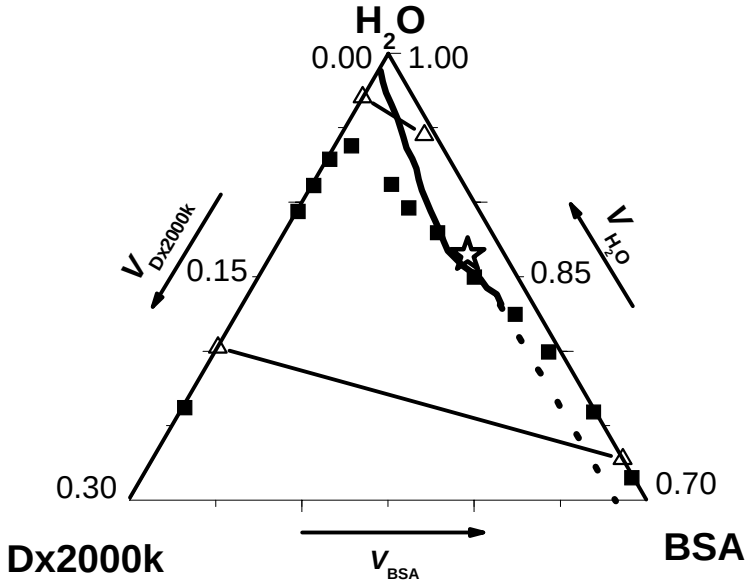

Figure 40. Water/Dx2000k/BSA at 25 °C was modeled using the parameter set Y1 (cf. Table XIV). The upper part of the Gibbs triangle is shown. Full squares are experimental cloud points, the line represents the modeled spinodal curve and the dashed line indicates the expected continuation of the spinodal line to higher polymer concentration. The open star gives the modeled critical point and the open triangles are the ends of tie lines.

Table XIV. Interaction parameters used for modeling with parameter set Y1.

components	Interaction parameters
water/Dx2000k (Model D2)	$g = \frac{0.5152}{(1-0.22)(1-0.22\varphi_2)} - 0.0203\left(1+(1-0.5134)\varphi_2\right)$
water/BSA (Model B3)	$g = \frac{0.5}{(1-0.1)(1-0.1\varphi_3)} + 0.1\left(1+(1-0.1)\varphi_3\right)$
Dx2000k/BSA (Model Z1)	$g = \frac{1}{(1-0.17)(1-0.17\varphi_3)} - 0.8\left(1+(1-0.5)\varphi_3\right)$

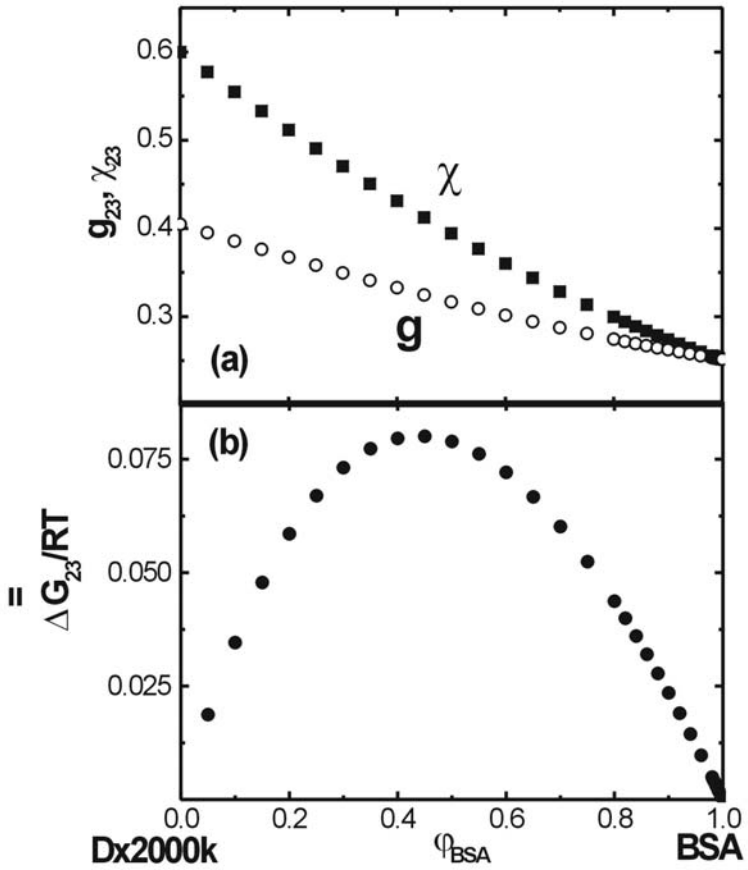

Figure 41. Dx2000k/BSA at 25 °C. Parameter set Z1 was used: $\alpha_{23} = 1$, $\zeta_{23} = 0.8$, $\lambda_{23} = 0.5$ and $\nu_{23} = 0.17$. (a) Full symbols represent χ, and open symbols represent g. (b) Segment molar Gibbs energy of mixing.

The system water/Dx2000k/BSA was modeled in a realistic manner, at least qualitatively. However, there are more combinations of different parameter sets to describe the interactions for the system water/BSA. Further investigation, including an answer to the question whether the theory of "Chain Connectivity and Conformational Variability" should hold true for globular macromolecules or not, is necessary.

4.8 Fractionation

4.8.1 Dx10k

The fractionation of 70 g of Dx10k was achieved through five fractionations, reducing the original non-uniformity of U=1.01 considerably (Cf. Figure 43). The phase diagram of the system water/methanol/Dx10k is given in Figure 42. It shows cloud points, connecting lines of FD and EA, and WP. The first three fractionations were achieved under the same condition. No swelling point was determined for Dx10k in methanol, because of the difficulties to prepare thin films; due to the crystallization tendency of the present polymer sample the resulting films are so brittle that they break immediately.

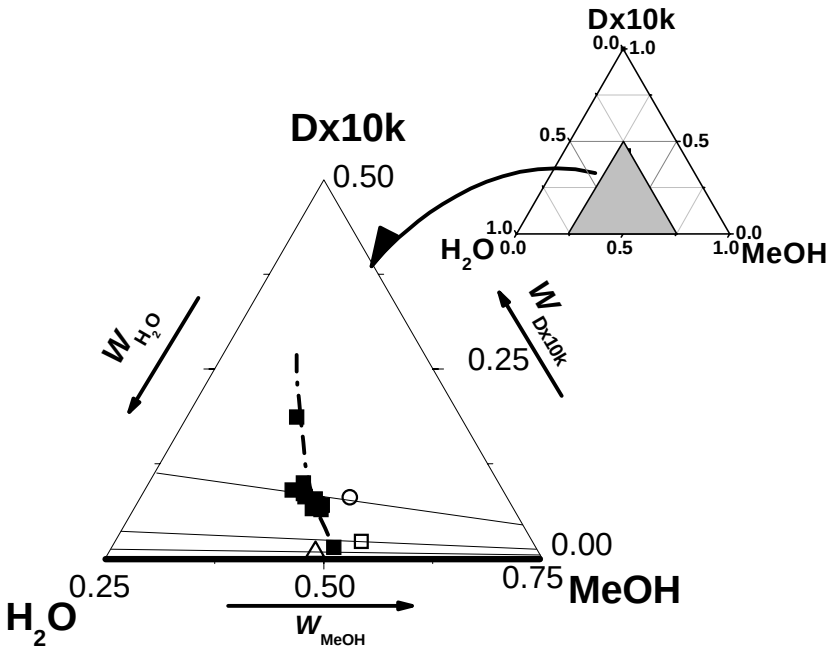

Figure 42. Part of the phase diagram of the system water/methanol/Dx10k that is relevant for CSF at room temperauture. Full squares represent the cloud points and the dashed line gives the expected cloud point curve for the original Dx10k. Open circle, triangle and square are WP of the fractionation No.1-3, 4 and 5, respectively. Lines are working lines.

During macroscopic phase separation the dextran contained in the gel phase starts to crystallize (because of the high polymer content), while the polymer that is present in the sol phase remains in solution. For fractionation this feature does not

represent a problem because it takes typically one hour for crystallization to set in. To regain the partially crystalline dextran of the gel phase for the next fractionation step it was redissolved in boiling water for about two hours and then freeze dried. Figure 43 shows the five fractionation steps that have been performed.

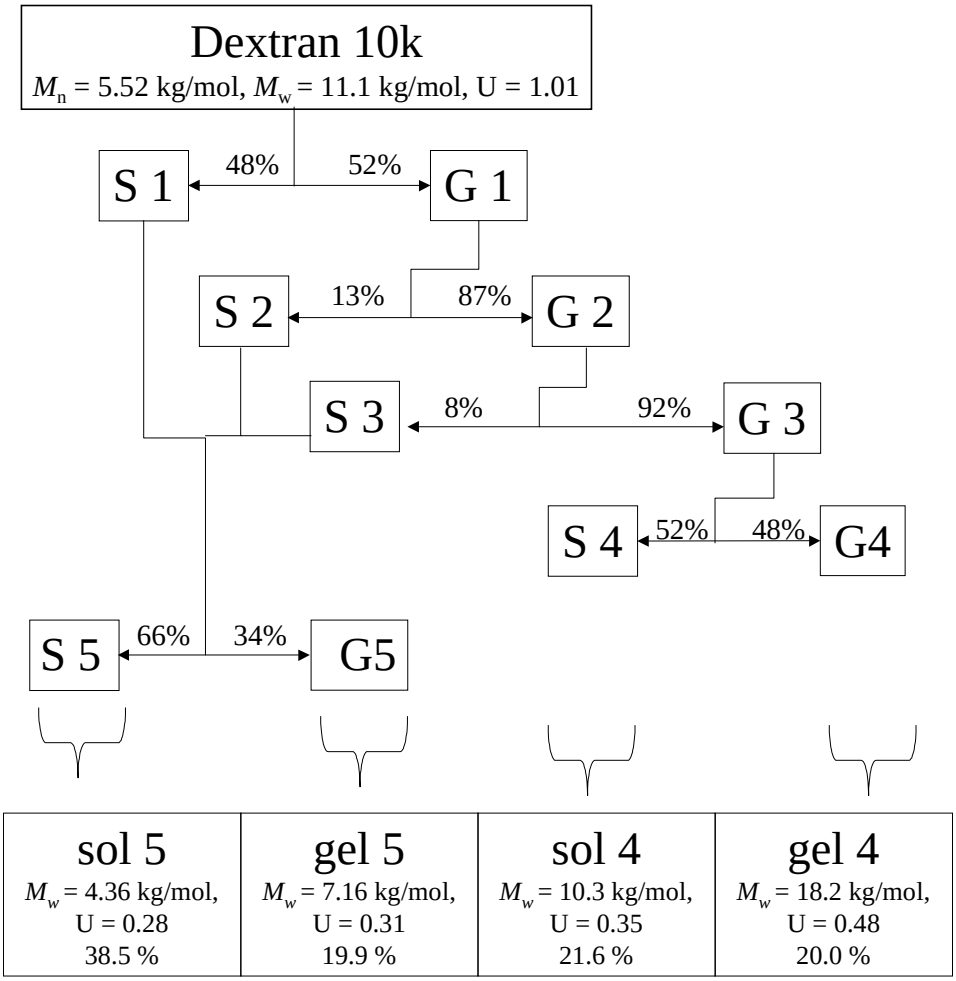

Figure 43. Scheme for the fractionation of 70 g of Dx10k. The percentage of the polymer contained in the feed that was found in the different phases is indicated. The sol fractions of the first three runs were combined and fractionated to yield sol 5 and gel 5; the gel fraction of run 3 was fractionated to result in sol 4 and gel 4. Weight average molecular weights and non-uniformities of the final products are also given.

For the first three CSF-runs, the same conditions were used, that is, FD:15wt% dextran in water, EA:100wt% methanol and WP:43wt%/49wt%/8wt% of water/ methanol/dextran. In the first CSF-run nearly the same fraction of the starting material

was found in the two phases. The polymer in the gel phase still contained considerable amounts of low molecular weight material. In order to take out the remaining short chain dextran this CSF run was repeated twice under the same conditions, using the previous gel fraction as starting material. The amount of polymer that can be found in the sol phase for the second and third CSF-run decreases because the miscibility gap expands (higher average molecular weight of the respective feed) and the working point is now located deeper inside the two phase region. In the third CSF-run only 8 wt % of the starting material was extracted into the sol phase. The sol fractions of the first three CSF-runs were combined due to their similar molecular weight distributions.

For the fourth CSF-run, which uses the gel fraction of the third run as starting material, the polymer concentration of the working point was reduced in order to transfer more polymer material into the sol phase and to produce a gel fraction that contains only the longest chains of the initial sample. The operation condition was FD:1.66 wt% dextran in water, EA:100 wt% methanol and WP:43 wt%/49 wt%/8 wt% of water/methanol/dextran. In a fifth CSF experiment we have removed the lower molecular weight components from the combination of sol fractions 1-3 at a total polymer concentration of 2 wt %.

Figure 44 shows the molecular weight distribution of the starting material and the four final fractions. The insert in the graph gives the molecular weights and the non-uniformity of the different samples showing that the molecular weight distribution has been significantly narrowed.

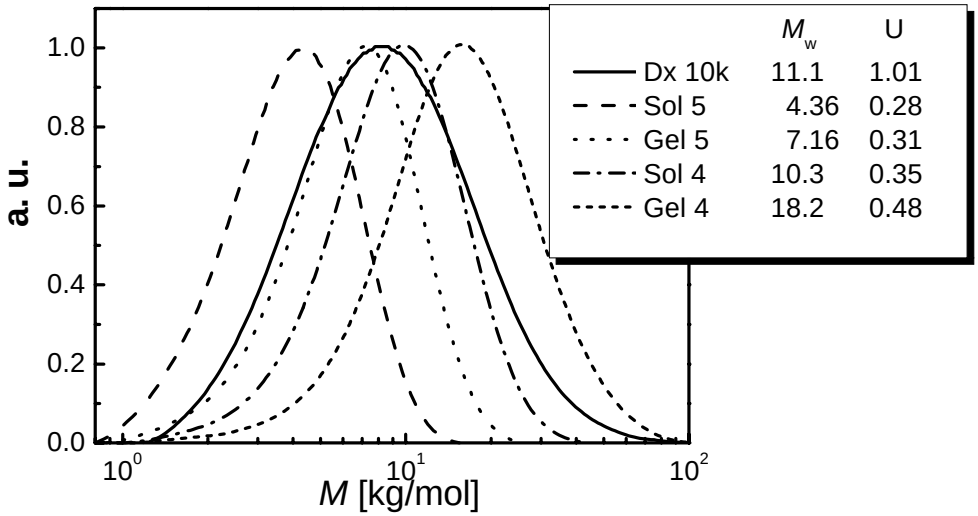

Figure 44. Molecular weight distributions of the initial Dx10k and of the four obtained fractions have been normalized to the same height. Weight average molecular weights and non-uniformities are indicated in the graph.

4.8.2 Dx70k

One CSF run was performed for Dx70k. Figure 45 shows cloud points, the critical point, the working line and the WP.

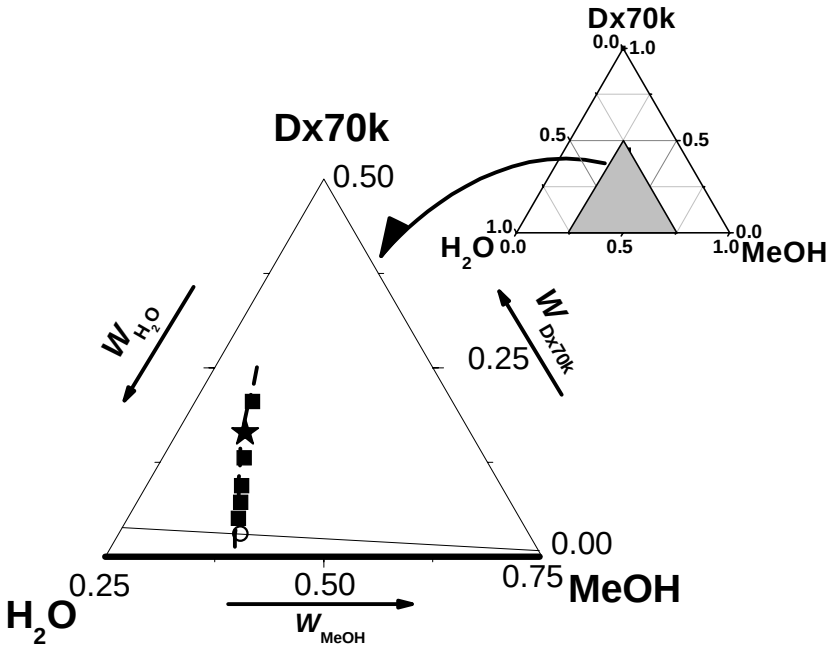

Figure 45. Part of the phase diagram of the system water/methanol/Dx70k relevant for CSF at room temperature. Symbols are the same as in Figure 42.

The operation conditions of CSF were FD: 5.4wt% dextran in water, EA: 100wt% methanol and WP: 58wt%/39wt%/3wt% of water/methanol/dextran. The fraction in the gel phase of Dx70k crystallizes much later than that of Dx10k at comparable compositions and temperatures. Figure 46 shows the molecular weight distributions of fractionations obtained under the same operating condition with different resting periods, (1 day, 2 days and 5 days). The gel fractionations kept for one day and two days did not crystallize, but after five days it crystallized. Figure 46 indicates that the sol phase separated one day after mixing contains a larger fraction of the original polymer as compared with five days of standing. The reason why the longer resting periods leads more polymer in the gel phase might be the temperature change during the resting periods. As the fractionation was performed in winter, the temperature during night should be lower than day. Therefore during the night, some polymer contained in the sol phase is precipitated (UCST) and migrates to the gel phase. This temperature influence is so large that in order to control the conditions for fractionation, it is necessary not only to consider the compositions of WP, FD and EA but also to control the temperature during the resting periods.

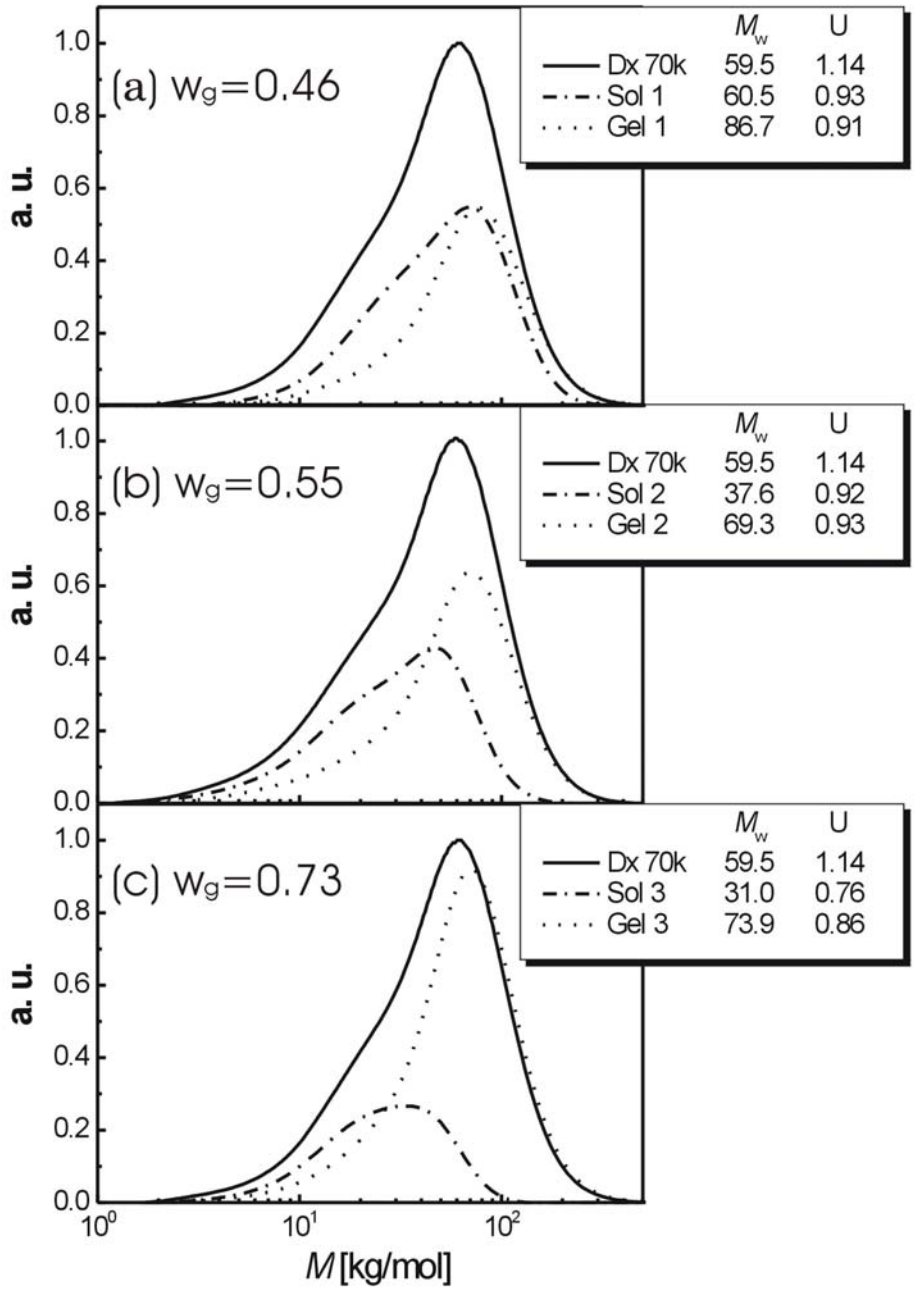

Figure 46. Molecular weight distributions of the initial Dx70k and the fractions obtained are normalized to the yields of the fractions. The resting periods before the separation is one day(a), two days(b) and five days(c), respectively. Weight fraction of the original polymer content in the gel phase(w_g), weight average molecular weights and non-uniformities are indicated in the graph.

4.8.3 Dx10000k

Figure 47 shows the cloud points, the working line and the WP of discontinuous fractionation, i.e. the fractionation scale was about 10ml of total mixture. Figure 48 represents the molecular weight distribution of the original sample and fractions from the discontinuous fractionation. The operation conditions of discontinuous fractionation were FD:4.7wt% dextran in water, EA:100wt% methanol and WP:57wt%/40wt%/3wt% of water/methanol/dextran

One CSF run has been made for Dx10000k, but it was not successful due to the high viscosity of the FD. The FD did not disperse evenly over the EA; instead of isolated droplet, coalescent threads are made. Two procedures were introduced in order to solve this problem One is to reduce the speed of pumping the FD (<<5mL/min). For Dx10k and Dx70k, the FD was pumped about 20mL/min. But for the highly viscous FD of Dx10000k, the pumping speed should be lower. Another solution is to pump the solutions in reverse way, that is: pump the EA into the FD. As is reported from the fractionation of hyaronic acid,[93] this way works even for the highly viscous FDs.

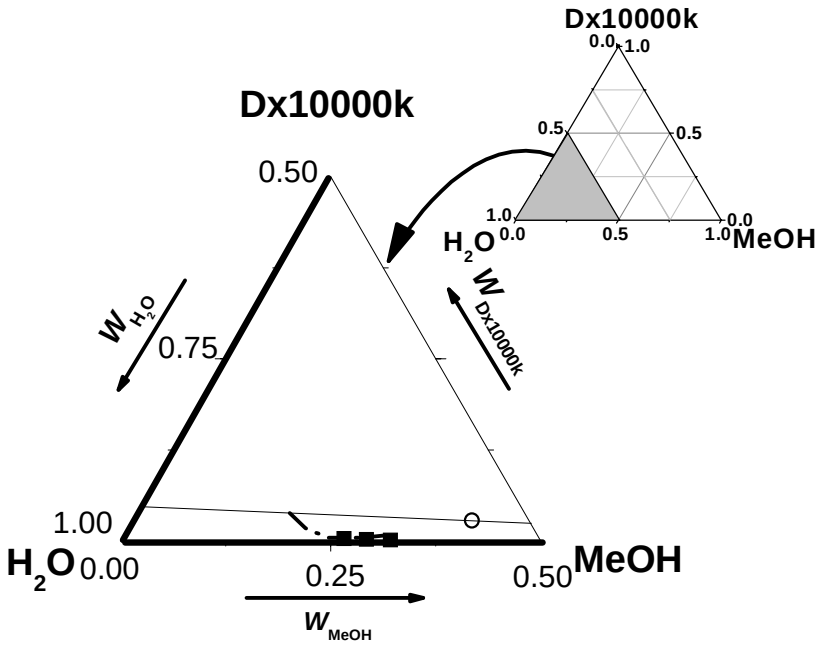

Figure 47. Part of the phase diagram of the system water/methanol/ Dx10000k relevant for discontinuous fractionation at room temperature. Symbols are same as in Figure 42.

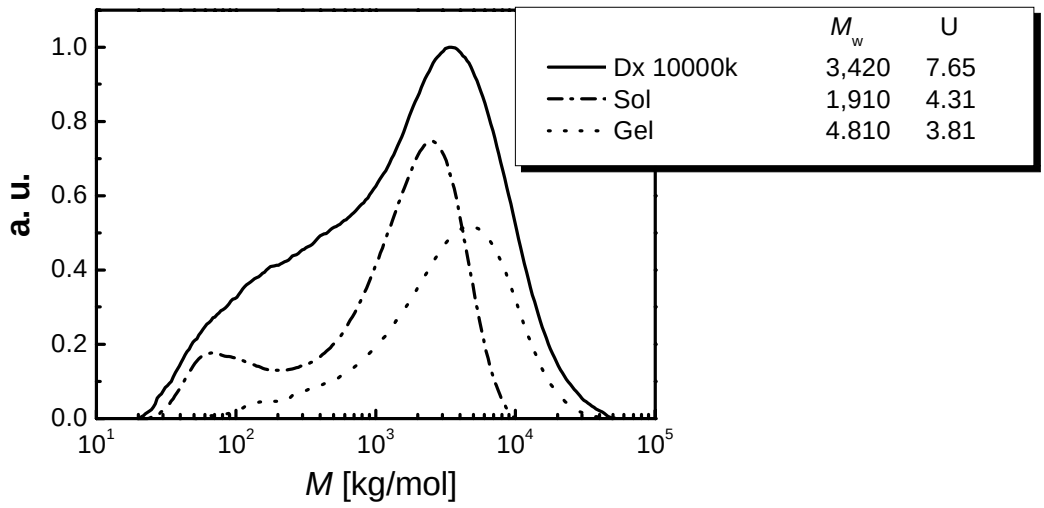

Figure 48. Molecular weight distributions of the initial Dx10000k and the fractions obtained are normalized to the yields of the fractions (sol: 65.8%, gel 34.2%). Weight average molecular weights and non-uniformities are indicated in the graph.

5 Conclusions

The applicability of the new approach of "Chain Connectivity and Conformational Variability" to biopolymers was verified. It was confirmed that the new approach is applicable for the solutions of dextran, a chain polymer with some short branches. Its applicability to the solution of BSA, a globular polymer is still questionable.

For the system water/dextran, the system specific parameters α, ζ and λ were determined from dilute solution information and they reasonably describe the phase diagram for the system water/methanol/dextran. Different parameter set was obtained from vapor pressure measurements. These data were less suited for the modeling of the ternary system.

For the system water/BSA, only partial information for the determination of the specific parameters was obtained from the information on the dilute solutions and it was necessary to guess the values to some extent. The chosen parameter set describes the measured vapor pressures in a realistic manner but it only qualitatively represents the phase diagram for the system water/dextran/BSA. The reason could be that the parameter sets chosen were not correct or that the new theory is in its present form not applicable for globular polymers. Additional investigation including an answer to a question whether globular polymers like BSA follow the new approach is necessary.

For further experimentation, dextran of low molecular weight (Dx10k) was efficiently fractionated by means of Continuous Spin Fractionation (CSF). Five fractionation steps yielded from the starting polymer with a molecular non-uniformity $U=(M_w/M_n)-1=1.0$ to four fractions with U values ranging from 0.28 to 0.48. It was also confirmed that CSF worked for the dextran in the mild-range of molecular weights (Dx70k). The high molecular weight dextran (Dx10000k) was efficiently fractionated on the small scale. But at the large scale, i.e. by means of CSF, it was not possible to fractionate due to the high viscosity of polymer solution (FD). This problem could be solved by reducing the pumping speed of FD and EA or by pumping the solutions in reverse way, i.e. pumping the EA into the FD.

6 Appendix

This chapter consists of three sections. 6.1 gives results of measurements concerning thermal diffusion of dextran; this work is submitted to *Biomacromolecules* for publication. 6.2 documents the data used for the different graphs of phase diagrams and vapor pressures. It also contains vapor pressure data for the system water/ Dx10000k, not used for modeling. 6.3 presents the list of symbols.

6.1 Thermal Diffusion of Dextran in Aqueous Solutions in the Absence and the Presence of Urea

*Publication submitted to Biomacromolecules (Aug. 2005)

*Authors:

Rei Sugaya[1] and Bernhard. A. Wolf[1]
[1]*Institut für Physikalische Chemie, Johannes Gutenberg-Universität Mainz, Jakob-Welder-Weg 13, D-55099 Mainz, Germany*

Rio Kita[2,3]
[2]*Max-Planck-Institut für Polymerforschung, Ackermannweg 10, D-55128 Mainz, Germany*

and [3]*Department of Physics, Tokai University, Hiratsuka 259-1292, Japan*

Abstract

The Ludwig-Soret effect was studied for aqueous solutions of dextran in the temperature range $15 < T < 55$ ^{o}C taking into account the effect of the addition of urea. In the absence of urea, the Soret coefficient S_T changes sign; it is positive for $T > 45.0$ ^{o}C, but negative for $T < 45.0$ ^{o}C. The positive sign of S_T means that the dextran molecules migrate towards the cold side of the fluid; this behavior is typical for polymer solutions, while a negative sign indicates the macromolecules move toward the hot side. The addition of urea to the aqueous solution of dextran rises S_T and reduces the inversion temperature. For 2 M urea the change in the sign of S_T is observed at $T = 29.7$ ^{o}C and beyond that value S_T is always positive in the studied temperature range. To rationalize these observations it is assumed that the addition of urea leads to an opening of hydrogen bonds similar to that induced by an increase in temperature.

6.1.1 Experiment

Sample

Dextran (Dx70k) was fractionated by Continuous Spinning Fractionation using water as a good solvent and methanol as a poor solvent. One fraction was used in this study and the weight- and the number-averaged molecular weight of dextran were determined as M_w=86.7 kg/mol and the non uniformity U= M_w/M_n-1=0.9 by GPC. Deionized water (milli-Q) was used as solvent. Urea was purchased from Acros Organics (New Jersey, U.S.A.). In this study, 1.0 g/L, 5.0 g/L and 10.0 g/L dextran in water and solutions of 5.0 g/L dextran in urea/water mixtures with different urea compositions were prepared with a trace amount of the dye, Basantol Yellow 215 (BASF). The absorption spectra of the dye in the solution of dextran/urea/water agreed well with the solutions of dextran/water and urea/water which indicates no special contributions of the dye to the system. Detailed descriptions about the absorption spectra were presented in Ref[55]. The sample solutions were filtered directly into a quartz cell for TDFRS experiments through 0.22 μm membrane filter (Millipore).

Methods

The experimental setup for TDFRS has been described in detail elsewhere.[55,94] In brief, the interference grating is written by an argon ion laser operating at the wavelength of λ=488 nm. The grating was read out by a He-Ne laser (λ=632.8 nm). A rectangular quartz cell with a path length of 0.2 mm (Hellma) was used for sample solutions. The intensity of the diffracted beam was measured by a photomultiplier. A mirror mounted on a piezocrystal was used for phase shifting and stabilization to obtain the heterodyne signal. TDFRS measurements were carried out at the temperature range from 15 ^{o}C to 55 ^{o}C, where the temperature of the sample cell was controlled by circulating water from a thermostat with an uncertainty of 0.01 ^{o}C.

In order to determine the Soret coefficient, the refractive index increments with respect to mass fraction ($\partial n/\partial w$) and to the temperature ($\partial n/\partial T$) have to be determined separately. The quantities $(\partial n/\partial w_1)_{P,\ T,\ w_2}$, $(\partial n/\partial w_2)_{P,\ T,\ w_1}$ and $(\partial n/\partial T)_{P,\ T,\ w_2}$ were measured by means of a scanning Michelson interferometer operating at a wavelength of 632.8 nm.[95-97] The values of ($\partial n/\partial w$) were measured at room temperature and ($\partial n/\partial T$) were obtained from interference signals in the temperature range of ± 0.5 K for the respective points. [98]

The diffusion coefficient of dextran in homogeneous solutions was measured for comparison purposes by dynamic light scattering (DLS) using a Kr-ion laser as the light source (λ =647.1 nm) and an ALV-5000E correlator to obtain correlation functions of scattered light. A cylindrical cell, having an inner diameter of 18 mm, was placed in a thermostatted bath, the temperature of which was controlled to ± 0.01 ^{o}C. The sample solution was filtered directly into the cylindrical cell through 0.22 μm membrane filter (Millipore). The sample solutions were kept at the measurement temperature for at least 1 hour to ensure equilibrium before starting data acquisition.

6.1.2 Results and Discussion

Contrast factors

Refractive index increments with respect to the mass fraction (∂n/∂w) for the systems of dextran in water with and without urea are shown in Table XV. ($\partial n/\partial w$) of urea in water was obtained from CRC Handbook of Chemistry and Physics[99] and is also shown in this table. Typical results of temperature dependence of ($\partial n/\partial T$) for the systems of 5.0 g/L dextran in water and 5.0 g/L dextran in urea/water are displayed in Figure 49. The values of ($\partial n/\partial T$) for 1.0 g/L, 5.0 g/L and 10.0 g/L dextran in water were identical within the experimental uncertainty in the measured temperature range.

Table XV. Refractive index increments with respect to the mass fraction $(\partial \mathrm{n}/\partial \mathrm{w}_2)_{P,\,T,\,\mathrm{w}_1}$ of dextran in the mixed solvent of 0, 2, and 5 M urea in water as well as $(\partial \mathrm{n}/\partial \mathrm{w}_1)_{P,\,T}$ of urea in water. The value was obtained from Ref.[99]

solution	$\partial n/\partial w$
dextran in water	0.1340
dextran in 2 M urea / water	0.1252
dextran in 5 M urea / water	0.1089
urea in water[(a)]	0.1583

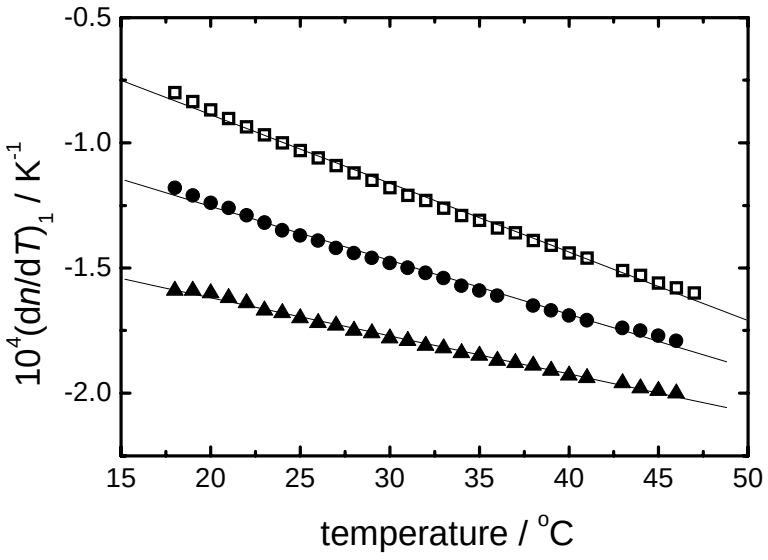

Figure 49. Refractive index increment with respect to the temperature $(\partial n/\partial T)_{P,w_1}$ for a solution of dextran (5.0 g/L) in the mixed solvent urea/water as a function temperature, where the urea concentrations in water are 0 M (□), 2 M (●) and, 5 M (▲).

Binary system of dextran in water

The temperature dependences of the Soret coefficient, S_T, of the diffusion coefficient, D, and of the thermal diffusion coefficient, D_T, are shown in Figures 50 and 51 for 1.0 g/L, 5.0 g/L and 10.0 g/L dextran in water. These values were obtained by a least squares fit of the experimental heterodyne signals ζ_{het} to Eq. 49. The error bars mean one standard deviation. At 45.0 °C the sign of S_T and D_T changes from negative to positive as T is raised. At $T > 45$ °C the dextran molecules migrate to the cold side of the fluid, as is typical for polymer solutions ($S_T > 0$), while at $T < 45$ °C they migrate to the warm side ($S_T < 0$). This seems to be the first observation of a change in sign for a polymer solution in pure water. The magnitude of S_T does not show any significant concentration dependence under the present experimental condition, consequently the above inversion temperature is identical for all concentrations measured. The diffusion coefficients of dextran in water at 25 °C obtained from TDFRS experiment are $D = 2.63 \times 10^{-7}$ cm^2/s for 1.0 g/L and $D = 2.98 \times 10^{-7}$ cm^2/s for 5.0 g/L; these data agreed well with those from DLS measurement, which are $D = 2.77 \times 10^{-7}$ cm^2/s for 1.0 g/L and $D = 3.16 \times 10^{-7}$ cm^2/s for 5.0 g/L. The diffusion coefficient was not obtained at $T = 45$ °C by TDFRS experiment where the signs of S_T and D_T change. Because the amplitude of

heterodyne signal of TDFRS vanishes at this temperature, the diffusion coefficient cannot be evaluated [cf. Eq. 49].

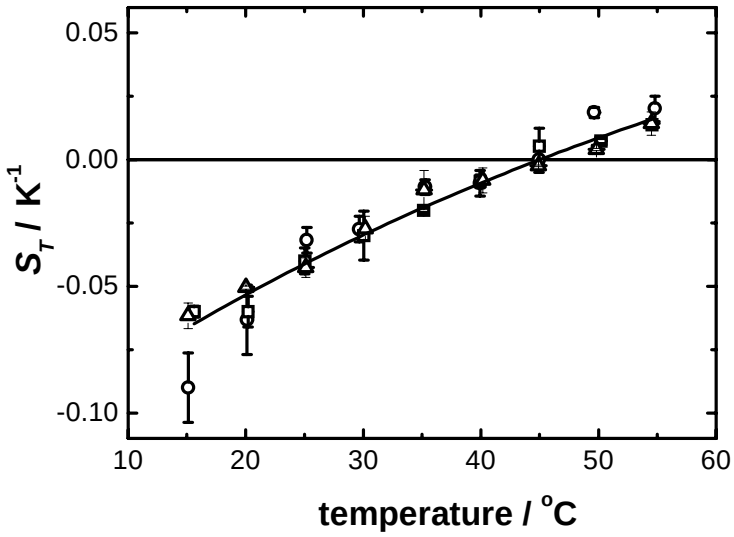

Figure 50. Soret coefficient, S_T, for aqueous dextran solutions of dextran of 1.0 g/L (○), 5.0 g/L (□) and 10.0 g/L (△), respectively, as a function of temperature. The solid line is fitted according to Eq. 77.

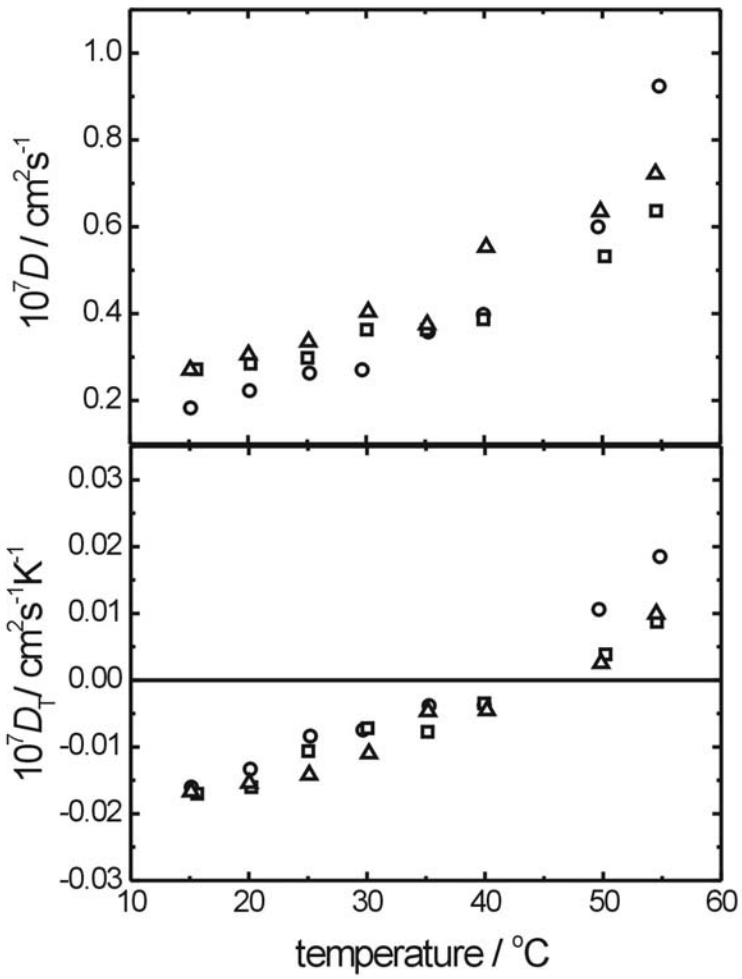

Figure 51. Soret coefficient, S_T, for aqueous dextran solutions of dextran of 1.0 g/L (○), 5.0 g/L (□) and 10.0 g/L (△), respectively, as a function of temperature. The solid line is fitted according to Eq. 77.

The curve describing the temperature dependence of the Soret coefficient in Figure 51 was obtained by a least squares fit to the empirical equation proposed by Iacopini and Piazza[100] as

$$S_T(T) = S_T^{\infty}\left[1-\exp\left[\frac{T_{inv}-T}{T_0}\right]\right] \tag{77}$$

Here, S_T^{∞} represents a saturation value of S_T at high temperature, T_{inv} is the temperature where S_T changes the sign, and T_0 indicates to the strength of temperature effects. The parameters obtained by means of Eq. 77 will be presented and discussed in the next section, which deals with the ternary system dextran/urea/water.

A thermally induced change in the sign of S_T was reported for solutions of poly(*N*-isopropylacrylamide) (PNiPAM) in ethanol where S_T was identical for both the dilute and the semidilute solutions.[101] It should be mentioned that S_T changed from positive to negative with increasing temperature, i.e., the slope of S_T versus temperature is opposite to that observed in the present study. Furthermore, ethanol is good solvent for PNiPAM at all temperatures according to the second virial coefficients obtained by static light scattering. The other systems which show thermally induced changes in the sign of S_T are solutions of PEO in ethanol/water[55] and of lysozyme in a sodium acetate buffer with added sodium chloride.[100] For these systems the slope is positive and thus agrees with the result obtained for the dextran solutions. The difference in the slope is probably related to the choice of solvent, i.e., water as the major component of solvent has a positive slope, while alcohol system yields negative one. It was suggested for low molecular mixtures that the simple energetic consideration for water systems qualitatively explains the sign change behavior,[102] whereas for alcoholic systems the energetic argument needs to be complemented with taking into account an entropic contribution.[103]

The exothermal Θ-temperature for aqueous dextran solutions is 44.7 ^{o}C and the solubility decreases by heating.[104,105] The solubility of polymers in water is closely related to the formation of hydrogen bonds, which shows a strong temperature dependence. The strength of hydrogen bonding is weakened by heating, thus the solubility of dextran becomes poorer. [106]Surprisingly, the Θ-temperature of dextran is in good agreement with the sign inversion temperature T_{inv}. At theta conditions the mixture is in a pseudo-ideal condition, i.e. the polymers are in the boundary between good and bad solvents where they behave as an unperturbed chain. Under these conditions it is speculated that the dextran molecules do not distinguish the gradient, thus they are not brought into a certain direction. The pseudo-ideal behavior refers to the Gibbs free energy of dilution and not to the heat of mixing. In order to clarify this hypothesis one needs to study various systems at theta condition with taking into account these thermodynamic parameters of polymer solutions. In a recent report concerning aqueous solutions PNiPAM, having a LCST with the second virial coefficient being zero at 30.6 ^{o}C, did not show any sign change of S_T in the temperature range 20 ^{o}C $<T<$ 38 ^{o}C.[107] PEO solutions in pure water exhibit a lower critical solution temperature (LCST) at around 100 ^{o}C[108] and show no sign change of S_T in the accessible temperature range (18 ^{o}C $< T <$ 38 ^{o}C).[55] These findings demonstrate that the coincidence of the inversion temperature of the present system with its theta temperature is not general. Further considerations in regard to the contribution of hydrogen bonding will be presented in the next section dealing with the effect of urea as a hydrogen bonding breaker.

Ternary system of dextran in urea/water mixture

Figure 52 presents typical normalized TDFRS signal of 5.0 g/L dextran in the solvent of 2 M urea/water as a function of time after the intensity grating has been switched on at time t=0. The insets show the same data on a semi logarithmic time scale. The linear plots include data from the rapid increase of $\zeta_{het}(t)$ as the temperature modulation is established on the time scale τ_{th}, which is less than 1 ms. For later times, two mode behavior was observed on typical time scales of $\tau_1 \sim 10^{-3}$ s and $\tau_2 \sim 10^{-1}$ s. This can be seen clearly in the semi logarithmic plots of $\zeta_{het}(t)$, where the signals of the establishment of the temperature modulation has been omitted for clarity. The solid and dashed lines in the insets were obtained by a least squares fit to Eq. 50 and represent the fast and the slow mode, respectively.

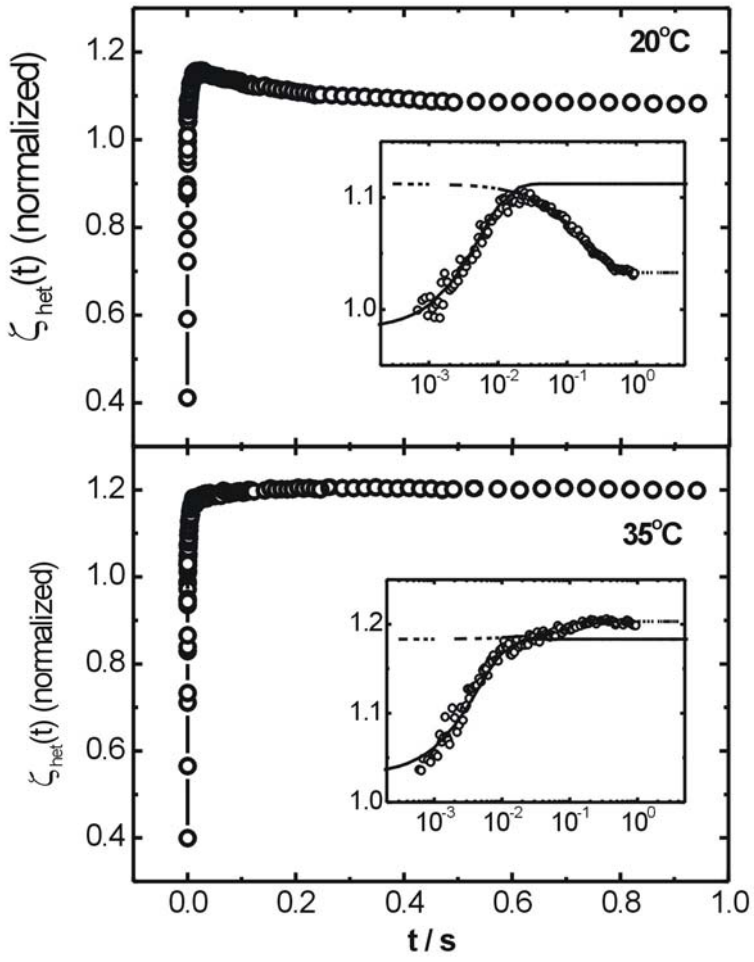

Figure 52. Typical normalized TDFRS signals of solutions of dextran (5.0 g/L) in the mixed solvent 2 M urea/water at 20.0 °C and at 35.0 °C. The insets show semi logarithmic plots in which the curves were obtained by fitting to Eq. 50 with the fast mode (full line) and slow mode (dashed line).

Figure 53 shows the Soret coefficient, S_T, the diffusion coefficient, D, and the thermal diffusion coefficient, D_T, obtained from the fast mode for the ternary system (filled symbols). Open symbols correspond to the values obtained from a 2 M and a 5 M solution urea in water; these data agreed well with the values obtained from the fast mode of ternary system. This finding suggests that the fast mode observed in the ternary system is associated with the diffusive mode of the solvent, i.e. the urea/water mixture. The diffusion coefficient of urea obtained from TDFRS experiment is in a good agreement with the reported value D= 1.38x10^{-5} cm^2 s^{-1} at 25 ^{o}C.[109] In the previous report for the ternary system of PEO in the mixed solvent ethanol/water, we also observed a similar two mode behavior with TDFRS experiments.[55] The respective modes were interpreted as the development of the concentration gradient for ethanol/water (fast mode), and the formation of the concentration gradient of PEO in the mixed solvent (slow mode). In analogy to PEO/ethanol/water, the fast observed in this study is associated with the concentration gradient of urea/water, while the slow mode corresponds to the signal of the concentration gradient of dextran in the mixed solvent. The positive value of Soret coefficient means that the urea molecules migrate to the cold side of the fluid. In the measured temperature range the values of S_T, D and D_T for 5 M urea solution tend to be larger than those of 2 M urea. However, we do not discuss the concentration and temperature dependences of resultant values obtained from the fast mode because of large uncertainty due to experimental difficulties for this aqueous solution and lack of experimental data for comparison. In Figure 52 the signal intensity of the slow mode (dashed line) decreases with time at 20 ^{o}C, whereas at 35 ^{o}C it increases. This observation implies a change in the sign of the Soret coefficient, where the slow mode corresponds to the establishment of concentration gradient of dextran molecules in the mixed solvent as mentioned above.

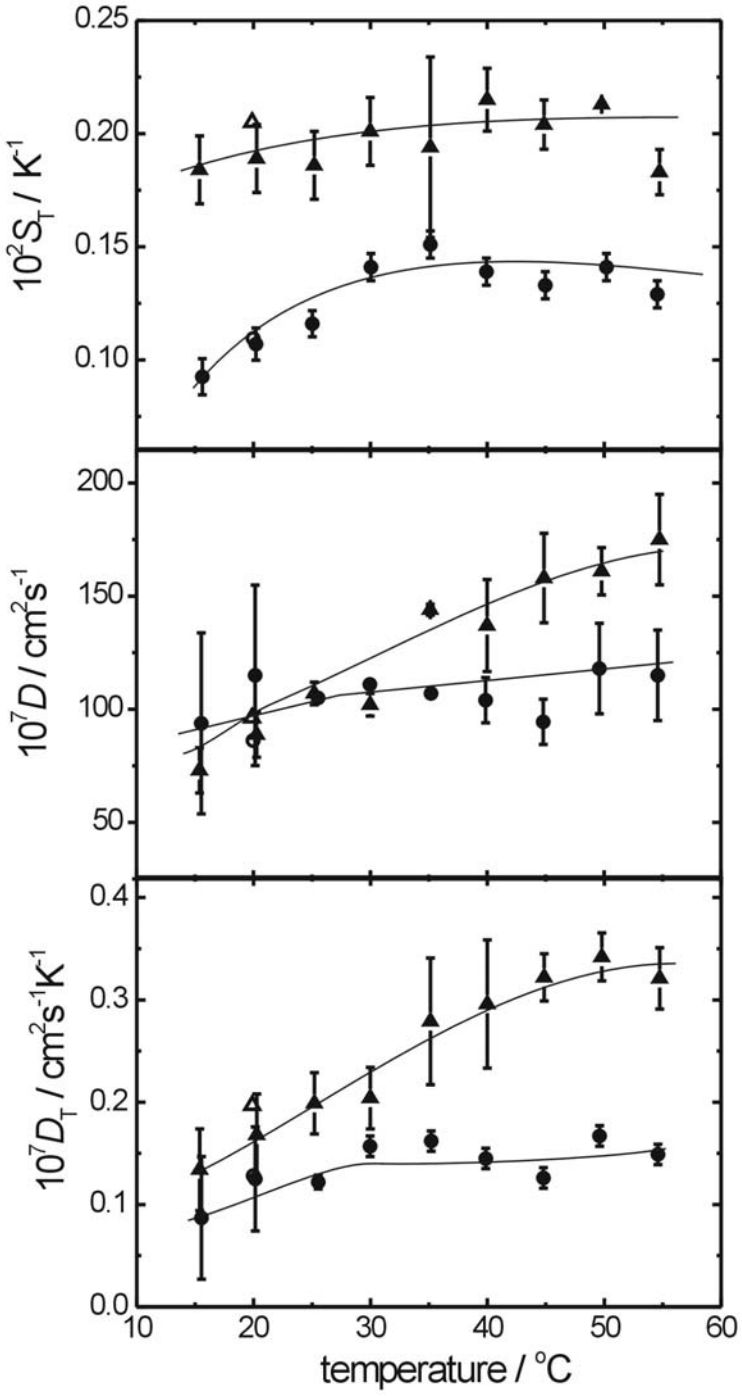

Figure 53. Soret coefficient, S_T, diffusion coefficient, D, and thermal diffusion coefficient, D_T, of urea as a function of temperature. Full symbols correspond to the results obtained from the fast mode for the ternary systems, dextran in 2 M urea/water (●) and dextran in 5 M urea/water (▲). The open symbols correspond to the results for the binary systems of 2 M urea in water (○) and 5 M urea in water (△).

Figure 54 shows the temperature dependence of the Soret coefficient obtained from the slow mode by a least squares fit to Eq. 50 for a solution of 5.0 g/L dextran in the mixed solvent. In the same way, the diffusion coefficient and the thermal diffusion coefficient of dextran were obtained as shown in Figure 55. The results for the binary solution of 5.0 g/L dextran in water (without urea) are also shown in Figures 54 and 55. A change in the sign of S_T was observed at 0M and 2M urea/water solvents. The corresponding temperatures are 45.0 ^{o}C for 0M urea and 29.7 ^{o}C with the addition of 2M urea. No inversion was found in the case of 5M urea within the measured temperature range. The diffusion coefficient D of dextran increases with increasing temperature, while the urea concentration dependence of D was not observed. As mentioned previously, the diffusion coefficient D of dextran obtained by TDFRS experiment is in good agreement with the results of DLS. The temperature dependence of thermal diffusion coefficient D_T showed similar tendency with the Soret coefficient, i.e. with increasing urea concentration the value of D_T increases and the inversion temperature T_{inv} shifts to lower values; for 5 M urea D_T does not have T_{inv}.

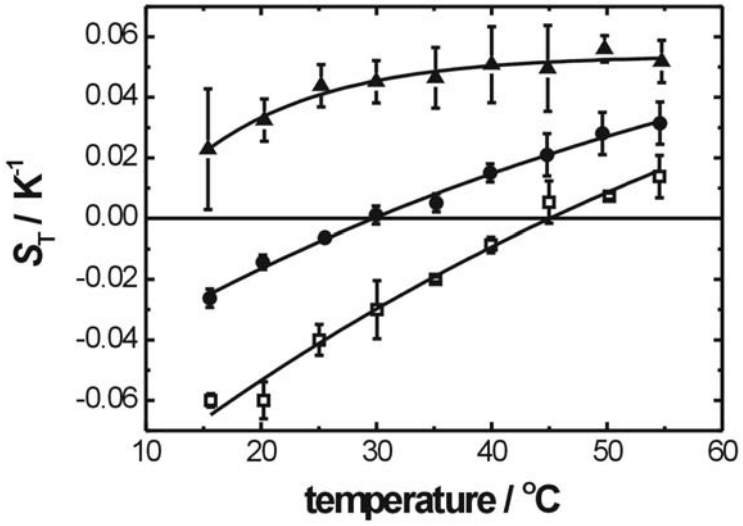

Figure 54. Soret coefficient, S_T, for solutions of dextran (5.0 g/L) as a function of temperature. Full symbols correspond to the values obtained from the slow mode for the ternary systems of dextran in 2 M urea/water (●) and of dextran in 5 M urea/water (▲). Open symbols represent the results for the binary system of dextran in water (□). The solid lines are fitted according to Eq. 77.

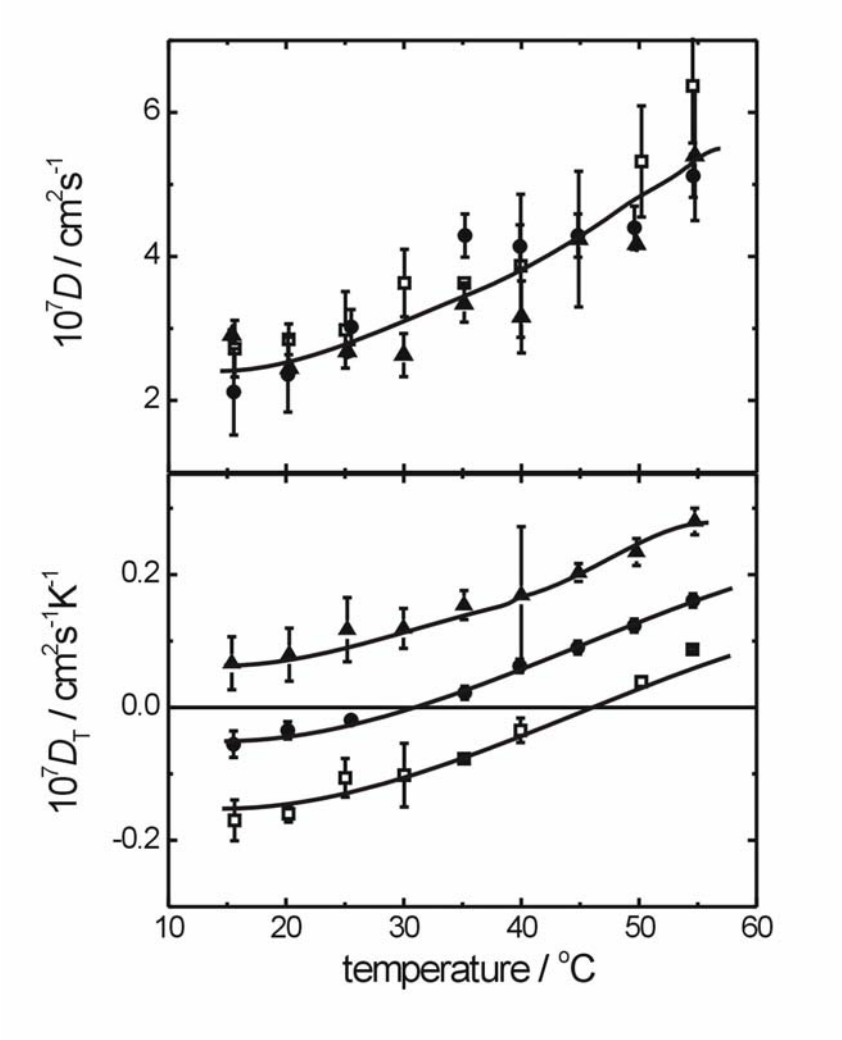

Figure 55. Diffusion coefficient, *D*, and thermal diffusion coefficient, D_T, for solutions of dextran (5.0 g/L) as a functions of temperature. Full symbols correspond to the values obtained from the slow mode for the ternary systems of dextran in 2 M urea/water (●) and of dextran in 5 M urea/water (▲). Open symbols represent the results for the binary system of dextran in water (□).

Fitting curves in Figure 54 for the Soret coefficient were obtained by a least squares fit to Eq. 77. The urea concentration dependence of the sign change temperatures T_{inv} were 45.0 °C (0 M), 29.7 °C (2 M), and 9.3 °C (5 M), although the temperature of 9.3 °C could not be achieved in the experiments. The asymptotic value of the Soret coefficient S_T^∞ of dextran decreases from 0.13 via 0.10 to 0.05 K^{-1} and the parameter T_0 declines from 71.4 via 63.5 to 11.1 K as the urea content is raised from 0M via 2M to 5M. For lysozyme solutions it is reported that the values of S_T^∞ and T_0 decrease with increasing the ionic strength of the solution.[100] The decreasing behaviors of S_T^∞ and T_0 with increase of ionic strength for lysoyzme solutions have a similar trend

to those with increase of the concentration of urea for dextran solution. It indicates existence of analogue mechanism of sign change behavior. However, in the lysozyme solution, electrostatic forces have a dominant role for the solution properties which could be different from the effect of urea for dextran molecules. As mentioned in the previous section for the binary system dextran/water, the strength of hydrogen bonding is weakened by heating which yields positive values of the Soret coefficient. In this study for the ternary system dextran/urea/water, the negative values of the Soret coefficient tends to become positive upon the addition of urea; this effect is analogous to that resulting from an increase in temperature. This observation implies that urea molecules destroy local structures of water, i.e. the addition of urea has a similar contribution with heating for the sign change behavior of dextran solution.

From the fact that solutions of PNiPAM in water did not show any sign change of S_T upon heating, even when passing through the Θ-temperature where liberation of solvated water takes place according to the consequence of the coil-globule transition of it, we conclude that there are no systematic trends for sign change behavior among these systems. The results suggest that chemical nature of polymers and the structure of water have complicated contributions for the sign change behavior and which is a sort of system dependence phenomena. The sign inversion behavior of S_T is diminished by the addition of urea. Although the role of urea for destroying the local water structure is still controversial,[110-116] it indicates that the thermal diffusion behavior is largely affected by the modification of local structures of water, i.e. a modification of short range interactions has a dominant role for the sign inversion of Soret coefficient of aqueous solutions of dextran.

Recently, inversions in S_T were studied by means of MD methods for aqueous solutions, where the sign change of alcohol/water mixtures was attributed to the strength of the molecular interactions.[117] By a thermodynamic consideration Ki and Wu predicted the sign change for the systems of ionic solutions.[118] At the present stage it is not clear whether these approaches established for associating solutions can be adopted for aqueous polymer systems. Semenov and Schimpf developed a theoretical model of thermal diffusion considering molecular interactions that depend on the temperature-induced pressure gradient.[119] According to these authors the Soret coefficient for polymer solutions should change sign, if the Hamaker constant between the solvent and the solute satisfies a certain condition. It is of interest to apply their theory for aqueous polymer solutions, whether the sign change behavior can be evaluated. However, in order to examine it one needs to acquire physical parameters of the aqueous solution of dextran for the calculations.

6.1.3 Conclusion

The thermally induced sign change of the Soret coefficient for dextran solutions in water was found at the temperature 45.0 ^{o}C. The temperature above 45.0 ^{o}C dextran molecules migrate toward the cold side of the fluid (S_T >0), whereas below 45.0 ^{o}C dextran molecules migrate toward the hot side (S_T <0). When urea is added to the solution, the value of Soret coefficient becomes large and the sign change temperature shifted to lower temperatures. The addition of urea makes the sign of S_T more positive. These observations imply that the strength of hydrogen bonding is weakened with increasing temperature which has a similar contribution with the local structure change of water with the addition of urea.

Acknowledgement

We would like to thank Prof. Dr. Gerhard Wegner (Director, MPIP) for his kind support and Christine Rosenauer and Beate Müller for their experimental help. Sample donation from Polymer Standard Service GmbH (Mainz, Germany) is gratefully acknowledged.

6.2 Measured data

6.2.1 Phase diagrams

Table XVI. Cloud points for the system water/methanol/Dx10k at 25 ^{o}C (Figure 20).

	w_{MeOH}	w_{Dx10k}	w_{H_2O}
Cloud points	0.376	0.186	0.438
	0.427	0.099	0.474
	0.438	0.081	0.481
	0.465	0.064	0.471
	0.450	0.076	0.474
	0.459	0.070	0.471
	0.463	0.070	0.466
	0.419	0.090	0.491
	0.434	0.085	0.481
	0.451	0.078	0.471
	0.456	0.072	0.472
	0.454	0.065	0.480
	0.463	0.070	0.468
	0.504	0.014	0.481

Table XVII. Cloud points for the system water/aceton/Dx10k at 25 ^{o}C.

	w_{AC}	w_{Dx10k}	w_{H_2O}
Cloud points	0.286	0.079	0.635
	0.297	0.049	0.654
	0.307	0.033	0.661
	0.354	0.025	0.621
	0.182	0.302	0.516
	0.211	0.220	0.569
	0.272	0.176	0.552
	0.251	0.165	0.584
	0.244	0.147	0.609
	0.266	0.101	0.634

Table XVIII. Cloud points, swelling point and critical point for the system water/methanol/Dx70k at 25 ^{o}C (Figures 19 and 20).

	w_{MeOH}	w_{Dx70k}	w_{H_2O}
Cloud points	0.236	0.091	0.674
	0.241	0.072	0.687
	0.254	0.059	0.688
	0.167	0.291	0.542
	0.180	0.244	0.576
	0.186	0.208	0.607
	0.208	0.165	0.627
	0.211	0.125	0.664
	0.231	0.073	0.696
	0.243	0.048	0.709
	0.263	0.030	0.707
	0.262	0.013	0.725
Swelling point	0.054	0.946	0.000
Critical point	0.333	0.157	0.510

Table XIX. Cloud points, swelling point, critical point and tie lines for the system water/aceton/Dx70k at 25 ^{o}C (Figure 19).

	w_{AC}	w_{Dx70k}	w_{H_2O}
Cloud points	0.236	0.091	0.674
	0.241	0.072	0.687
	0.254	0.059	0.688
	0.167	0.291	0.542
	0.180	0.244	0.576
	0.186	0.208	0.607
	0.208	0.165	0.627
	0.211	0.125	0.664
	0.231	0.073	0.696
	0.243	0.048	0.709
	0.263	0.030	0.707
	0.262	0.013	0.725
Swelling point	0.054	0.946	0.000
Critical point	0.206	0.153	0.640
Tie line1	0.273	0.014	0.714
	0.115	0.456	0.430
Tie line2	0.287	0.039	0.674
	0.115	0.500	0.385
Tie line3	0.271	0.013	0.716
	0.125	0.313	0.562

Table XX. Cloud points for the system water/iso-propanol/Dx70k at 25 °C (Figure 18).

	w_{iPOH}	w_{Dx70k}	w_{H_2O}
Cloud points	0.274	0.066	0.659
	0.288	0.043	0.669
	0.300	0.027	0.672

Table XXI. Cloud points for the system water/ethanol/Dx70k at 25 °C (Figure 18).

	w_{EtOH}	w_{Dx70k}	w_{H_2O}
Cloud points	0.340	0.043	0.617
	0.350	0.023	0.627
	0.352	0.017	0.631

Table XXII. Cloud points for the system water/tetra-hydrofuran/Dx70k at 25 °C (Figure 18).

	w_{THF}	w_{Dx70k}	w_{H_2O}
Cloud points	0.389	0.071	0.541
	0.411	0.018	0.571

Table XXIII. Cloud points for the system water/acetic acid/Dx70k at 25 °C (Figure18).

	w_{AA}	w_{Dx70k}	w_{H_2O}
Cloud points	0.556	0.029	0.414
	0.572	0.017	0.411
	0.581	0.010	0.409

Table XXIV. Cloud points for the system water/dimethyl-acetamid/Dx70k at 25°C (Figure18).

	w_{DMAC}	w_{Dx70k}	w_{H_2O}
Cloud points	0.741	0.018	0.241
	0.767	0.010	0.223
	0.789	0.007	0.204

Table XXV. Cloud points and swelling point for the system water/methanol/ Dx10000k at 25 ^{o}C (Figure20).

	w_{MeOH}	$w_{Dx10000k}$	w_{H_2O}
Cloud points	0.291	0.002	0.706
	0.320	0.001	0.679
	0.264	0.003	0.733
Swelling point	0.028	0.972	0.000

Table XXVI. Cloud points and swelling point for the system water/aceton/ Dx10000k at 25 ^{o}C.

	w_{AC}	$w_{Dx10000k}$	w_{H_2O}
Cloud points	0.189	0.010	0.800
	0.206	0.006	0.788
	0.205	0.003	0.792

Table XXVII. Cloud points and tie lines for the system water/Dx2000k/BSA at 25 ^{o}C (measured by Yurij Antonov).

	w_{BSA}	w_{H_2O}	$w_{Dx2000k}$
Cloud points	0.343	0.656	0.001
	0.293	0.706	0.001
	0.239	0.751	0.010
	0.201	0.780	0.019
	0.157	0.808	0.035
	0.112	0.843	0.044
	0.081	0.862	0.057
	0.059	0.882	0.060
	0.013	0.912	0.075
	0.002	0.899	0.099
	0.002	0.875	0.124
	0.001	0.851	0.148
	0.001	0.685	0.314
Tie line1	0.171	0.669	0.160
	0.001	0.791	0.208
	0.716	0.283	0.000
Tie line2	0.232	0.666	0.102
	0.001	0.837	0.162
	0.609	0.391	0.001
Tie line3	0.253	0.666	0.081
	0.001	0.856	0.143
	0.578	0.422	0.001

Table XXVIII. Determination of the critical point for the system water/methanol/Dx70k at 25 ^{o}C (Figure 56). Because gel phase segregated crystals at higher concentration of dextran, it was not possible to determine the volume ratio of sol and gel phases.

w_{MeOH}	w_{Dx70k}	w_{H_2O}	V_{sol}	V_{gel}	$R= V_{sol} /V_{gel}$
0.368	0.108	0.524	0.759	0.241	3.158
0.379	0.081	0.540	0.809	0.191	4.231

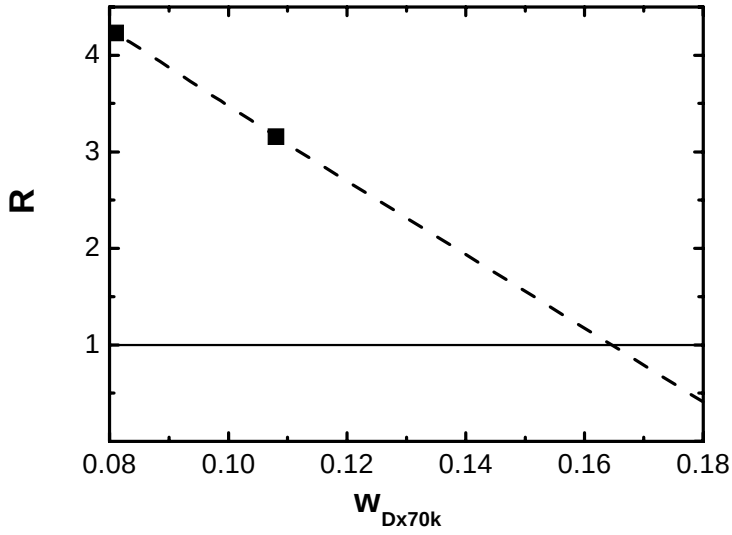

Figure 56. Determination of the critical point for the system water/methanol/Dx70k at 25 ^{o}C: R (the volume ratio of sol and gel phases, R= Vsol/Vgel) as a function of w_{Dx70k}. The dashed line gives the linear fit of $R(w_{Dx70k})$; R = -38.4* w_{Dx70k} +7.32. From the intersection of the linear fit to $R(w_{Dx70k})$=1, the critical point is obtained as w_{Dx70k}=0.165.

Table XXIX. Determination of the critical point for the system water/aceton/Dx70k at 25 ^{o}C (Figure 57).

w_{AC}	w_{Dx70k}	w_{H_2O}	V_{sol}	V_{gel}	$R= V_{sol} /V_{gel}$
0.208	0.188	0.604	0.329	0.671	0.490
0.219	0.160	0.621	0.444	0.556	0.797
0.251	0.089	0.660	0.690	0.310	2.227

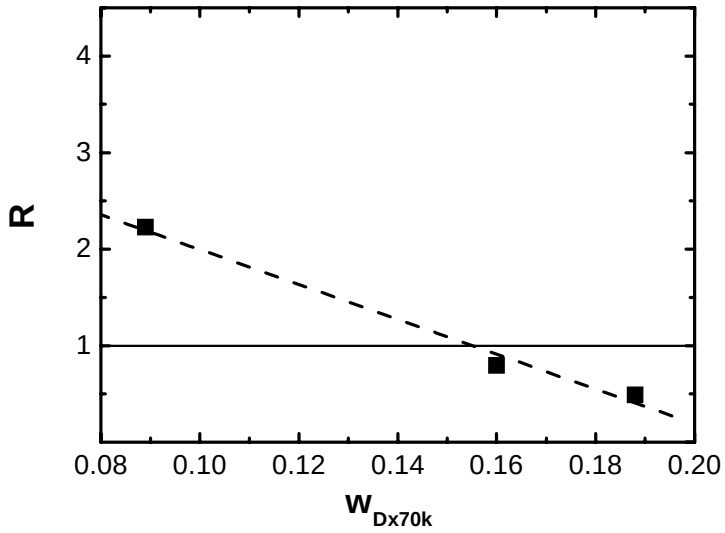

Figure 57. Determination of the critical point for the system water/aceton/ Dx70k at 25 ^{o}C: R (the volume ratio of sol and gel phases) as a function of w_{Dx70k}. The dashed line gives the linear fit of R(w_{Dx70k}); R = -18.0* w_{Dx70k} +3.79. From the intersection of the linear fit to R(w_{Dx70k})=1, the critical point is obtained as w_{Dx70k}=0.155.

6.2.2 Vapor Pressures

Table XXX. Vapor pressures for the system water/Dx70k at 25 °C for different standing times (Figure 22).

Standing time	φ_{Dx70k}	P/P_0	Error (P/P_0)
1 day	0.940	0.000	0.000
	0.931	0.097	0.003
	0.848	0.384	0.033
	0.781	0.707	0.016
	0.713	0.741	0.025
	0.594	0.893	0.035
	0.387	0.994	0.040
1 week	0.950	0.044	0.001
	0.933	0.115	0.002
	0.851	0.392	0.032
	0.777	0.665	0.021
	0.718	0.808	0.014
	0.596	0.972	0.004
	0.387	0.994	0.028
3 weeks	0.975	0.055	0.005
	0.933	0.127	0.007
	0.857	0.343	0.018
	0.777	0.641	0.040
	0.718	0.710	0.043
	0.596	0.893	0.054
	0.387	0.952	0.054

Table XXXI. Vapor pressures for the system water/Dx10000k at 25 °C for different standing times (Figure 58).

Standing time	$\varphi_{Dx10000k}$	P/P_0	Error (P/P_0)
1day	0.957	0.059	0.005
	0.928	0.123	0.007
	0.842	0.531	0.023
	0.778	0.638	0.047
	0.718	0.745	0.102
	0.595	0.894	0.063
	0.414	1.001	0.056
	0.213	0.955	0.054
1week	0.960	0.062	0.004
	0.930	0.146	0.017
	0.840	0.591	0.034
	0.780	0.742	0.045
	0.720	0.827	0.042
	0.390	0.972	0.046
	0.210	0.987	0.049
3 weeks	0.960	0.076	0.006
	0.930	0.166	0.012
	0.840	0.566	0.034
	0.780	0.653	0.039
	0.720	0.740	0.046
	0.390	0.984	0.059
	0.210	1.033	0.111

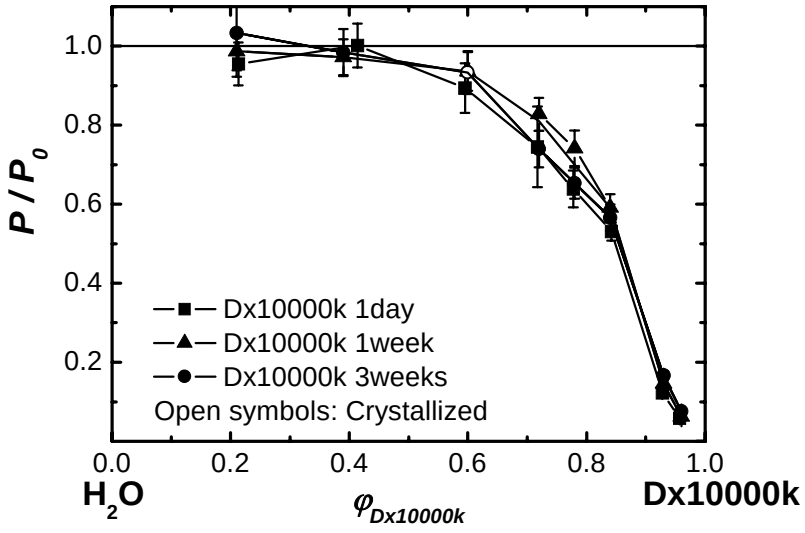

Figure 58. Vapor pressures for the system water/Dx10000k at 25 °C.

Table XXXII. Vapor pressures for the system water/Dx70k at 25 °C for different standing times (Figure 23).

Standing time	φ_{BSA}	P/P_0	Error (P/P_0)
1 day	0.936	0.120	0.010
	0.872	0.370	0.024
	0.806	0.610	0.040
	0.747	0.760	0.047
	0.639	0.950	0.058
	0.531	0.960	0.056
	0.431	0.940	0.054
	0.246	0.990	0.061
1 week	0.935	0.120	0.020
	0.876	0.401	0.018
	0.812	0.685	0.018
	0.750	0.850	0.029
	0.641	0.990	0.022
	0.533	1.000	0.022
	0.433	1.000	0.024
	0.247	0.965	0.034
3 weeks	0.968	0.042	0.011
	0.935	0.148	0.015
	0.876	0.439	0.048
	0.812	0.658	0.058
	0.750	0.854	0.076
	0.641	0.930	0.077
	0.533	0.940	0.078
	0.433	0.950	0.078
	0.247	0.962	0.096

6.3 List of Symbols

G	Gibbs energy
H	enthalpy
S	entropy
T	absolute temperature
R	universal gas constant
$^{-}$	quantities referring to mole fraction
$^{=}$	quantities referring to volume fraction
x_i	mole fraction of component i
φ_i	volume fraction of component i
w_i	weight fraction of component i
a	activity
P	vapor pressure
N	number of segment
V_i	molar volume of component i
n_i	moles of component i
μ	chemical potential
T_c	critical temperature
w_c	critical weight fraction of the polymer
g	integral interaction parameter
χ, ξ	differential interaction parameters
g_c	critical interaction parameter
φ_c	critical volume fractions
α, ζ, λ , ν	specific parameters accounting for interaction parameters according to the "Chain Connectivity and Conformational Response" theory
s_i	surface area of component i
A_2	second osmotic virial coefficient
A_2^{∞}	second osmotic virial coefficient of infinitely long chains

a	exponent of the Kuhn-Mark-Houwink equation
K	factor of the Kuhn-Mark-Houwink equation
κ	$K_N \rho_2$
K_N	$K\left(\frac{\rho_2}{\rho_1}M_1\right)^a$
σ	slope of A_2 vers $N^{-(1-a)}$
ρ	density
M	molar mass
FD	feed
EA	extract agent
WP	working point
S_T	Soret coefficient
D	translational diffusion coefficient
D_T	thermal diffusion coefficient
ζ_{het}	heterodyne signal intensity
τ_{th}	time constant of the temperature grating
n	index of refraction
q	wave vector
R	absolute Rayleigh ratio
K	optical constant
$P(q)$	particle scattering factor
R_g	radius of gyration
R_h	hydrodynamic radius
k_B	Boltzmann's constant
η	viscosity
T_g	glass transition temperature
T_{cr}	crystallization temperature
T_m	melting temperature

7 Reference List

1. Bercea, M.; Cazacu, M.; Wolf, B. A. *Macromolecular Chemistry and Physics* **2003**, *204*, 1371-1380.
2. Wolf, B. A. *Macromolecular Chemistry and Physics* **2003**, *204*, 1381-1390.
3. Stryuk, S.; Wolf, B. A. *Macromolecular Chemistry and Physics* **2003**, *204*, 1948-1955.
4. Horst, R. *Macromolecular Theory and Simulations* **1995**, *4*, 449.
5. Guo, M.; Narsimhan, G. *Biotechnology Progress* **1991**, *7*, 54-59.
6. Schmitt, C.; Sanchez, C.; Desobry-Banon, S.; Hardy, J. *Critical Reviews in Food Science AndNutrition* **1998**, *38*, 689-753.
7. Atkins, P. W. *Physical Chemistry, Fourth Edition* **1994**.
8. Flory, P. J. *Principle of Polymer Chemistry* **1953**.
9. Flory, P. J. *J. Chem. Phys.* **1944**, *12*, 425.
10. Huggins, M. L. *J. Phys. Chem.* **1942**, *46*, 151.
11. Stryuk, S.; Wolf, B. A. *Macromolecules* **2005**, *38*, 812-817.
12. Schneider, A.; Schuld, N.; Bercea, M.; Wolf, B. A. *J. Polym. Sci., Part B: Polym. Phys.* **2004**, *42*, 1601-1609.
13. Stryuk, S.; Wolf, B. A. *Macromolecules* **2005**, *38*, 812-817.
14. Stryuk, S.; Wolf, B. A. *Macromolecular Chemistry and Physics* **2003**, *204*, 1948-1955.
15. Schneider, A.; Schuld, N.; Bercea, M.; Wolf, B. A. *J. Polym. Sci., Part B: Polym. Phys.* **2004**, *42*, 1601-1609.
16. Bercea, M.; Cazacu, M.; Wolf, B. A. *Macromolecular Chemistry and Physics* **2003**, *204*, 1371-1380.
17. Wolf, B. A. *Macromolecules* **2005**, *38*, 1378-1384.
18. Koningsveld, R.; Stockmayer, W. H.; Nies, E.Oxford University Press: 1st. New York, 2001,

19. Horst, R. *Macromolecular Theory and Simulations* **1996**, *5*, 789-800.

20. Horst, R. *Macromolecular Theory and Simulations* **1995**, *4*, 449.

21. Flory, P. J. *Principle of Polymer Chemistry* **1953**.

22. Horst, R. *Macromolecular Theory and Simulations* **1996**, *5*, 789-800.

23. Weidler, B.; Vonbormann, K.; Sommermeyer, K.; Lohmann, E.; Peil, J.; Hempelmann, G. *Arzneimittel-Forschung/Drug Research* **1991**, *41-1*, 215-218.

24. Sommermeyer, K.; Cech, F.; Hildebrand, U.; Pfitzer, E.; Baumbach, C. *Starch-Starke* **1992**, *44*, 215-218.

25. Schulz, G. V. *Zeitschrift Für Elektrochemie* **1956**, *60*, 199.

26. Staudinger, H.; Heuer, W. *Berichte Der Bunsen-Gesellschaft Für Physikalische Chemie* **1930**, *B63*, 222.

27. Meyerhoff, G. *Advances in Polymer Science* **1961**, *3*, 59-105.

28. LeGrand, D. G.; Gaines, G. L. Jr. *J. Colloid Interface Sci.* **1975**, *50*, 272-279.

29. Fleischer, C. A.; Koberstein, J. T.; Krukosnis, V.; Wetmore, P. A. *Macromolecules* **1993**, *26*, 4172-4178.

30. Shi, T. F.; Ziegler, I. C.; Welge, L.; An, L.; Wolf, B. A. *Macromolecules* **2004**, *37*, 1591-1599.

31. Szwarc, M.; Levy, M.; Milkovich, R. *J. Am. Chem. Soc.* **1956**, *78*, 2656-2657.

32. Waack, R.; Rembaum, A.; Coombes, J. D.; Szwarc, M. *J. Am. Chem. Soc.* **1957**, *79*, 2026-2027.

33. Szwarc, M.; Van Beylen, M.*Ionic Polymerization and Living Polymers;* Chapman & Hall: New York London, 1993,

34. Schwarc, M. *Advances in Polymer Science* **1983**, *49*, 1-177.

35. Matyjaszweski, K.; Xia, J. H. *Chemical Review* **2001**, *101*, 2921-2990.

36. Patten, T. E.; Matyjaszewski, K. *Advanced Materials* **1998**, *10*, 901.

37. Meyer, V. R.Wiley: New York, 1994,

38. Snyder, L. R.; Kirkland, J. J.Wiley: New York, 1979,

39. Potschka, M.American Chemical Society: Washington DC, 1996,

40. Tung, L. H.; Moore, J. C.*Gel Permeation Chromatography;* Marcel Dekker: New York, 1977,

41. Schimpf, M. E. *Trends in Polymer Science* **1996**, *4*, 114-121.

42. Colfen, H.; Antonietti, M. *New Developements in Polymer Analytics I* **2000**, *150*, 67-187.

43. Eckelt, J.; Haase, T.; Loske, S.; Wolf, B. A. *Chem. Abstr.* **2003**, *139*, 134096.

44. Eckelt, J.; Haase, T.; Loske, S.; Wolf, B. A. *Macromolecular Materials and Engineering* **2004**, *289* , 393-399.

45. Wolf, B. A.*Continuous Polymer Fractionation;* Pergamon Press: Oxford, New York, Seoul, Tokyo, 1994, S. 881-885.

46. Meißner, K.; Wolf, B. A. *Papier (Darmstadt)* **1998**, *52*, 749-755.

47. Wolf, B. A. In *Encyclopedia of Advanced Materials*; Bloor, D.; Brook, R. J.; Flemings, M. C.; Mahajan, S., Eds.; Pergamon Press: Oxford, New York, Seoul, Tokyo, 1994; pp 881-885.

48. Rayleigh, J. W. S. *Proc. Lond. Math. Soc.* **1879**, *10*, 4.

49. Tomotika, S. *Proc. R. Soc. London* **1936**, *A153*, 302-18.

50. Tomotika, S. *Proc. R. Soc. London, A* **1936** , *A153*, 302-318.

51. Ludwig, C. *Sitz. Ber. Akad. Wiss. Wien Math-Naturw. Kl* **1856**, *20*, 539.

52. Soret, C. *Arch. Geneve* **1879**, *3*, 48.

53. Tyrell, H. *Diffusion and Heat Flow in Liquids* **1961**.

54. Köhler, W.; Wiegand, S. *Thermal Non-Equilibrium Phenomena in Fluid Mixtures* **2002**.

55. Kita, R.; Wiegand, S.; Luettmer-Strathmann, J. *J. Chem. Phys.* **2004**.

56. de Groot, S. R.; Mazur, P. *Non-Equilibrium Thermodynamics* **1984**.

57. Moore, F. A.; Mckinley, B. A.; Moore E. E. *Lancet* **2004**, *363*, 1988-1996.

58. Blijdenstein, T. B. J.; Hendriks, W. P. G.; van der Linden, E.; van Vliet, T.; van Aken, G. A. *Langmuir* **2003**, *19*, 6657-6663.

59. Brondsted H.; Hovgaard L.; Simonsen L. *European Journal of Pharmaceutics and Biopharmaceutics* **1996**, *42*, 85-89.

60. Dickinson, E. *Trends in Food Science and Technology* **1998**, *9*, 347-354.

61. Stenekes, R. J. H.; Talsma, H.; Hennink, W. E. *Biomaterials* **2001**, *22*, 1891-1898.

62. Hirayama, K. *BBRC* **1990**, *173*, 639.

63. Frank, W. *Strucure, Function and Genetic Control, 2nd ed.;* Academic Press: New York, 1975, S. 141, 147.

64. Dickenson, E. *Food Hydrocolloids* **2003**, *17*, 25-39.

65. Dumitriu, S.; Chornet, E. *Advanced Drug Delivery Reviews* **1998**, *31*, 223-246.

66. Axelsson, I. *J. Chromatogr.* **1978**, *152*, 21.

67. Foster, J. F.Oxford: Pergamon, 1977 , S. 53-84.

68. Brandrup, J.; Immergut, E. H.; Grulke, E. A.John Wiley & Sons, Inc.: 4th. New York, Chichester, Weinheim, Brisbane, Singapore, Tronto, 1999,

69. Wünsch, M.; Wolf, B. A. *Polymer* **2002**, *43*, 5027-5034.

70. Schneider, A.; Wünsch, M.; Wolf, B. A. *Macromolecular Chemistry and Physics* **2002**, *203*, 705-711.

71. Krause, C.; Wolf, B. A. *Macromolecules* **1997**, *30*.

72. Petri, H. M.; Wolf, B. A. *Macromolecules* **1994**, *27*, 2714.

73. Petri, H. M.; Schuld, N.; Wolf, B. A. *Macromolecules* **1995**, *28*, 4975.

74. Hachenberg, H. *Die Headspace Gaschromatographie Als Analysen- Und Meßmethode. Ein Überblick;* Eigenverlag: Frankfurt Höchst, 1991.

75. Gottwald, W.*GC für Anwender;* VCH: Weinheim, New York, Basel, Cambridge, Tokyo, 1995,

76. Hachenberg, H.*Die Headspace Gaschromatographie als Analysen- und Meßmethode. Ein Überblick;* Eigenverlag: Frankfurt Höchst, 1991,

77. Güner, A.; Kibarer, G. *Eur. Polym. J.* **2001**, *37*, 619-622.

78. Nordmeier, E. *J. Phys. Chem.* **1993**, *97*, 5770-5785.

79. Ioan, C. E.; Aberle, T.; Buchard, W. *Macromolecules* **2000**, *33*, 5730-5739.

80. Ioan, C. E.; Aberle, T.; Buchard, W. *Macromolecules* **2001**, *34*, 326-336.

81. Burchard, W.; Cowie, J. M. G.*17. Selected Topics in Biopolymeric Systems;* Academic Press: London and New York, 1972,

82. Tmasheff, S. N.; Dintzis, H. M.; Kirkwood, J. G.; Coleman, B. D. *Proceedings of the National Academy of Sciences* **1955**, *41*, 710-714.

83. Cojazzi, G.; Pizzoli, M. *Macromolecular Chemistry and Physics* **1999**, *200*, 2356-2364.

84. Burghoff, H. G.; Push, W. *J. Appl. Polym. Sci.* **1979**, *23*, 473-484.

85. Hall, D. J.; Mash, C. J.; Pemberton, R. C. *Nat. Phys. Lab. Chem. Rep* **1979**, *95*.

86. Kooner, Z. S.; Phutela, R. C.; Fenby, D. V. *Aust. J. Chem.* **1980**, *33*, 9-13.

87. Jianhua, H. U.; Haynes, C. A.; Wu, A. H. Y.; Cheung, C. M. W.; Chen, M. M.; Yee, E. G. M.; Ichioka, T.; Nishikawa, K.; Westh, P.; Koga, Y. *Can. J. Chem.* **2003**, *81*, 141-149.

88. Senti, F. R.; Hellman, N. N.; Ludwig, N. H.; Babcock, G. E.; Tobin, R.; Class, C. A.; Lamberts, B. L. *Journal of Polymer Science* **1955**, *17*, 527.

89. Brandrup, J.; Immergut, E. H.; Grulke, E. A.John Wiley & Sons, Inc.: 4th. New York, Chichester, Weinheim, Brisbane, Singapore, Tronto, 1999,

90. Bondi, A. John Wiley & Sons, Inc. : New York, London, Sydney, 1968,

91. Timasheff, S. N.; Dintyis, H. M.; Kirkwood, J. G.; Coleman, B. D. *J. Am. Chem. Soc.* **1956**, *79*, 782-788.

92. Anotonov, Y. Private Conversation. 2005.

93. Haase, T. Conversation. 2005.

94. Perronace, A.; Leppla, C.; Leroy, F.; Rousseau, B.; Wiegand, S. *Jounal of Chemical Physics* **2002**, *116*, 3718.

95. Rauch, J.; Köhler W. *Phys. Rev. Lett.* **2002**, *88*, 185901.

96. Becker, A.; Köhler, W.; Muller, B. B. *Bunsen-Ges. Phys. Chem. Chem. Phys.* **1995**, *99* , 600-608.

97. Becker, A.; Köhler, W.; Muller, B. B. *Bunsen-Ges. Phys. Chem. Chem. Phys.* **1995**, *99* , 600-608.

98. Perronace, A.; Leppla, C.; Leroy, F.; Rousseau, B.; Wiegand, S. *Jounal of Chemical Physics* **2002**, *116*, 3718.

99. Lide, D. R. *Handbook of Chemistry and Physics 65th Edition* **1984**.

100. Iacopini, S.; Piazza, R. *Europhys. Lett.* **2003**, *63*, 247.

101. Kita, R.; Kircher, G.; Wiegand, S. *J. Chem. Phys.* **2004**, *121*, 9140-9146.

102. Rousseau, B.; Nieto-Draghi, C.; Avalos, J. B. *Europhys. Lett.* **2004**, *67*, 976-982.

103. Prigogine, I.; De Brouckere, L.; Amand, R. *Physica* **1950**, *16*, 851-860.

104. Güner, A.; Kibarer, G. *Eur. Polym. J.* **2001**, *37*, 619-622.

105. Güner, A. *J. Appl. Polym. Sci.* **1999**, *72*, 871-876.

106. Güner, A.; Kibarer, G. *Eur. Polym. J.* **2001**, *37*, 619-622.

107. Kita, R.; Wiegand, S. *Macromolecules* **2005**, *38*, 4554-4556.

108. Amu, T. *Polymer* **1982**, *23*, 1775.

109. Lide, D. R. *Handbook of Chemistry and Physics 76th Edition* **1995**.

110. Frank, H. S.; Franks, F. *J. Chem. Phys.* **1968**, *48*, 4746-4757.

111. Hoccart, X.; Turell, G. *J. Chem. Phys.* **1993**, *99*, 8498-8503.

112. Shimofune, S.; Kubota, K.; Kita, R.; Dobashi, T. *J. Chem. Phys.* **1999**, *111*, 4199-4204.

113. Kuramoto, N.; Nishikawa, S. *J. Phys. Chem.* **1995**, *99*, 14372-14376.

114. Hoccart, X.; Turell, G. *J. Chem. Phys.* **1993**, *99*, 8498-8503.

115. Shimofune, S.; Kubota, K.; Kita, R.; Dobashi, T. *J. Chem. Phys.* **1999**, *111*, 4199-4204.

116. Kuramoto, N.; Nishikawa, S. *J. Phys. Chem.* **1995**, *99*, 14372-14376.

117. Niet-Draghi, C.; Avalos, J. B. *J. Chem. Phys.* **2005**, *122*, 114503.

118. Li, H.; Wu, L. *Journal of Physical Chemistry B* **2004**, *108*, 13821-13826.

119. Semenov, S.; Schimpf, M. *Physical Review E* **2004**, *69*, 011201.

120. Wolff, I. A.; Mehltretter, C. L.; Mellies, R. L.; Watson, P. R.; Hofreiter, B. T.; Patrick, P. L.; Rist, C. E. *Industrial and Engineering Chemistry* **1954**, *46*, 370

121. Wolf, B. A. *Adv. Polym. Sci.* **1972**, 10, 109